iScience

CellPress
OPEN ACCESS

Article

Comprehensive characterization of migration profiles of murine cerebral cortical neurons during development using FlashTag labeling

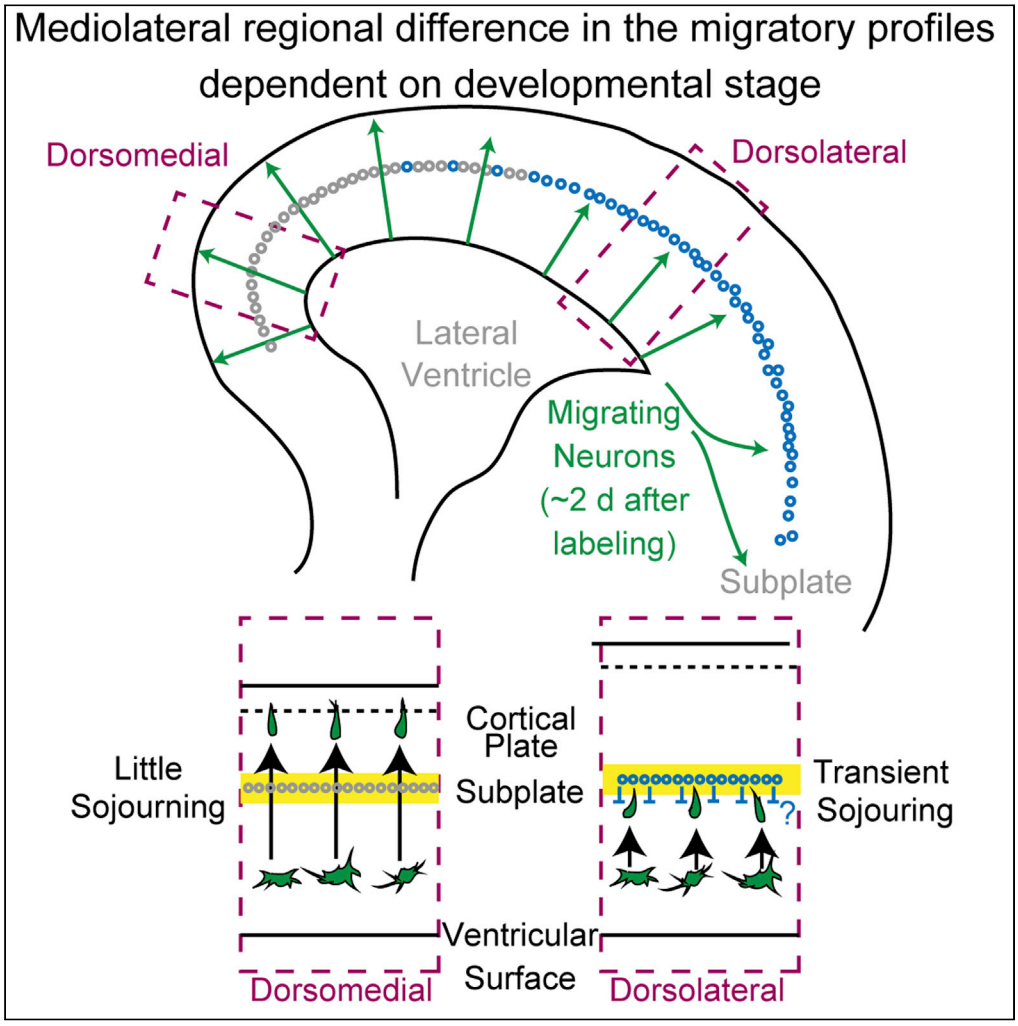

Satoshi Yoshinaga, Minkyung Shin, Ayako Kitazawa, ..., Hitoshi Hashimoto, Ken-ichiro Kubo, Kazunori Nakajima

ken16@jikei.ac.jp (K.-i.K.)
kazunori@keio.jp (K.N.)

HIGHLIGHTS

FlashTag visualized mediolateral regional differences of cortical migratory profiles

Mediolateral differences were observed when neurons were labeled at E12.5–15.5

Late-born neurons transiently sojourned below the dorsolateral subplate (SP) cells

The difference was unclear in *reeler* cortex, where SP cells position superficially

Yoshinaga et al., iScience *24*, 102277
April 23, 2021
https://doi.org/10.1016/j.isci.2021.102277

iScience

CellPress
OPEN ACCESS

Article

Comprehensive characterization of migration profiles of murine cerebral cortical neurons during development using FlashTag labeling

Satoshi Yoshinaga,[1] Minkyung Shin,[1,8] Ayako Kitazawa,[1] Kazuhiro Ishii,[1,9] Masato Tanuma,[2] Atsushi Kasai,[2] Hitoshi Hashimoto,[2,3,4,5,6] Ken-ichiro Kubo,[1,7,*] and Kazunori Nakajima[1,10,*]

SUMMARY

In the mammalian cerebral neocortex, different regions have different cytoarchitecture, neuronal birthdates, and functions. In most regions, neuronal migratory profiles are speculated similar based on observations using thymidine analogs. Few reports have investigated regional migratory differences from mitosis at the ventricular surface. In this study, we applied FlashTag technology, in which dyes are injected intraventricularly, to describe migratory profiles. We revealed a mediolateral regional difference in the migratory profiles of neurons that is dependent on developmental stage; for example, neurons labeled at embryonic day 12.5–15.5 reached their destination earlier dorsomedially than dorsolaterally, even where there were underlying ventricular surfaces, reflecting sojourning below the subplate. This difference was hardly recapitulated by thymidine analogs, which visualize neurogenic gradients, suggesting a biological significance different from the neurogenic gradient. These observations advance our understanding of cortical development and the power of FlashTag in studying migration and are thus resources for future neurodevelopmental studies.

INTRODUCTION

The mammalian cerebral neocortex is a well-organized, six-layered structure that contains a diversity of neurons. Neuronal migration is an essential step in the precise formation of the complex cortical cytoarchitecture, which underlies the evolution of mammalian cognitive function. At the earliest stage of cortical development, neural stem cells form a pseudostratified structure called the neuroepithelium, and these stem cells undergo self-renewal to expand the cortical areas (Caviness et al., 1995; His, 1889; Rakic, 1995; Sauer, 1935; Subramanian et al., 2017). They then begin to produce the earliest-born neurons (Bystron et al., 2006; Iacopetti et al., 1999), which form the preplate (PP) or primordial plexiform layer (Marin-Padilla, 1971) (see Figures S1A and S1B, Table 1, and the *histological terminology* section in transparent methods). These neurons include Cajal-Retzius cells and future subplate (SP) neurons, most of which are transient populations that undergo cell death postnatally (Hoerder-Suabedissen and Molnár, 2015; Kostovic and Rakic, 1990; Price et al., 1997). In the pallium, the production of cortical projection neurons follows. They derive from radial glial cells in the ventricular zone (VZ). Some daughter cells become postmitotic soon after they exit the VZ (Tabata et al., 2009) whereas others divide in a more basal structure (the subventricular zone [SVZ]) (Boulder-Committee, 1970; Takahashi et al., 1996). In both cases, they migrate radially through the intermediate zone (IZ), SP, and the cortical plate (CP) to the primitive cortical zone (PCZ) (Sekine et al., 2011, 2012), the most superficial part of the CP. Migrating neurons overtake earlier-born neurons to finish their migration in the PCZ. This process serves as a basis for the inside-out pattern of neuronal positioning, in which earlier-born neurons position deeply and later-born neurons position superficially (Sekine et al., 2011; Shin et al., 2019).

Different cortical regions have different functions. The cerebral cortex is subdivided into many cortical areas based on cytoarchitectonics (Brodmann, 1909), which have high correlations with function. According to the protomap hypothesis, the neural stem cells in the VZ provide a protomap of prospective cytoarchitectonic areas (Rakic, 1988). At a time of concurrent innervation from the thalamus (Moreno-Juan et al., 2017), neuronal migration takes place between proliferation at the ventricular surface and the formation of cytoarchitectonics. Therefore, the whole-brain visualization of neuronal migratory profiles from mitosis

[1]Department of Anatomy, Keio University School of Medicine, Shinjuku, Tokyo 160-8582, Japan

[2]Laboratory of Molecular Neuropharmacology, Graduate School of Pharmaceutical Sciences, Osaka University, Suita, Osaka 565-0871, Japan

[3]Molecular Research Center for Children's Mental Development, United Graduate School of Child Development, Osaka University, Kanazawa University, Hamamatsu University School of Medicine, Chiba University, and University of Fukui, Suita, Osaka 565-0871, Japan

[4]Division of Bioscience, Institute for Datability Science, Osaka University, Suita, Osaka 565-0871, Japan

[5]Open and Transdisciplinary Research Initiatives, Osaka University, Suita, Osaka 565-0871, Japan

[6]Department of Molecular Pharmaceutical Sciences, Graduate School of Medicine, Osaka University, Suita, Osaka 565-0871, Japan

[7]Department of Anatomy, The Jikei University School of Medicine, Minato, Tokyo 105-8461, Japan

[8]Present address: Korea Brain Research Institute, Dong-gu, Daegu, 41,068, Republic of Korea

[9]Present address: Department of Psychiatry, The Jikei University School of Medicine, Minato, Tokyo, 105-8461, Japan

[10]Lead contact

*Correspondence: ken16@jikei.ac.jp (K.-i.K.), kazunori@keio.jp (K.N.)

https://doi.org/10.1016/j.isci.2021.102277

Table 1. Definitions of abbreviations used in the text and figures

Abbreviations	Explanations
3H-TdR	Tritiated thymidine
BrdU	5-bromo-2′-deoxyuridine
CAS	Caudal amygdaloid stream
CC	Corpus callosum
CFSE	Carboxyfluorescein succinimidyl ester
CGE	Caudal ganglionic eminence
CP	Cortical plate
DAPI	4′,6-diamidino-2-phenylindole
E	Embryonic days
EdU	5-ethynyl-2′-deoxyuridine
FT	FlashTag
GM	Gray matter
i-GONAD	Improved genome editing via oviductal nucleic acids delivery
Ins	Insular cortex
IZ	Intermediate zone
LCS	Lateral cortical stream
LGE	Lateral ganglionic eminence
LI	Cortical layer I
LV	Lateral ventricle
MAZ	Multipolar cell accumulation zone
MGE	Medial ganglionic eminence
moRG	Mouse outer radial glial cells
MZ	Marginal zone
P	Postnatal days
PCZ	Primitive cortical zone
pH3	Phospho-histone H3
Pir	Piriform cortex
PP	Preplate
PSB	Pallial-subpallial boundaries
R	Reservoir
REP	Rapidly exiting population
SEP	Slowly exiting population
SP	Subplate
SVZ	Subventricular zone
VZ	Ventricular zone
WM	White matter

For detailed explanations, see Figures S1A and S1B, and the histological terminology section of transparent methods.

at the ventricular surface to arrival at their final destinations may serve as basic information to further understand the formation of the complex mammalian brain.

To reveal the above-mentioned neuronal behaviors (neurogenesis, positioning, and neuronal migration), thymidine analogs have long been used. Interkinetic nuclear migration of the VZ stem cells (Fujita, 1963) and the inside-out pattern of neuronal birthdate (Angevine and Sidman, 1961; Bayer and Altman, 1991; Hicks and D'Amato, 1968) were clearly shown by tritiated thymidine (^{3}H-TdR). The limitation of the use of these S-phase markers to study neuronal migration was hardly discussed; however, in the last 20 years,

growing evidence suggests that many projection neurons, especially superficial layer neurons, are generated indirectly in the SVZ from intermediate neural progenitors (Haubensak et al., 2004; Kowalczyk et al., 2009; Miyata et al., 2004; Noctor et al., 2004; Takahashi et al., 1996) and basal radial glial cells (Fietz et al., 2010; Hansen et al., 2010) that derive from (apical) radial glial cells, in addition to direct neurogenesis (Tabata et al., 2009). In addition, interneurons are born in the ventral forebrain and migrate to the cortex (tangential migration) (Anderson et al., 1997; Marin and Rubenstein, 2001; Tamamaki et al., 1997). Thymidine analogs are incorporated in the S-phase and retained by the progeny of dividing cells that undergo final mitosis irrespective of the anatomical position. Basal progenitors are already in the midst of migration when they are in the S-phase and because interneurons incorporate thymidine analogs ventrally, migratory "profiles" of neurons revealed by thymidine analogs contain those with different "starting points" (i.e., cellular positions when thymidine analogs are incorporated).

As a method of aligning the "starting points," we previously developed *in utero* electroporation, in which expression plasmids are injected into the lateral ventricle (LV), and electrical pulses are given to transfect the cells lying along the ventricular surface at the time of labeling (Tabata and Nakajima, 2001, 2008). This method is supposed to label apical progenitors in the S/G2/M phase preferentially (Pilaz et al., 2009). Using this method, we previously described (1) different migratory profiles between the direct progeny of apical progenitors and basal progenitors and (2) regional differences in the abundance of the two modes of neurogenesis between the dorsomedial and dorsolateral cortices (Tabata et al., 2009). As it is well known that neurogenic events progress along the lateral-to-medial gradient (Hicks and D'Amato, 1968; Smart and McSherry, 1982; Smart and Smart, 1982; Takahashi et al., 1999), we hypothesized that the migratory profiles of the dorsomedial (future cingulate) cortex and the dorsolateral cortex (future somatosensory cortex where there is an underlying VZ prenatally) differ significantly. On the other hand, the aforementioned work (Bayer and Altman, 1991) and others (Hicks and D'Amato, 1968) using thymidine analogs did not describe this. The former studied regional differences in the migration of later-born cortical neurons in rats and observed that it took approximately 2 days for labeled neurons to reach the top of the CP in the dorsomedial and dorsolateral cortices, where there is an underlying VZ, whereas neurons migrating to the lateral (future presumptive insular and piriform) cortex, which lacks an underlying VZ, took longer because they migrate in a sigmoid manner to circumvent the growing striatum along the lateral cortical stream (LCS). The overall migratory profiles of neurons born at ventricular surfaces in different cortical regions at different stages remain to be described.

To visualize the migration of neurons of different cortical regions that undergo mitosis at the ventricular surface at a given time, we decided to take advantage of FlashTag (FT) technology (Govindan et al., 2018; Telley et al., 2016), in which fluorescent dyes are injected into the ventricle. This technique is used to label ventricular cells specifically in the M-phase. Once the hydrophobic precursor fluorescent molecules (5(6)-carboxyfluorescein diacetate succinimidyl ester; CFDA-SE), often called carboxyfluorescein succinimidyl ester (CFSE) in biological contexts, diffuse into the cell, cellular esterases cleave them to produce carboxyfluorescein succinimidyl ester, which is fluorescent and covalently bonded to intracellular proteins (Telley et al., 2016). FT also refers to the use of other compounds with identical modes of action, including CytoTell Blue (Telley et al., 2016). Here, we successfully visualized the migration of projection neurons in different cortical regions with high temporal resolution. We describe mediolateral regional differences in the migratory profiles of neurons born at different stages in regions where there is an underlying VZ, which were not clearly detected by experiments using thymidine analogs.

RESULTS

Characterization of cell population labeled with FT

FT technology has been increasingly used to label neuronal progenitors on the ventricular surfaces and their positioning (Govindan et al., 2018; Mayer et al., 2018; Oberst et al., 2019; Telley et al., 2016, 2019), but has rarely been used to study overall migratory profiles. Therefore, we first characterized the cellular population labeled with FT to ensure the validity of our analyses. We performed an intraventricular injection of ~0.5 μL of 1 mM CFSE. We decreased the concentration of CFSE and the quantity of organic solvent to one-tenth of that used in the previous studies (Govindan et al., 2018; Telley et al., 2016) to minimize any possible but unknown side effects from injection, although the original concentration was successfully used. To characterize the population of cells labeled with FT, we injected CFSE into the LV of E14 Institute of Cancer Research (ICR) mouse embryos and fixed them 0.5–9.5 h later (Figures 1A–1E). When brains were fixed 0.5 h after dye injection, strong fluorescence was observed in the most apical cells in the pallial VZ,

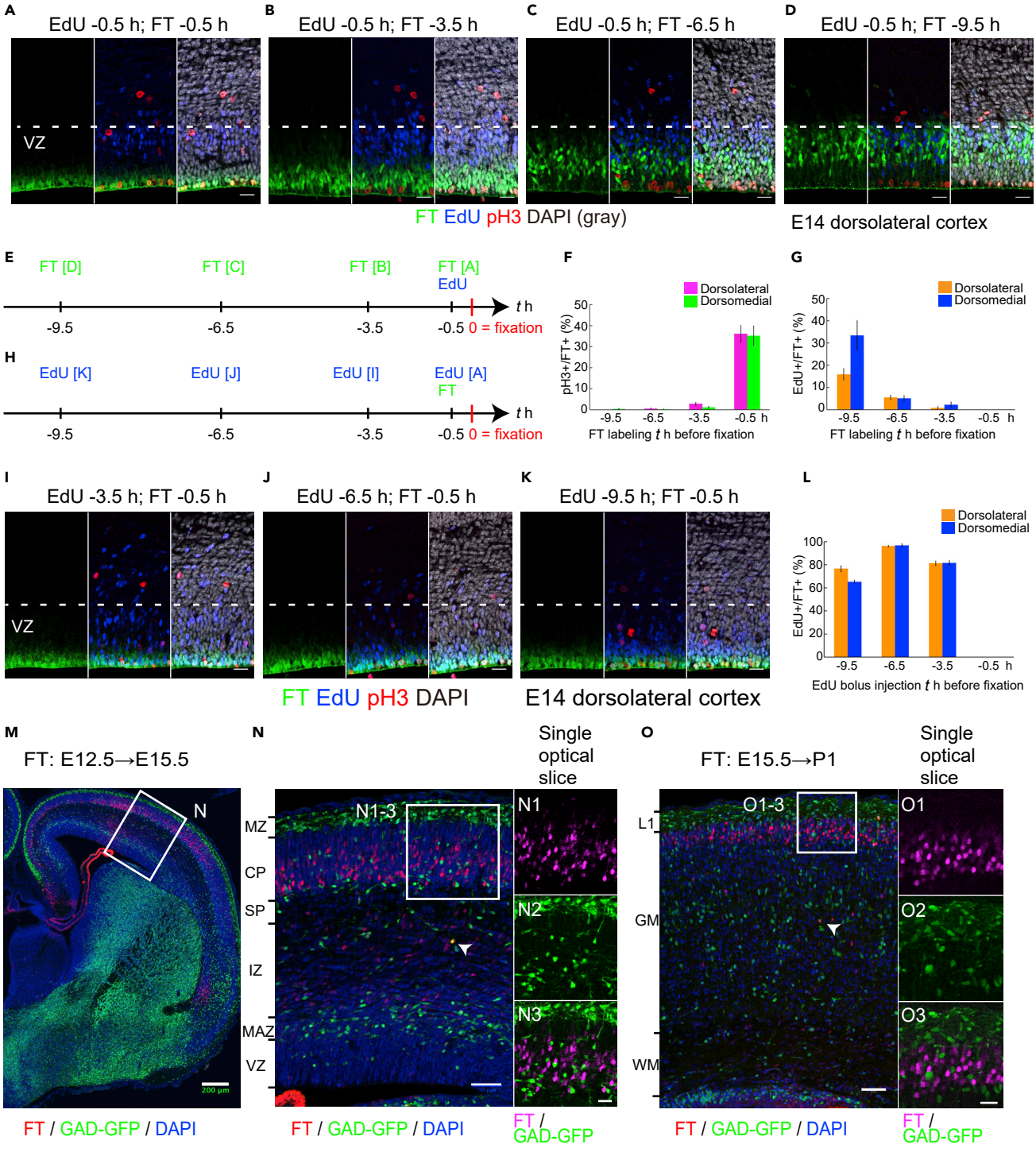

Figure 1. Characterization of cell populations labeled with the FlashTag (FT) technology

(A–G) 1 mM 5- or 6-(N-succinimidyloxycarbonyl) fluorescein 3′,6′-diacetate (CFSE) was injected into the lateral ventricles (LV) at embryonic day (E)14 of ICR mice and fixed 0.5 (A), 3.5 (B), 6.5 (C), and 9.5 (D) h later. Intraperitoneal bolus injection of 5-ethynyl-2′-deoxyuridine (EdU) was performed maternally 0.5 h before fixation. Photomicrographs from the dorsolateral cortex are shown. In (A), FT-labeled cells are positioned most apically and are often positive for phospho-histone H3 (pH3) (F, −0.5 h, dorsolateral: 36.1% ± 4.0%, 339 cells from five brains; dorsomedial: 35.2% ± 4.7%, 249 cells from 5 brains, *t* test, p = 0.82) but negative for EdU administered at the same time (G, −0.5 h, dorsolateral: 0.0% ± 0.0%, 339 cells from 5 brains; dorsomedial: 0.0% ± 0.0%, 249 cells from 5 brains, *t* test not applicable). The nuclei of EdU-positive cells are positioned basally in the VZ. 3.5 h after FT injection, FT-labeled cells have left the ventricular surface but are still near it and are no longer positive for pH3 (B) (F, pH3, −3.5 h, dorsolateral: 2.8% ± 0.7%, 530 cells from 5 brains; dorsomedial:

Figure 1. *Continued*

1.1% ± 0.5%, 415 cells from 5 brains, *t* test, p = 0.22) (G, EdU, −3.5 h, dorsolateral: 0.76% ± 0.58%, 530 cells from 5 brains; dorsomedial: 2.3% ± 1.2%, 415 cells from 5 brains, *t* test, p = 0.38). At 6.5 h after labeling, almost no cells are adjacent to the lateral ventricle (C) (F, pH3, −6.5 h, dorsolateral: 0.48% ± 0.34%, 695 cells from 5 brains; dorsomedial: 0.17% ± 0.17%, 501 cells from 5 brains, *t* test, p = 0.52) (G, EdU, −0.5 h, dorsolateral: 5.6% ± 0.87%, 695 cells from 5 brains; dorsomedial: 5.1% ± 1.3%, 501 cells from 5 brains, *t* test, p = 0.83). At 9.5 h after labeling, most of the labeled cells are in about the basal two-thirds of the VZ and some are double-labeled for EdU, suggesting that some re-enter the S-phase (D, G) (F, pH3, -9.5 h, dorsolateral: 0.0% ± 0.0%, 711 cells from 5 brains; dorsomedial: 0.37% ± 0.23%, 546 cells from 5 brains, *t* test, p = 0.19) (G, EdU, −9.5 h, dorsolateral: 15.9% ± 2.5%, 711 cells from 5 brains; dorsomedial: 33.4% ± 6.6%, 546 cells from 5 brains, *t* test, p = 0.025). A schematic representation of these experiments is shown in (E). In (F), percentages of pH3+ cells based on all FT-labeled cells are shown. Magenta, pH3+ FT+/FT+ in the dorsolateral cortex. Green, pH3+ FT+/FT+ in the dorsomedial cortex. In (G), percentages of EdU+ cells of all FT-labeled cells are shown. Orange, EdU+ FT+/FT+ in the dorsolateral cortex. Blue, EdU+ FT+/FT+ in the dorsomedial cortex.

(H–L) EdU was administered 3 (I), 6 (J), and 9 (K) h before FT labeling. At 0.5 h after FT labeling, the brains were harvested. A schematic representation of these experiments is shown in (H). Nuclei of the EdU-labeled cells are positioned more apically in brains in which EdU was administered 3.5 h before fixation (I) compared with (A), and some of the EdU-labeled cells are positioned at the ventricular surface to enter the M phase (interkinetic nuclear migration). In brains in which EdU was administered 6.5 (J) and 9.5 (K) h before fixation, EdU-labeled cells positioned even more apically. In mice treated with EdU 3–9 h before FT, FT-labeled cells are often co-labeled with EdU (I–K) (L, −9.5 h: dorsolateral, 76.6% ± 2.4%, 328 cells from 5 brains, dorsomedial, 65.1% ± 1.5%, 369 cells from 5 brains, *t* test, p = 0.014; −6.5 h: dorsolateral, 96.1% ± 0.5%, 304 cells from 5 brains, dorsomedial, 96.7% ± 1.2%, 217 cells from 5 brains, *t* test, p = 0.58; −3.5 h: dorsolateral, 81.2% ± 1.9%, 263 cells from 6 brains, dorsomedial, 81.5% ± 1.9%, 287 cells from 6 brains, *t* test, p = 0.92). Note that EdU and FT never co-label when administered simultaneously (A). In the graph in (L), the percentage of EdU+ cells based on all FT-labeled cells is shown. Data for −0.5 h in (L) correspond to those for −0.5 h in (G). Orange, EdU+ FT+/FT+ in the dorsolateral cortex. Blue, EdU+ FT+/FT+ in the dorsomedial cortex.

(M–O) CytoTell Blue was injected into the LV of the E12.5 (M–N) and 15.5 (O) *GAD67-GFP* brains. In the E15.5 dorsolateral cortex labeled at E12.5, most of the labeled cells (red) are in the deep part of the cortical plate (CP) (M, N). The majority of the labeled cells are negative for GFP (E12.5–15.5 dorsolateral cortex, 93.3% ± 2.5%, 1,653 cells from 3 brains) (N, N1–3). In postnatal day (P)1 dorsolateral cortex labeled at E15.5 (O), most of the labeled cells are found in the superficial gray matter (GM). Again, most of the labeled cells are negative for GFP (E15.5–P1, 95.5% ± 0.5%, 1,455 cells from 5 brains) (O, O1–3). Arrowheads in (N) and (O) show rare examples of cells positive for both FT and GFP.

Scale bars: 20 μm in (A–D, I–K, N3, O3), 50 μm in (N, O), and 200 μm in (M). See also Figure S1. Data are presented as mean ± standard error of the mean (SEM). The sample numbers in the statistical analyses refer to the number of brains.

which often overlapped with phospho-histone H3 (pH3, a mitosis marker) (Hendzel et al., 1997; Kim et al., 2017)-positive cells along the ventricular surface (Figure 1A). More than one-third of the labeled cells were positive for pH3 (Figure 1F, −0.5 h). This mitosis rate will be underestimated due to the time lag between dye injection and fixation and the dephosphorylation of histone H3 after telophase (Hendzel et al., 1997). Almost all pH3-positive cells on the ventricular surface were labeled with FT 0.5 h after injection (dorsolateral: 97.9% ± 1.3%, 71 cells from 5 brains; dorsomedial: 98.9% ± 1.1%, 55 cells from 5 brains; mean ± standard error of means [SEM], *t* test, p = 0.37, the sample numbers in the statistical analyses were the number of brains), suggesting that almost all cells undergoing mitosis on the ventricular surface were labeled with FT when CFSE occupied the LV. FT-labeled cells moved basally to leave the ventricular surface (Figures 1A–1D), and 3.5 h after FT labeling, FT-labeled cells had already left the ventricular surface and were almost never immunolabeled with pH3 (Figures 1B and 1F, −3.5 h). This observation suggests that the labeling time window is less than a few hours, which is compatible with previous observations (Telley et al., 2016). To visualize the difference between cellular populations labeled with FT and thymidine analogs, we performed bolus injection of 5-ethynyl-2′-deoxyuridine (EdU, a thymidine analog) into the intraperitoneal cavity of the mother mice at the same time as, or 3–9 h after, FT labeling (Figures 1A–1E). No cells were double-positive for FT and EdU when EdU and FT labeling were performed simultaneously (Figures 1A and 1F, -0.5 h). Nine hours after FT, some FT-labeled (FT+) cells were also labeled with EdU (EdU+), indicating that they had reentered the S-phase (Figures 1D and 1G, −9.5 h). We observed slight differences in EdU+/FT+ between the dorsomedial and dorsolateral cortices (Figure 1G, -9.5 h; the definitions of dorsomedial, dorsal, and dorsolateral cortices as well as the cortical zones mentioned in this study are shown in Figures S1A and S1B). This observation might reflect differences in cell-cycle lengths and/or the proportions of direct neurogenesis (Polleux et al., 1997).

To further define the differences in the labeled cellular populations, we performed bolus injection of EdU into the intraperitoneal cavity of the mother mice at the same time as, or 3–9 h before, FT (Figures 1H–1L). Brains were harvested 0.5 h after FT. Approximately 60%–90% of FT-labeled cells in mice treated with EdU 3–9 h before FT were co-labeled with EdU (Figure 1L, −3.5, −6.5, 9.5 h). As EdU is incorporated in the S-phase, these observations suggest that S-phase cells move apically to the ventricular surface by interkinetic nuclear migration over the course of several hours and are labeled with FT when they are around the M-phase. Collectively, these observations suggest that FT labels cells around the M phase on the ventricular surface and that FT can serve as a method to describe neuronal migration from a single starting point, that is, the ventricular surface.

To investigate whether cortical interneurons were also labeled with FT, CytoTell Blue, another fluorescent dye used for FT labeling (Govindan et al., 2018; Telley et al., 2016), was injected into the LV of the E12.5 (Figures 1M and 1N) and E15.5 (Figure 1O) *GAD67-GFP* knock-in mouse brains (Tamamaki et al., 2003), in which interneurons are labeled with GFP. Several days after labeling, most of the FT-labeled cells were in the CP/gray matter (GM) and a vast majority of the cells were negative for GFP. Many migrating cells in the LCS or "reservoir" (Bayer and Altman, 1991) were also mostly negative for GFP (Figure S1C, C1–C3). More ventrally, FT-labeled cells were identified in the caudal amygdaloid stream (CAS) (Remedios et al., 2007) and were negative for GFP (Figure S1C, C4–C6). GFP-labeled interneurons that migrated into the dorsal pallium were rarely labeled with FT, except for a small number of cells that were positive for both FT and GFP (Figures 1N and 1O, arrowheads), suggesting that when FT labeling is performed at E12.5–15.5, most of the FT-labeled cells in the cortex are projection neurons.

Why did we observe only a few FT-labeled interneurons in the cortex, although the ventral progenitors of the interneurons are also labeled with FT (Mayer et al., 2018) (Figures S1D and S1E)? We reasoned that frequent abventricular cell division might dilute the fluorescent dyes, thereby attenuating the fluorescent labeling. Indeed, when we performed immunohistochemistry against pH3, we confirmed that abventricular mitosis is very frequent in the ganglionic eminences (Figures S1D and S1E), which is consistent with previous reports (Katayama et al., 2013; Smart, 1976; Tan et al., 2016; Tan and Shi, 2013). We next reasoned that injection of a fluorescent dye into the SVZ might prevent loss of fluorescence by dilution upon abventricular mitosis. To address this question, we injected CytoTell Blue into the parenchyma of the ganglionic eminences of *GAD67-GFP* mice at E12.5 (the injection sites were retrospectively identified, e.g., a presumptive injection site is shown by an asterisk in Figure S1F). Cells were far more strongly labeled than with intraventricular injections. FT and GFP-double-labeled cells with tangential morphologies were distributed throughout the hemispheres, especially in the SVZ and the marginal zone (MZ) of the dorsal pallium at E15.5 (Figure S1F, F1–10). These observations are compatible with the idea that FT-labeled interneuron progenitors in the VZ undergo mitosis in the SVZ, resulting in loss of FT fluorescence in the migrating cortical interneurons when fluorescent dyes are delivered intraventricularly. Another group independently reported that projection neurons formed the majority of the FT-labeled cells, based on single-cell RNA sequencing (Telley et al., 2019).

In summary, when fluorescent dyes were injected intraventricularly, the FT-labeled cells at early (E12.5) and late (E15.5) stages of neurogenesis were mostly non-GABAergic projection neurons. We do not preclude a small subpopulation of interneurons from being labeled with FT, which will be described later in the late and very late stages of neurogenesis (E15.5 and E17.0 cohort).

FT visualizes clear regional differences in neuronal migration profiles in the cerebral cortex

Using FT technology, we noticed regional differences in neuronal migration during the development of the cerebral cortex. We performed FT labeling at E14.5 and fixation 2 days later (Figure 2A). Many FT-labeled cells had reached the top of the CP in the dorsomedial cortex, whereas most of the labeled cells were still below the SP in the dorsolateral cortex (the lower border of the SP is represented by yellow dotted lines). This suggests the presence of clear regional differences in neuronal migration profiles, for example, in the times required for cells to reach the top of the CP, even where there is an underlying ventricular surface, when mitotic cells on the ventricular surface are selectively labeled with FT.

To compare migration profiles visualized with FT with those visualized with thymidine analogs, EdU was co-administered with FT. The distribution of EdU-positive cells was similar to that reported previously (Bayer and Altman, 1991). As expected, we found no clear difference between the distributions of labeled cells in the dorsomedial and dorsolateral regions when examined where there was an underlying VZ (Figures 2B and 2C). A small number of EdU-positive GABAergic interneurons were distributed sparsely, mainly in the multipolar cell accumulation zone (MAZ) and IZ (Figure S2). The EdU-labeled neurons in the dorsolateral CP (Figure 2B) should have passed the SP to enter the CP earlier than the FT-labeled cells (Figure 2A), although the M-phase-labeled (FT-labeled) cells should have started migration earlier than the S-phase-labeled (EdU-labeled) cells if they were labeled in the VZ. Therefore, EdU-labeled neurons in the dorsolateral CP in Figure 2B would have been in the S-phase in the SVZ at the time of FT labeling and EdU administration. We previously reported that a mitotically active population leaving the VZ (rapidly exiting population [REP]) (Tabata et al., 2009), most of which corresponds to the basal and glial progenitors (Tabata et al., 2009, 2012), is more abundant in the dorsolateral cortex than in the dorsomedial cortex. This population would have contributed to the EdU-labeled cells in the dorsolateral CP.

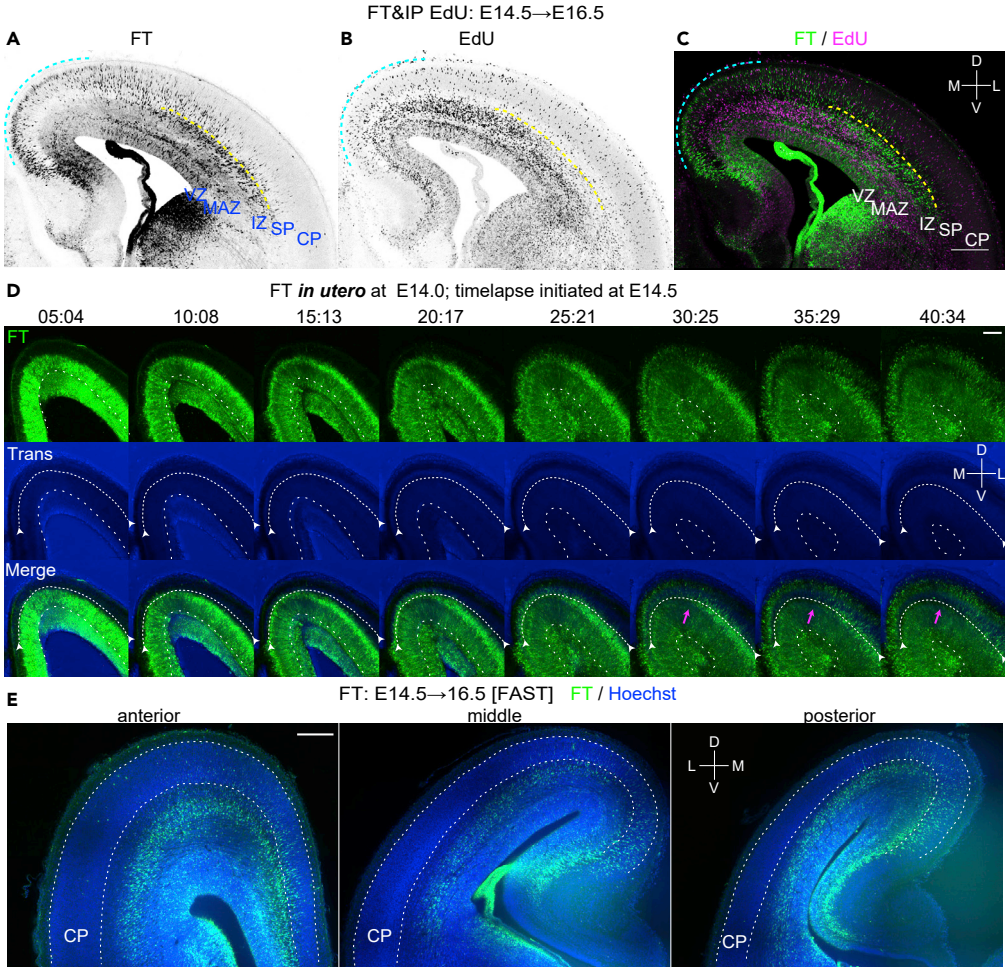

Figure 2. Regional differences in neuronal migration in the cerebral cortex revealed by FT

(A–C) To visualize the migration profile of the whole telencephalon, CFSE was injected into the ventricles of the E14.5 embryos, and 5-ethynyl-2′-deoxyuridine (EdU) was injected into the peritoneal cavity of the mother at the end of the surgery. Harvested at E16.5, many cells labeled with FT reach the superficial part of the CP in the dorsomedial cortex (cyan dotted line), whereas almost no cells reach the CP in the dorsolateral cortex (A, C). In the dorsolateral cortex, many neurons are just below the subplate (SP) (yellow dotted line). Such a clear difference in neuronal migration is not detected by EdU (B, C).

(D) FT labeling was performed at E14.0, and slice culture was prepared at E14.5. Labeled cells left the VZ and migrate in the MAZ in multipolar morphology (10:08–25:21). They gradually acquire polarity and migrate in the intermediate zone (IZ) (20:17–30:25), reaching points just below the SP (the relatively dark band in the transmitted light channel, highlighted by white arrows). Neurons in the dorsomedial cortex (more medial than the magenta arrow) migrate smoothly to reach the most superficial part of the cortical plate (25:21–30:25), whereas in the dorsolateral cortex (more lateral than the magenta arrow), neurons seem to sojourn transiently below the SP (clear in the regions lateral to the magenta arrow; 30:25–35:29). These cells subsequently migrate into the CP in locomotion mode (35:29–40:34).

(E) FAST 3D imaging of E16.5 brains in which FT labeling was performed at E14.5. Anterior and posterior representative sections are shown in addition to a section at the interventricular foramen. Video S1 shows a 3D video taken from this brain. M, medial; L, lateral; D, dorsal; V, ventral. Scale bars: 200 μm in (A–C and E) and 100 μm in (D).

See also Figure S2.

To further characterize these regional differences, we performed time-lapse imaging of the FT-labeled cells (Figure 2D). In the dorsolateral cortex, labeled cells left the VZ to enter and accumulate in the MAZ, a zone enriched in postmitotic multipolar cells (Tabata et al., 2009, 2012) (Figure 2D, 10:08–25:21). They then migrated through the IZ and transiently sojourned just below the SP (Figure 2D, 30:25–35:29) before entering the CP (Figure 2D, 40:34). This sojourning behavior below the SP corresponds to the stationary period (Ohtaka-Maruyama et al., 2018). It should be noted that this sojourning behavior was not clear in

the dorsomedial cortex. To visualize the migratory profile in three dimensions (3D), we injected the dye at E14.5, fixed approximately 2 days later, and subjected the brains to 3D FAST imaging (Seiriki et al., 2017, 2019). The mediolateral difference in the migratory profile was preserved along the anteroposterior axis (Figure 2E, Video S1). The difference was somewhat clearer in the posterior cortex (presumptive retrosplenial-visual cortex) than in the anterior (presumptive medial prefrontal cortex—somatosensory cortex). These observations suggest that this mediolateral difference in neuronal migration profiles may, at least in part, result from a transient pause just below the dorsolateral SP.

Regional migratory/positional profiles differ from neuronal birthdates at the ventricular surface

It was previously reported that early- and late-born neurons migrate differently (Hatanaka et al., 2004). Do both early-born and late-born neurons show similar regional differences? Do regional differences have birthdate-dependent characters? To better understand the migration profiles of neurons born at different embryonic stages, we injected CFSE at E10.5, 11.5, 12.5 13.5, 14.5, 15.5, and 17.0 and fixed chronologically. Subsequent observations were carried out on the coronal section in which the interventricular foramen was visible.

E10.5 cohort

One day after injection, at E11.5, some labeled cells were already located in the PP in both the dorsomedial and dorsolateral cortex (Figures 3D, 3E, and S3A), although the PP was then very thin, especially in the dorsomedial cortex (Figure 3D). Many other labeled cells were still in the VZ, which consisted of densely packed, radially oriented (Boulder-Committee, 1970) Pax6-positive (Englund et al., 2005) nuclei of radial glia. Two days after injection, at E12.5, most of the labeled cells were in the PP (Figures 3A, 3D, 3E, and S3B). Mediolateral migratory differences were not clear in these observations.

Three days after injection, at E13.5, chondroitin sulfate proteoglycan (CSPG) (Bicknese et al., 1994) and nuclear staining showed PP splitting proceeding in a lateral-to-medial direction, and the emergence of the CP was apparent in the dorsolateral cortex (asterisks in Figure 3B, blue arrows in Figure 3E) but not in the dorsomedial cortex (Figures 3B and 3D; the upper and lower borders of the nascent CP are shown by blue lines in Figures 3D and 3E), which is consistent with the lateral-to-medial neurogenic gradient. In the dorsolateral cortex, most of the labeled cells were in the CP and MZ, whereas in the dorsomedial cortex, most of the labeled cells were in the PP. Note that strongly labeled cells were hardly found in the SP just below the CP at E13.5 (Figures 3B, 3D, 3E, and S3C). At E14.5–15.5 in the dorsomedial cortex, labeled cells were found at the boundary between the SP and CP as well as in the MZ (Figures 3D, S3D, and S3E), which was similar to the dorsolateral cortex at E14.5 (Figures 3E and S3D). In the E15.5 dorsolateral cortex, many labeled cells were distributed in the CSPG-positive SP below the CP (Figures 3E and S3E). At E16.5, in both the dorsomedial and dorsolateral cortices, labeled cells were mainly found in the SP (Figures 3C–3E, and S3F) and were Tbr1 (Hevner et al., 2001)-positive (Figure S3G), suggesting that they are of pallial origin. Some cells were also found in the MZ (Figures 3C–3E, and S3G) and were also positive for Reelin (Ogawa et al., 1995) (Figures S3G), suggesting that FT labeling at E10.5 mainly labels Tbr1-positive SP cells and Cajal-Retzius cells. These observations suggest that at least some future SP neurons in the PP are in the CP and MZ when the CP begins to be formed. They might eventually move down to the SP layer in a lateral-to-medial fashion. This view is compatible with previous observations (Bayer and Altman, 1991; Osheroff and Hatten, 2009; Saito et al., 2019). Recent observations have shown that future SP neurons migrate tangentially in the PP (Pedraza et al., 2014; Saito et al., 2019), but FT failed to explicitly detect tangential migration of the future SP neurons, probably because FT labels the whole hemisphere.

In summary, the E10.5 cohort reached the PP in less than 1 day after they exited the VZ in both the dorsomedial and dorsolateral cortices. Among the E10.5 cohort, future SP neurons formed a distinct layer below the CP in a lateral-to-medial fashion, reflecting the well-described neurogenic gradient.

E11.5 cohort

As early as half a day after injection, at E12.0, most of the labeled cells were in the VZ, and some cells were in the CSPG-positive PP in both the dorsomedial (Figure 4D, arrowhead in Figures 4D and S4A) and dorsolateral cortices (Figure 4E, arrowheads in Figures 4E and S4A). At E12.5 and 13.0, more labeled cells were found in the PP in both dorsomedial (Figures 4A, 4D, S4B, and S4C) and dorsolateral cortices (Figures 4A, 4E, S4B, and S4C) and in the VZ. Many labeled cells had reached points just beneath the meninges. At E13.5, in the dorsomedial cortex, where PP splitting has not yet occurred at this stage, many neurons were in the PP just beneath the meninges (Figures 4D and S4D). However, in the dorsolateral cortex, where the

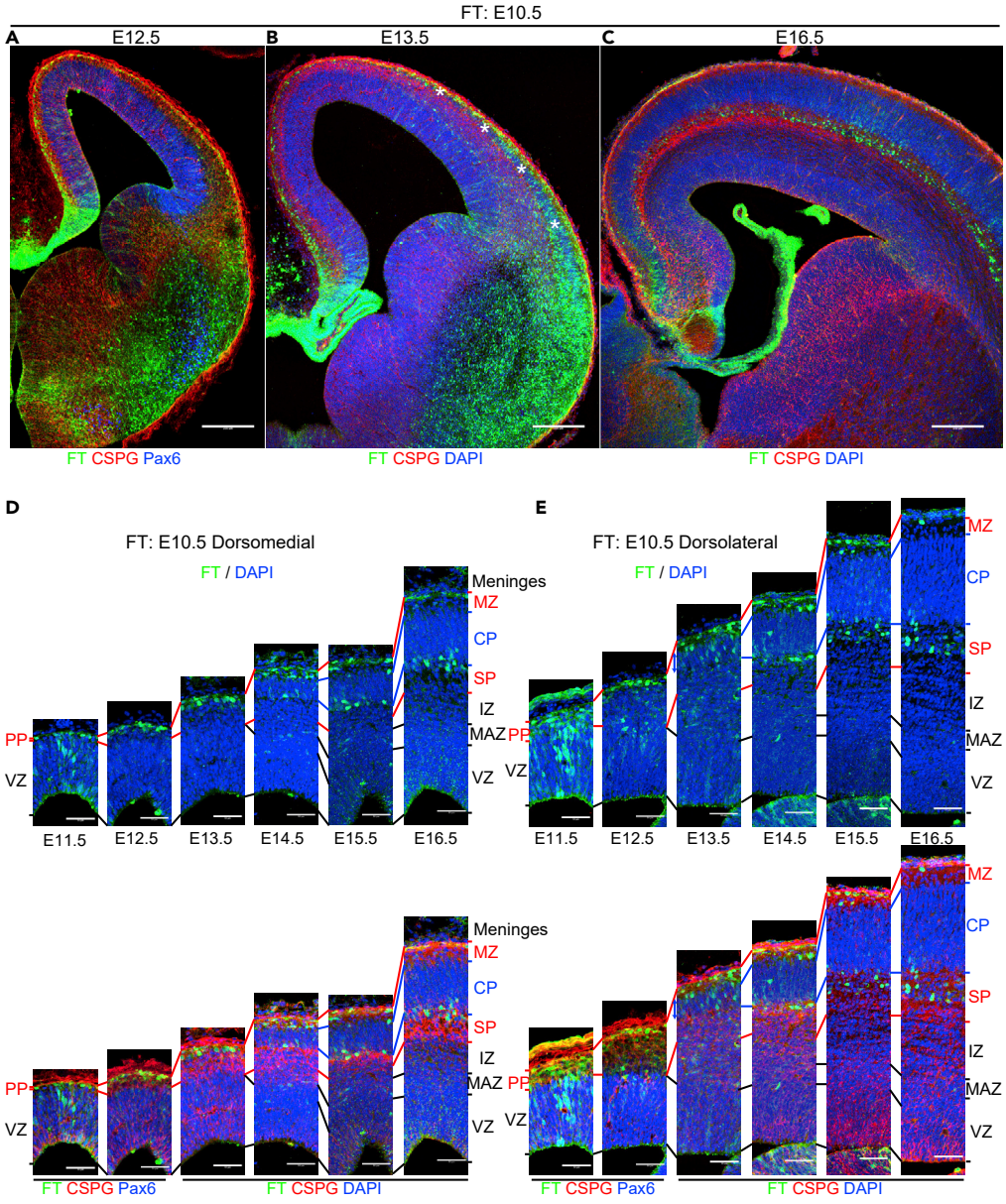

Figure 3. Cohort of cells born at E10.5

(A–E) Coronal sections of 12.5 (A), 13.5 (B), and 16.5 (C) brains labeled at E10.5. See also Figure S2 for coronal sections from E11.5 to 16.5, shown with FT and 4′,6-diamidino-2-phenylindole (DAPI). Higher-magnification micrographs from the dorsomedial cortex and dorsolateral cortices from E11.5 to 16.5 are shown in (D) and (E), respectively. As early as E11.5, some cells are found in the preplate (PP), which is very thin in the dorsomedial cortex, as well as in the VZ (D, E, Figure S3A). At E12.5, many cells are in the PP, sometimes in a tangential morphology (A, D, and E). At E13.5, CSPG and nuclear staining show that PP splitting proceeds in a lateral-to-medial direction, and the CP (asterisks) is observed in the dorsolateral cortex but not in the dorsomedial cortex (B). In the dorsomedial cortex, labeled cells are in the PP, often with a somewhat rounded morphology (D). In the dorsolateral cortex, on the other hand, many labeled cells are in the CP (shown with blue arrows) and MZ (E). Note that few cells are found below the CP, as identified by nuclear and CSPG staining (B, E, Figure S3C). At E14.5, a thin CP is also identified in the dorsomedial cortex (D, E, Figure S2D). Some labeled cells are seen in the deep part of the CP in the dorsomedial cortex, but many labeled cells are still in the MZ (D). In the dorsolateral cortex, many labeled cells are found near the boundary between the CP and SP (E, Figure S3D). At E15.5, labeled cells are found at the boundary between the SP and CP as well as in the MZ in the dorsomedial cortex (D, Figures S3E and S3E′), which is similar to the dorsolateral cortex of E14.5 (E, Figure S3D). In the E15.5 dorsolateral cortex, many labeled cells are in the CSPG-positive SP (D, E, Figures S3E and S3E′). At E16.5, in both the dorsomedial and dorsolateral

Figure 3. *Continued*
cortices, labeled cells are mainly found in the SP (C, D, and E). Some cells are also found in the MZ (D, E, Figure S3G). Note that CSPG staining in the SP shows some double-track immunoreactivity strongly just above and below a distinct cell layer in the SP in the dorsal and dorsolateral cortex at E15.5–E16.5 (E). The emergence of the labeled cells in the SP seems to coincide with the emergence of a distinct layer. Scale bars: 200 μm in (A–C) and 50 μm in (D, E).

PP was split, many labeled cells showed radial (parallel to the apicobasal axis) alignment in the newly formed CP (Figures 4E and S4D). The formation of the CP coincided with this radial alignment of the labeled cells at E13.5 in the dorsolateral cortex and at E14.5 in the dorsomedial cortex (Figures 4D, 4E, and S4E). At E15.5, some cells were in the MZ, others remained in the deep part of the CP and expressed the deep-layer marker Ctip2 (Arlotta et al., 2005), and still others emerged below the CP (Figures 4C–4E and S4F–S4H).

In summary, the E11.5 cohort reached the PP soon after they exited the VZ in both the dorsomedial and dorsolateral cortices, similarly to the E10.5 cohort. Radial alignment occurred just below the meningeal surface in a lateral-to-medial fashion, in parallel with the formation of the CP. As in the E10.5 cohort, future SP neurons formed a distinct layer below the CP after the CP formed in the E11.5 cohort.

E12.5 cohort

As early as half a day after injection, at E13.0, many labeled cells were observed in the VZ, but a small number of labeled cells were also found in the PP in the dorsomedial cortex (Figures 5A, 5G, S5A, and S5G). The latter cells were often weakly positive for Pax6 (Figure S5G, arrowheads) (number of FT+/Pax6+ cells, 9.0 $\pm$ 2.0 cells [mean $\pm$ SEM]; dorsomedial low-power field, $n = 4$ brains). On the other hand, in the dorsolateral cortex, many labeled cells were in zones just above the VZ in addition to the VZ proper and were mostly negative for Pax6 (Figures 5A, 5H, S5A, and S5H; arrows). FT+/Pax6+ cells outside the VZ were relatively rare in the dorsolateral cortex (number of FT+/Pax6+ cells, 1.6 $\pm$ 0.8 cells; dorsolateral low-power field, $n = 4$ brains). One day after injection, at E13.5, in the dorsomedial cortex, more labeled cells were seen in the PP in addition to the VZ, and labeled cells in the PP were no longer positive for Pax6 (Figures 5B, 5G, and S5B). In the dorsolateral cortex, the incipient CP appeared at this stage (E13.5) (see also Figure 3B), and the majority of the labeled cells were below the CP and still migrating in the IZ (Figures 5B, 5H, and S5B). Some entered and were radially aligned in the CP; others were migrating in the IZ at E14.0 (Figures 5C, 5H, and S5C). In the dorsomedial cortex of E14.0, however, when the incipient CP is about to be formed, many labeled cells had already reached points just beneath the meningeal surface (Figures 5C, 5G, and S5C). The radial alignment of the labeled cells coincided with the formation of the CP at E14.5 in the dorsomedial cortex (2 days after injection) (Figures 5D, 5G, and S5D), as in the E11.5 cohort. Most of the labeled cells occupied the CP at E15.5 in both the dorsomedial and dorsolateral cortex (Figures 5E, 5G, 5H, and S5E), and some emerged in the SP at E16.5 in the dorsomedial cortex (Figures 5F, 5G, and S5F).

Taken together, the results suggest slight signs of mediolateral differences in the migration profiles of neurons labeled at E12.5, that is, the dorsomedial E12.5 cohort reached the outermost region of the PP just beneath the pial surface relatively soon after leaving the VZ, whereas the dorsolateral E12.5 cohort migrated slowly in the lower part of the PP or IZ before they entered the CP. Radial alignment of the labeled cells, on the other hand, occurred in a lateral-to-medial fashion in parallel with the formation of the CP.

E13.5 cohort

Half a day after injection, at E14.0, most of the labeled cells were in or just above the VZ, that is, the MAZ, a zone enriched in postmitotic multipolar cells (Tabata et al., 2009, 2012), in both the dorsomedial and dorsolateral cortex (Figures S6A, S7A, and S7B). One day after injection, at E14.5, many labeled neurons were migrating in the IZ below the CSPG-positive SP (Figures S6B, S7A, and S7B). One and a half days after injection, at E15.0, many labeled cells reached the top of the CP in the dorsomedial cortex (Figures S6C and S7A), whereas in the dorsolateral cortex, few cells reached the CP and many cells were still migrating in the superficial IZ or beneath the SP (Figures S6C, S6H, and S7B). In the dorsolateral cortex, it was at E15.5–16.5 when most of the labeled cells reached the superficial CP (Figures S6D, S6E, and S7B). These observations suggest clear regional differences in the times required for neurons to reach the CP in the E13.5 cohort. At E16.5, E17.5, and E18.5, labeled neurons were overtaken by neurons presumptively born later and settled in the deep part of the CP (Figures S6E–S6G, S7A, and S7B) in both the dorsomedial and dorsolateral cortices. In the ventrolateral cortex, some labeled neurons were still in the reservoir, and others had migrated out of the reservoir to the insular and piriform CP (Figure S6G, G1) at E17.5, compatible with a previous observation that neurons that migrate along the LCS take

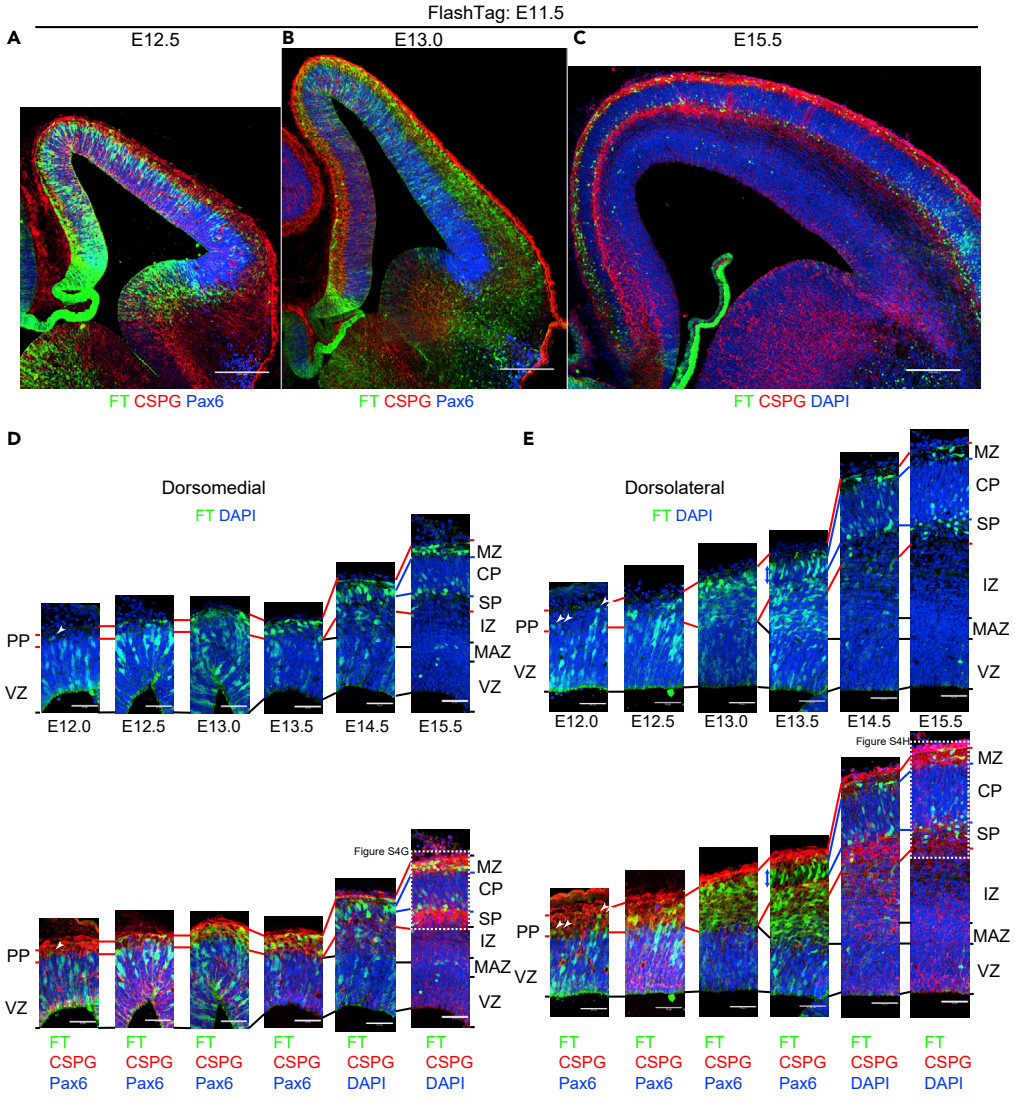

Figure 4. Cohort of cells born at E11.5

(A–E) Coronal sections of E12.5 (A), 13.0 (B), and 15.5 (C) brains, all labeled at E11.5. Higher-magnification micrographs from the dorsomedial and dorsolateral cortices of E12.5 through E15.5 are shown in (D) and (E), respectively. See also Figure S4 for low-magnification micrographs of brains fixed at E12.5 through E15.5. At E12.0, most of the labeled cells are in the VZ, and some cells are in the CSPG-positive PP in both the dorsomedial and dorsolateral cortices (D, E, arrowheads, Figure S4A). At E12.5 and 13.0, more labeled cells are found in the PP in both dorsomedial (A, B, D, Figures S4B and S4C) and dorsolateral cortices (A, B, E, Figures S4B and S4C). At E13.5, in the dorsomedial cortex, where PP splitting does not occur at this stage, many neurons reach the PP just beneath the meninges (D, Figure S4D). Many labeled cells are in the newly formed CP and intermediate zone (IZ) in the dorsolateral cortex (E, Figure S4D). At E14.5, many cells are in the newly formed CP in both the dorsomedial and dorsolateral cortices (D, E, Figure S4E). At E15.5, many cells are in the lower part of CP and, to a lesser extent, the MZ (C, D, E, Figures S4F–S4H). Some cells are also found in the SP in the dorsolateral cortex (C, E, Figures S4F and S4H).

Scale bars, 200 μm in (A–C) and 50 μm in (D, E).

longer to reach their final destinations (Bayer and Altman, 1991). Labeled neurons were also observed in the presumptive CAS (Remedios et al., 2007) (Figure S6G2).

To characterize the regional differences quantitatively, we counted the proportion of FT-labeled cells in the CP at E15.0. Consistent with the above description, significantly more neurons were observed in the CP in the dorsomedial cortex than in the dorsolateral cortex (Figure S6H).

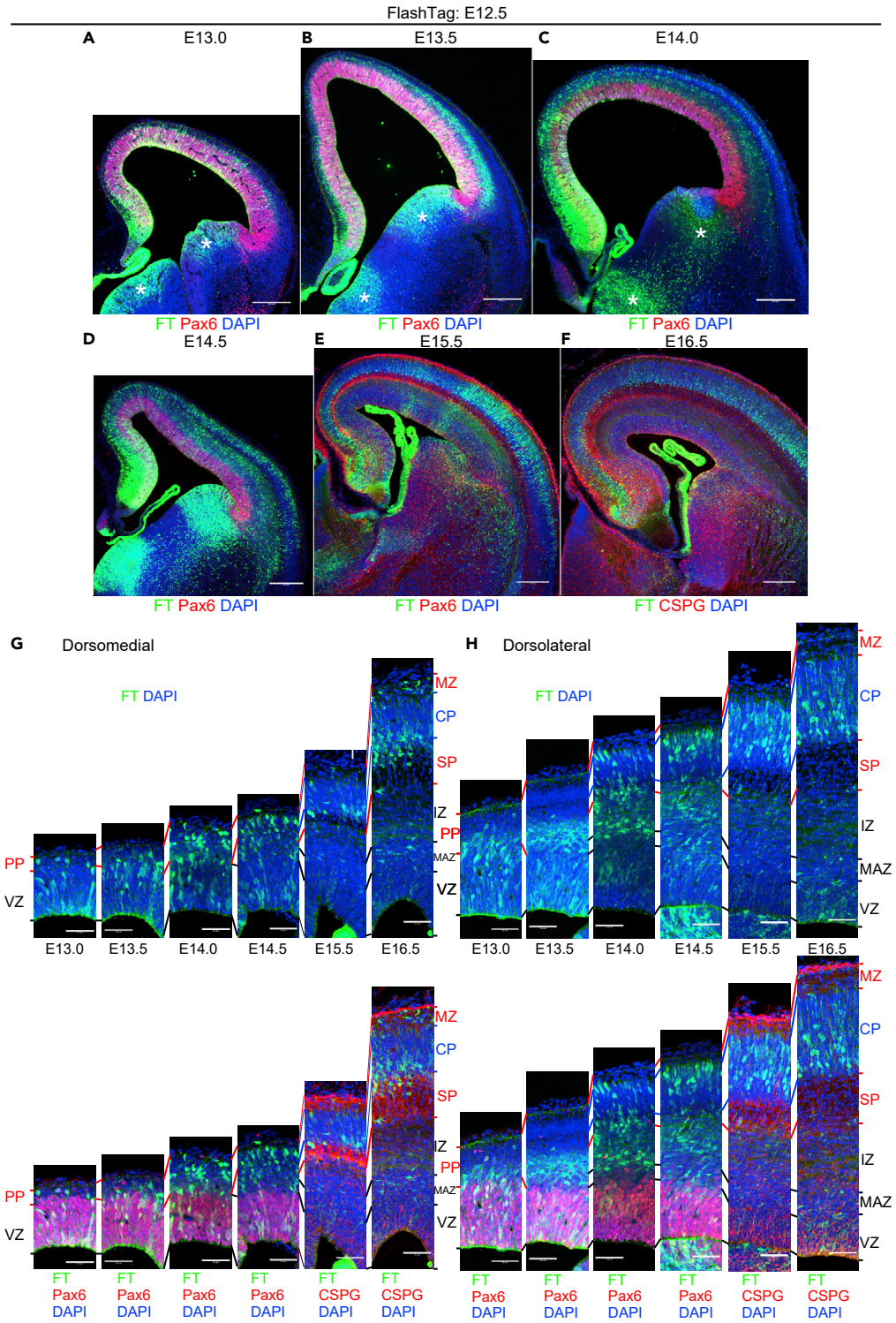

Figure 5. Cohort of cells born at E12.5

(A–H) Coronal sections of E13.0 (A), 13.5 (B), 14.0 (C), 14.5 (D), 15.5 (E), and 16.5 (F), all brains labeled at E12.5. Higher-magnification micrographs from the dorsomedial cortex and dorsolateral cortex are shown in (G) and (H), respectively. In the dorsomedial cortex at E13.0, many labeled cells are in the VZ, but a small number of labeled cells are also found in the PP (A, G, Figure S5G). At E13.5, more labeled cells are in the PP in addition to the VZ in the dorsomedial cortex (B, G). At this stage, the incipient CP appears in the dorsolateral cortex, and many labeled neurons are migrating in the IZ (B, H). In

Figure 5. *Continued*
the dorsomedial cortex of E14.0, when the incipient CP is beginning to form, some labeled cells reach points just beneath the meningeal surface, whereas others seem to be still migrating (C, G). In the dorsolateral cortex, many neurons reach the superficial part of the CP, whereas others continue migrating in the IZ and CP (C, H). At E14.5, labeled cells in the dorsomedial cortex begin to be oriented radially just beneath the MZ (D, G). In the dorsolateral cortex, many strongly labeled cells are in the CP in addition to the IZ (D, H). At E15.5, most of the labeled cells distribute not only the superficial CP but also in the deep part of the CP in both the dorsomedial and dorsolateral CP, suggesting that some begin to move deeper (E, G, H). At E16.5, the main population of the labeled cells is in the somewhat deeper part of the CP in both the dorsomedial and dorsolateral cortices. In the dorsomedial cortex, many labeled cells are also distributed in the SP. Scale bars: 200 μm in (A–F) and 50 μm in (G, H).

In summary, cells labeled at E13.5 reached points just beneath the meningeal surface in approximately 1.5 days in the dorsomedial cortex, whereas those in the dorsolateral cortex took longer to enter the CP and reach comparable locations. This areal difference was similar to that observed in the E14.5 cohort in Figure 2 and is likely explained, at least in part, by transient sojourning below the SP.

E14.5 cohort

Half a day after injection, at E15.0, most of the labeled cells were in the VZ (Figures 6A, 6H, 6I, and S8A). A small number of labeled cells had left the VZ mainly in the dorsolateral cortex (Figures 6H, 6I, and 6K) (dorsomedial, 3.7 ± 0.9 cells/low-power field, $n = 3$ brains; dorsolateral, 23.0 ± 3.5 cells/low-power field, $n = 3$ brains). They had long ascending processes and retraction bulbs and were mitotically active, as shown by Ki-67 immunoreactivity (Figure 6K), which presumably corresponds to the mitotically active REP that we reported previously (Tabata et al., 2009). They were also positive for the stem cell markers Pax6 and Sox2, although outside the VZ (Figure 6K) (Pax6 positive, dorsomedial, 91.7% ± 8.3%, 11 cells from 3 brains; dorsolateral, 80.8% ± 2.9%; 69 cells from 3 brains), suggesting that most of the cells in this population have features of mouse outer radial glial cells (moRG) (Shitamukai et al., 2011; Vaid et al., 2018; Wang et al., 2011). The progeny of this population was often difficult to identify, probably because the fluorescent signals decreased upon mitosis in the SVZ. One day after injection, at E15.5, the major population of labeled cells had left the VZ and accumulated in the MAZ (Figures 6B, 6H, 6I, and S8B). One and a half days after injection, at E16.0, most of the labeled cells had migrated in the IZ (Figures 6C, 6H, 6I, and S8C). Until this time point, the mediolateral migratory difference of the major population was not clear. However, 2 days after injection, at E16.5, many cells had reached the most superficial part of the CP in the dorsomedial cortex, whereas the majority were still migrating in the IZ just beneath the SP in the dorsolateral cortex (Figures 6D, 6H, 6I, and S8D), showing a clear mediolateral difference in migration. These observations are consistent with the view that mediolateral migratory differences are attributable to the migratory behavior of neurons in the dorsolateral IZ or just beneath the dorsolateral SP. In the dorsomedial cortex, most of the labeled cells settled in the most superficial CP, or PCZ, a zone composed of densely packed immature neurons (Sekine et al., 2011, 2012; Shin et al., 2019), at E16.5–17.5 (Figures 6D, 6E, 6H, S8D, and S8E). By E18.5, they were overtaken by presumptive later-born neurons and positioned in a slightly deeper part of the CP as NeuN-positive mature neurons in the dorsomedial cortex (Figures 6F, 6H, and S8F). In the dorsolateral cortex, one additional day was required for neurons to reach the CP (Figures 6E, 6I, and S8E) compared with dorsomedial neurons; they settled in the PCZ (indicated by the double-headed arrows in Figures 6G–6I) at E17.5–18.5 (Figures 6E, 6F, 6I, S8E, and S8F). At P0.5, they were positioned in a slightly deeper part of the CP as NeuN-positive mature neurons (Figure 6G) because of being overtaken by immature neurons in the PCZ. At P7, labeled neurons were mainly positioned in layers II/III in the dorsomedial and lateral cortices and in layer IV in the dorsolateral cortex (Figure S8H).

In summary, labeled cells showed similar migratory profiles until they entered the IZ in both dorsolateral and dorsomedial cortices. In the dorsolateral cortex, cells pass the SP and enter the CP more slowly, compatible with our *in vitro* observations in Figure 2 and similar to the E13.5 cohort. This time lag to enter the CP was not caught up until they had settled in their final destinations. These observations suggest that regional differences in the migration patterns of the E14.5 cohort derive, at least in part, from transient sojourning in the IZ below the SP.

To validate these observations quantitatively, we performed a bin analysis of the migratory profiles of neurons labeled at E14.5, from E15.0 to E18.5 (Figure 6J). We used relative rather than definitive positions to correct for individual variations in brain thickness and variations due to artifacts of histological processing.

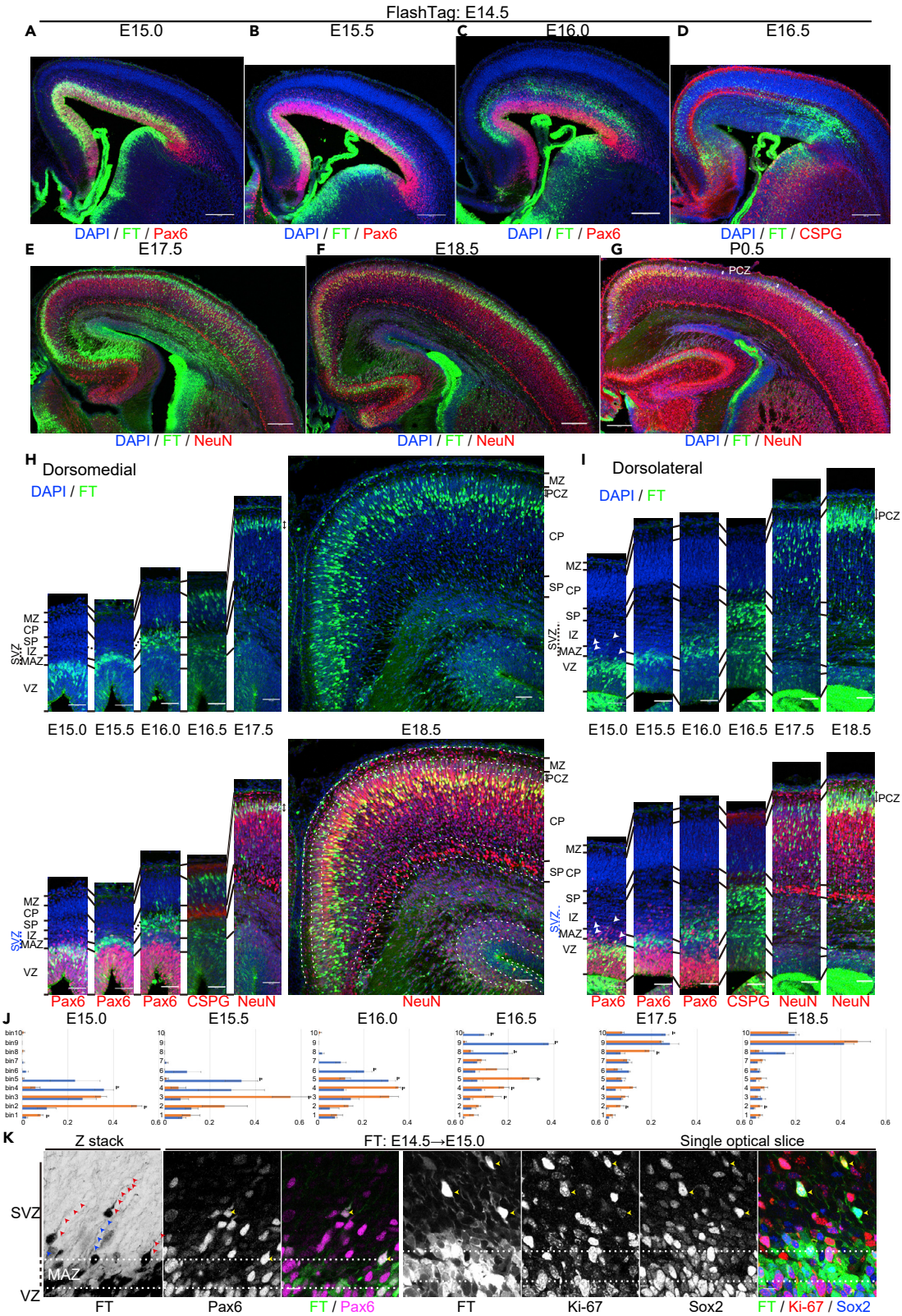
FlashTag: E14.5
A
E15.0
B
E15.5
C
E16.0
D
E16.5
DAPI / FT / Pax6
DAPI / FT / Pax6
DAPI / FT / Pax6
DAPI / FT / CSPG
E
E17.5
F
E18.5
G
P0.5
PCZ
DAPI / FT / NeuN
DAPI / FT / NeuN
DAPI / FT / NeuN
H
Dorsomedial
DAPI / FT
MZ
CP
SP
IZ
SVZ
MAZ
VZ
E15.0 E15.5 E16.0 E16.5 E17.5
E18.5
I
Dorsolateral
DAPI / FT
IPCZ
E15.0 E15.5 E16.0 E16.5 E17.5 E18.5
Pax6 Pax6 Pax6 CSPG NeuN
NeuN
Pax6 Pax6 Pax6 CSPG NeuN NeuN
J
E15.0
E15.5
E16.0
E16.5
E17.5
E18.5
K
Z stack
FT: E14.5→E15.0
Single optical slice
SVZ
MAZ
VZ
FT
Pax6
FT / Pax6
FT
Ki-67
Sox2
FT / Ki-67 / Sox2

Figure 6. Cohort of cells born at E14.5

(A–K) Coronal sections of E15.0 (A), 15.5 (B), 16.0 (C), 16.5 (D), 17.5 (E), 18.5 (F), and P0.5 (G) brains, all labeled at E14.5. Higher-magnification micrographs from the dorsomedial and dorsolateral cortices are shown in (H) and (I), respectively. Quantitative data of migratory profiles of the dorsolateral and dorsomedial cortices are shown in (J). Higher magnification of the apical part of the dorsolateral cortical wall of E15.0 (0.5 days after injection) brains is shown in (K). At E15.0, most of the labeled cells are in the VZ in both the dorsomedial and dorsolateral cortices (A, H, and I). Some labeled cells are located outside the VZ in the dorsolateral cortex (A, I, and K), but such cells are not frequently found in the dorsomedial cortex (A, H). The labeled cells located basally often have a long ascending process (red arrowheads, K, left) as well as some retraction bulbs (blue arrowheads) and are immunoreactive for Pax6, Sox2, and Ki-67 (yellow arrowheads, K, right). Note that the ascending processes are so long that it is difficult to observe their full length in the IZ crowded with radial fibers, which are also labeled with FT. At E15.5, most of the labeled neurons are in the MAZ with multipolar morphology in both the dorsomedial and dorsolateral cortices (B, H, and I). At E16.0, most of the labeled cells are in the IZ (C, H, and I). At E16.5 in the dorsomedial cortex, many cells reach the most superficial part of the CP (D, H). On the other hand, in the dorsolateral CP, most of the labeled cells migrate in the IZ just beneath the SP (D, I; see also Figures 2A and 2C). At E17.5, the vast majority of the labeled cells in the dorsomedial cortex are in the PCZ, which is the most superficial part of the CP (E, H). In the dorsolateral cortex, most of the labeled cells continue migrating in the CP (E, I). At E18.5, the labeled cells in the dorsomedial cortex are distributed not only in the PCZ but also in the slightly deeper part of the CP as NeuN-positive mature neurons (F, H). In the dorsolateral cortex, most of the labeled cells are in the PCZ (F, I). At P0.5, in the dorsolateral cortex, many labeled cells are distributed in the slightly deeper part of the CP as NeuN-positive mature neurons (G). Small double-headed arrows show the PCZ. A bin analysis was performed for these migration profiles by dividing the cortical wall between the top of the MZ and the ventricular surface into 10 equal areas (10 bins), and the proportion of FT-labeled cells in each bin was calculated from three or more different brains (J) (E15.0, $n = 4$ brains; E15.5, $n = 3$; E15.5, $n = 3$; E16.6, $n = 4$; E17.5, $n = 3$; E18.5, $n = 3$). *$p < 0.05$ (t test). Data are presented as mean ± SEM. At earlier stages, such as E15.0, cellular positions in the dorsomedial cortex are biased superficially because the dorsomedial cortex is thinner (Figure S8J).
Scale bars: 200 μm in (A–G), 50 μm in (H, I), and 10 μm in (K). See also Figures S6–S11.

Note that the cortical thickness increases as development proceeds (Figure S8J). FT-labeled dorsomedial neurons reached the superficial part of the cortex (bin8–10) at E16.5. At this stage, many labeled neurons in the dorsolateral cortex were still below bin 6, reflecting sojourning below the dorsolateral SP. They eventually migrated into the CP and settled in the most superficial part of the cortex at E17.5–18.5. We also calculated the proportion of FT-labeled cells in the CP at E16.5, when the mediolateral migratory difference was apparent. Significantly more neurons were in the CP in the dorsomedial cortex compared with the dorsolateral cortex (paired t test, $p = 0.0043$, $n = 3$ brains). These quantitative analyses supported the observation of regional differences in neuronal migration.

E15.5 cohort

Half a day after injection, at E16.0, many of the labeled cells were in the VZ (Figures S9A, S10A, and S11A). We also observed some cells outside the VZ (Figures S9A and S11A, arrowheads), which were often positive for Pax6, as in the E14.5 cohort. Around the pallial-subpallial boundaries (PSB) were scattered a small number of cells with single long ascending processes with various orientations (Figure S11B; similar cells were observed in the E17.0 cohort and analyzed in detail).

One day after injection, at E16.5, most of the labeled cells had accumulated in the MAZ both in the dorsomedial and dorsolateral cortex (Figures S9B, S10A, and S11A). At 1.5 days after injection, at E17.0, some labeled cells had entered the IZ, which is rich in L1-positive axons including thalamocortical and corticofugal axons (Fukuda et al., 1997; Kudo et al., 2005; Yoshinaga et al., 2012), both in the dorsomedial and dorsolateral cortex (Figures S9C, S10A, and S11A). Two days after injection, at E17.5, most of the labeled cells had migrated in the superficial and deep part of the IZ in the dorsomedial cortex (Figures S9D and S10A), but in the dorsolateral cortex, migrating cells were mainly located in the deep part of the IZ (Figures S9D and S11B).

Three days after injection, at E18.5, most of the labeled cells were in the PCZ in the dorsomedial cortex (Figures S9E and S10A). On the other hand, in the dorsolateral cortex, only a small population of labeled cells had reached the PCZ, and others were still migrating in the CP and SP with a locomotion morphology (Figures S9E and S11A). In the dorsolateral cortex, one additional day was required for most to reach the PCZ, at P0.5 (Figures S9F and S11A).

At P1.5, cells labeled at E15.5 had settled in the GM both in the dorsomedial and dorsolateral cortices (Figures S9G, S10A, and S11A). In the dorsolateral cortex, some of these labeled cells had shifted to slightly deeper positions, thereby leaving the top of the CP, which was not prominently observed in the dorsomedial cortex (Figures S9G, S10A, and S11A).

These observations suggest mediolateral differences in migratory profiles in the E15.5 cohort, similar to those observed for the E13.5 and E14.5 cohorts.

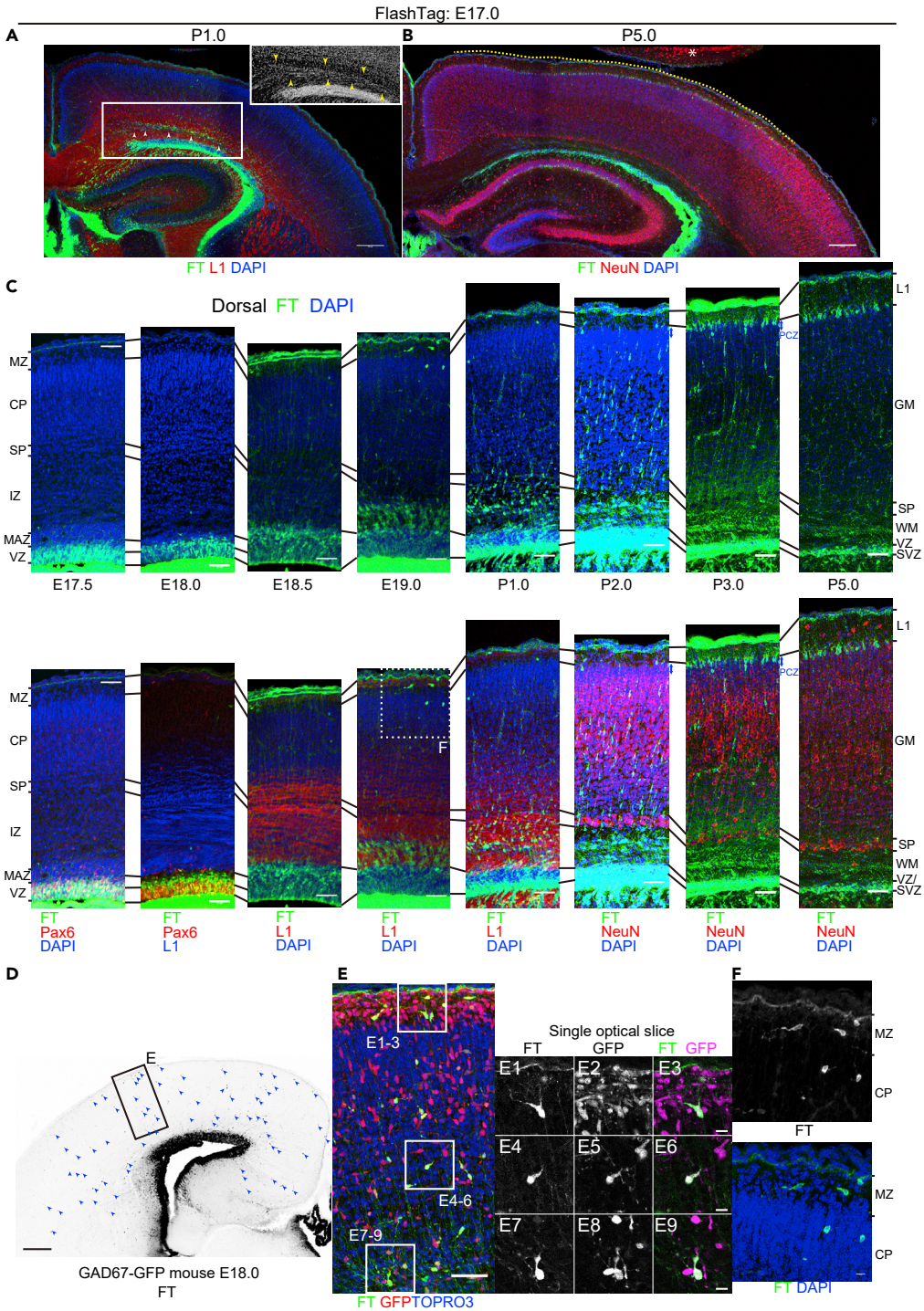

Figure 7. Cohort of cells labeled at E17.0

(A–C) Coronal sections of P1.0 (A) and P5.0 (B) brains labeled at E17.0. See also Figure S12 for lower-magnification micrographs of E17.5 through P5. Higher-magnification images of E17.5 through P5 from the dorsal cortex are shown in (C). At E17.5, most of the labeled cells are in the VZ (C). At E18.0, most of the labeled cells are in the VZ and MAZ (C). A small number of labeled cells are also found throughout the cortex sparsely (D). At E18.5, many labeled cells are found in the MAZ (C). Some labeled cells are sparsely distributed throughout the cortex. At E19.0, many cells enter the L1-positive IZ dorsally (C). A small number of cells are also found in the MZ and CP (F). At P1.0, many labeled cells are migrating in the IZ/white matter (WM) (A, C). Migrating cells form a slightly denser cellular structure (inset in A) sandwiched between

Figure 7. *Continued*

L1-positive axon bundles (arrowheads in A). At P2.0, many neurons are migrating in the CP/cortical gray matter (GM) with a locomotion morphology (C). At P3.0, many labeled cells reach the dorsal PCZ (C). At P5.0, most of the labeled cells are in the most superficial part of the GM (B, C). Note that many cells are in the dorsal (and dorsolateral) cortex (yellow dotted line), and few cells are in the dorsomedial and lateral cortices.

(D–F) Analyses of GABAergic interneurons. Cells labeled with FT (CytoTell Blue) at E17.0 are sparsely distributed throughout the cortex at E18.0 (D, E), and they are mostly positive for GFP in *GAD67-GFP* mice (E). Labeled cells with similar morphologies are found in the MZ/Layer I and in the CP at E19.0 before the main population of labeled cells reaches the CP (F). Scale bars: 200 μm in (A, B, and D), 50 μm in (C, E), and 10 μm in (E3, E6, E9, F). * indicates another brain on the same slide.

E17.0 cohort

Half a day after injection, at E17.5, labeled cells were seen mainly in the VZ (Figures 7C and S12A). One to 1.5 days after injection, at E18.0–18.5, the main population of labeled cells had migrated out of the VZ into the MAZ (Figures 7C, 7D, S12B, and S12C). They entered the IZ 2 days after injection, at E19.0 (Figures 7C and S12D). In the dorsal part of the IZ/white matter (WM) at P1.0, we observed a band-like zone where cellular density was somewhat greater than in the deeper and more superficial parts of the IZ/WM (Figure 7A, inset). This slightly denser cellular zone in the IZ/WM was sandwiched by L1-positive axon bundles that were skewed. At this time point, some of the labeled cells were found in this cellular zone in the dorsal part of the IZ/WM (Figure 7A). We also observed a small number of labeled cells with single leading processes extending medially (Figures 7A and S12J). Most of the labeled cells at this stage were positive for the neuronal marker Hu (Figures S12J2–6). As late as P2.0, or 4 days after injection, labeled neurons began to migrate in the CP/GM with a bipolar morphology (Figures 7C and S12F). Approximately 5 or more days after injection, or later than P3.0, labeled cells settled in the PCZ, or the top of the GM, of the dorsal cortex (Figures 7C, S12G, and S12H). These cells had a pyramidal morphology and became positive for NeuN by P5.0 (Figure S12I), suggesting that they were indeed mature neurons.

Collectively, labeled cells were mainly distributed dorsally, and only a few cells settled in the dorsomedial and lateral cortex. We did not observe clear sojourning just below the dorsal and dorsolateral SP as in the E13.5–15.5 cohort, but the appearance of a slightly dense zone consisting of migrating neurons may suggest sojourning and/or deceleration in the midst of migration in the IZ/WM. Axon bundles just above this zone may contain axons from the SP (Figures 7A and S12E, positive for Nurr1 and Cplx3).

Half a day after injection, at E17.5, some strongly labeled cells with long ascending processes were scattered around the PSB (Figure S12A), as with the E15.5 cohort (Figure S11B). As early as 1 day after injection, at E18.0, these cells were distributed throughout the cortex (Figures 7D and S12B). This population was mostly negative for the radial glial marker Pax6 (Figures 7C, S12A, and S12B), the glial lineage markers Gfap, Sox10 (Stolt et al., 2002; Zhou et al., 2000), and Olig2 (Tatsumi et al., 2018) (except for the ventromedial cortex) (data not shown). However, they were positive for GFP in *GAD67-GFP* mice (Figure 7E), suggesting that they were GABAergic interneurons. Some of these cells were positive for the caudal ganglionic eminence -derived interneuron markers *Htr3a* (Murthy et al., 2014) and Couptf2 (Kanatani et al., 2008, 2015), whereas others were negative, suggesting that they constitute a heterogeneous population. In addition, a few were positive for bromodeoxyuridine (BrdU) administered at E13.5, suggesting that at least some of these cells underwent final mitosis days before E17.0. These observations raise the possibility that the FT-labeled interneurons that leave the VZ earlier than the main population of FT-labeled cells are not labeled with FT at mitosis but are labeled after they become postmitotic. Labeled cells with similar morphologies were found in the MZ/Layer I and CP before the main population of the labeled cells reached the CP (Figures 7F and S12C–S12E).

We present schematic migratory profiles of the main population labeled with FT at different embryonic days in Figures 9A, 9B, and 9F.

Mechanisms of regional differences in neuronal migration

Finally, we sought to gain insight into the mechanisms of regional differences in neuronal migration. We focused on sojourning just below the SP in the E14.5 cohort. Based on our observations in Figure 2, we hypothesized that SP neurons or other structures in the SP transiently decelerate the migration of later-born neurons in the dorsolateral cortex (Figure 9C). First, to see if the SP neurons regulate the migration of neurons born at E14.5, we used *reeler* mice, in which SP neurons that are normally positioned below the CP are

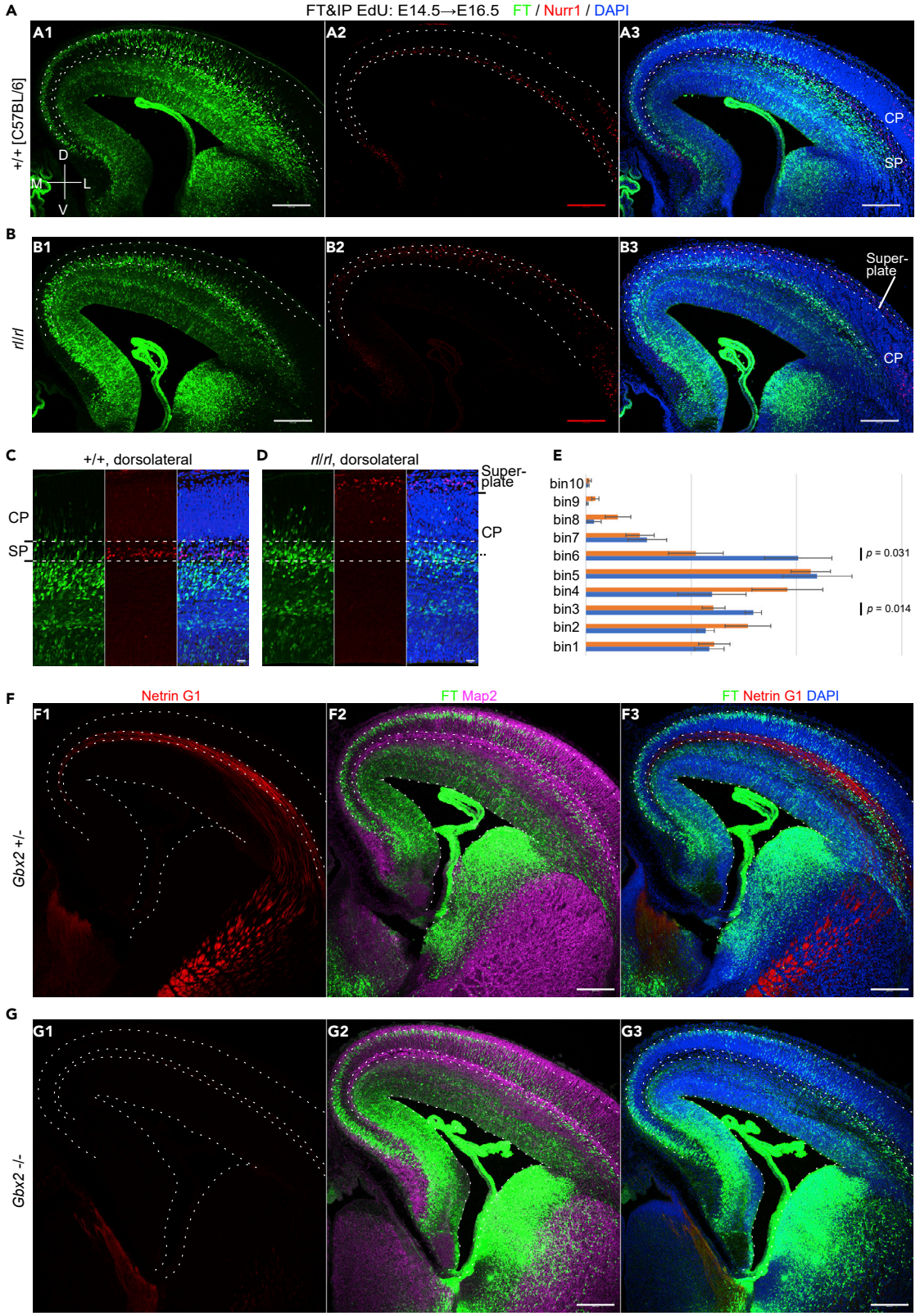
A
FT&IP EdU: E14.5→E16.5 FT / Nurr1 / DAPI
A1
A2
A3
+/+ [C57BL/6]
D
M
L
V
CP
SP
B
B1
B2
B3
rl/rl
Super-plate
CP
C
+/+, dorsolateral
CP
SP
D
rl/rl, dorsolateral
Super-plate
CP
E
bin10
bin9
bin8
bin7
bin6
bin5
bin4
bin3
bin2
bin1
p = 0.031
p = 0.014
F
Netrin G1
FT Map2
FT Netrin G1 DAPI
F1
F2
F3
Gbx2 +/-
G
G1
G2
G3
Gbx2 -/-

Figure 8. Regional differences in neuronal migration in *reeler* mutants and *Gbx2* −/− mice

(A–E) In wild-type brains, Nurr1+ cells are observed in the SP (A), whereas in *reeler* mice, Nurr1+ cells are mostly observed in the superplate or beneath the meninges (B). FT was performed at E14.5, and the brains were fixed at E16.5. In contrast to wild-type mice, which clearly show regional differences in neuronal migration (A), regional differences are not clear in *reeler* mice (B). The main population of labeled cells in the dorsolateral cortex is observed below the SP in the controls (C). In *reeler* mice, many neurons migrate in a zone that roughly corresponds to the deep part of the CP where SP neurons should normally position (D). Quantitatively, we observed more labeled neurons in bin 6 (E) of *reeler* mice (*rl*/*rl*: 20.2% ± 3.2%, 10 brains; control: 10.5% ± 2.6%, 8 brains [3 +/+ brains and 5 *rl*/+ brains] from 4 mother mice; $p = 0.031$, *t* test). Bins other than bin 6 and bin 3 ($p = 0.014$) did not reach statistical significance ($p > 0.05$). The sample numbers in the statistical analyses are the number of brains.

(F and G) In *Gbx2* +/− brain, Netrin G1-positive thalamocortical axons run through the SP (F1). In *Gbx2* −/− brain, Netrin G1-positive thalamocortical axons are almost absent in the cortex (F2). In both cases, many neurons are observed just beneath the SP. FT labeling was performed at E14.5, and the brains were fixed 50 h later. Coronal sections slightly caudal to the main part of the interventricular foramina are shown to confirm Netrin G1 immunoreactivity in the dorsal thalamus of *Gbx2* −/− brains, where cortical Netrin G1 immunoreactivity was almost absent (positive control of Netrin G1 staining). M, medial; L, lateral; D, dorsal; V, ventral. Scale bars: 200 μm in (A, B, F, G) and 50 μm in (C, D).

See also Figures S13. Data are presented as mean ± SEM.

mispositioned above the CP, as revealed by Nurr1 staining (Figures 8A–8D) (Hoerder-Suabedissen et al., 2009; Ozair et al., 2018; Pedraza et al., 2014). FT labeling was performed at E14.5, and the brains were harvested at E16.5. Compared with wild-type, the mediolateral migratory differences were less clear in *reeler* mice (Figures 8A and 8B). In *reeler* mice, after neurons enter the CP, they often stop along the internal plexiform zone (Tabata and Nakajima, 2002). We believe that this resulted in the deceleration of the migration of dorsomedial neurons. In fact, we observed that FT-labeled cells tended to position along the internal plexiform zone in the dorsomedial cortex (Figure S13A). To evaluate the regulatory functions of the dorsolateral SP neurons on the profiles of migrating neurons, we examined whether there was earlier entry of migrating neurons into the CP in *reeler* mice in the dorsolateral cortex. We performed a bin analysis of dorsolateral migrating neurons of E16.5 *reeler* and control mice in which FT was applied at E14.5. In *reeler* mice, we observed more labeled neurons in bin 6 (Figure 8E), which roughly corresponds to the deep part of the CP of the *reeler* mice and the SP of the control mice (Figures 8C and 8D), suggesting that the absence of SP cells beneath the CP in *reeler* mice caused the earlier entry of migrating neurons into the CP (Figures 8B, 8D, and 9D).

Thalamocortical axons run to the SP at this stage (Figure 8F1). To determine whether the thalamocortical axons (Bicknese et al., 1994; Molnár et al., 1998) regulate neuronal migration, we used a Crispr-Cas9-based improved genome editing via oviductal nucleic acids delivery (i-GONAD) (Gurumurthy et al., 2019; Ohtsuka et al., 2018; Takabayashi et al., 2018) to generate *Gbx2* knockout mice (Figures S13B and S13C), which lack thalamocortical axons (Hevner et al., 2002; Miyashita-Lin et al., 1999). *Gbx2* knockout mice provide a great opportunity to study the role of thalamocortical axons in the regulation of cortical neuron migration, because *Gbx2* is expressed in the dorsal thalamus but not in the cortex (Miyashita-Lin et al., 1999). As expected, immunoreactivity against the thalamocortical axon marker Netrin G1 (Nakashiba et al., 2002; Vue et al., 2013) was almost absent in the homozygous mice (Figure 8G1). In these mice, we performed FT labeling at E14.5 and harvested 50 h later. FT-labeled migrating neurons showed a migration profile almost identical to that of the control brains (Figures 8F, 8G, and 9E), suggesting that thalamocortical axons are not likely to regulate neuronal migration around the SP.

Taken together, these observations are compatible with the notion that the SP neurons or some other structures in the SP transiently decelerate the migration of later-born neurons in the dorsolateral cortex, although further analyses of other structures in the SP are warranted, as well as of cell-autonomous regulation of neuronal migration, which differs among cortical regions. Further direct observations, including those in brains in which SP cells are specifically and efficiently ablated, are required to draw a conclusion.

DISCUSSION

Using FT technology, we demonstrated clear regional differences in neuronal migration in the pallium, even where there is an underlying VZ. The regional differences were dependent on the embryonic stages when the apical radial glial cells divide at the ventricular surface to produce neuronal progenitors and neurons. In the E10.5 and E11.5 cohorts, regional differences in neuronal migration, defined in the current study as movement from mitosis at the ventricular surface to settlement just beneath the meningeal surface, were not clear. In the E12.5 cohort, we described slight regional differences. In the E13.5, E14.5, and E15.5 cohorts, neurons in the dorsomedial cortex reached the top of the CP about 1 day earlier than those in the dorsolateral cortex. In the E17.0 cohort, we observed that labeled neurons were positioned nearly dorsally. We also observed migratory

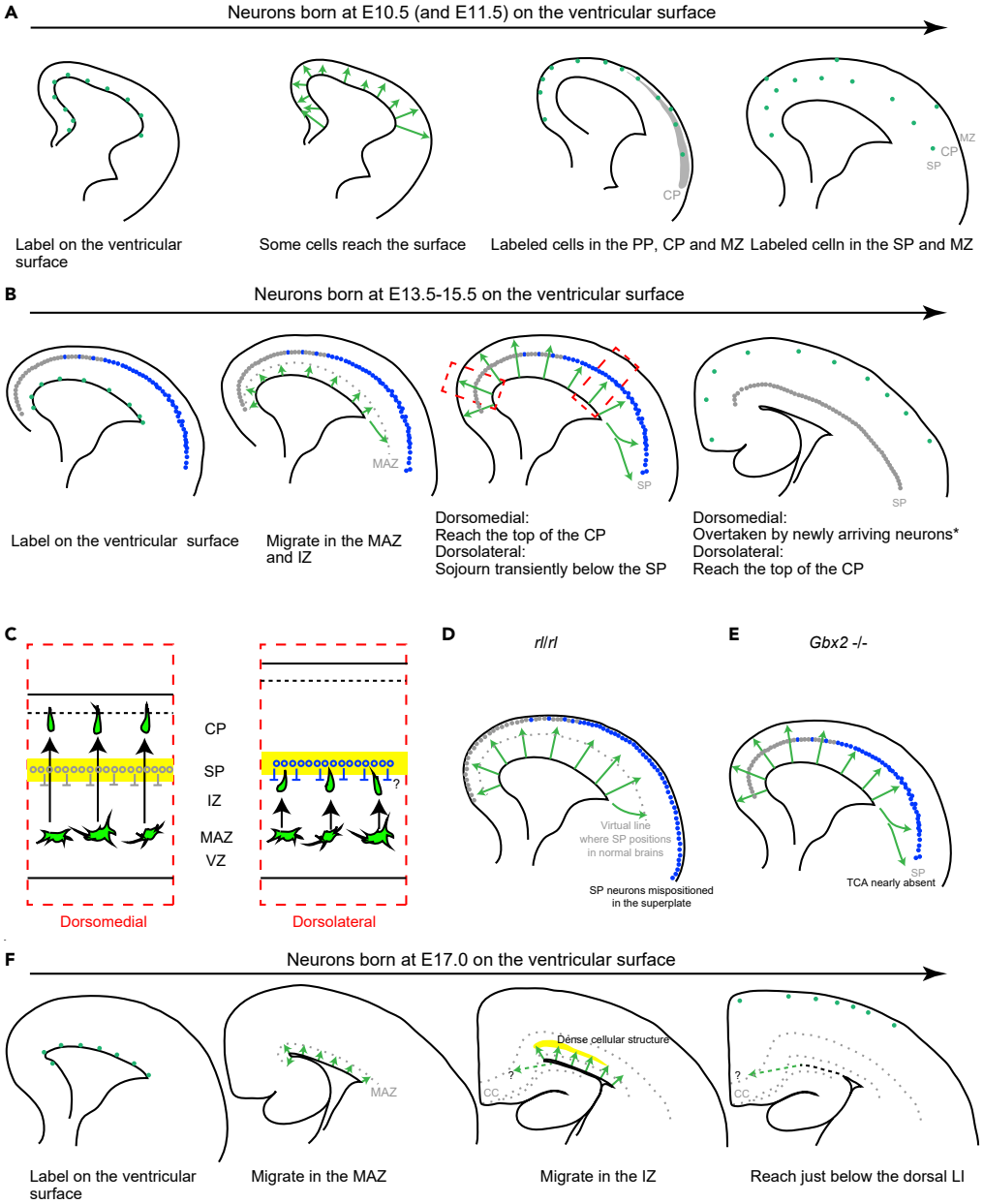

Figure 9. Schematic representation of migratory profiles of the main population labeled at different embryonic stages

(A) Cells labeled at very early stages (E10.5–E11.5) enter the PP soon after they leave the VZ. They next position in the incipient CP and MZ. They then move down their somata deeply to locate below the CP, or in the SP, in a lateral-early to medial-late fashion. At these stages, Cajal-Retzius cells are also labeled.

(B) Cells labeled at early to late stages (E13.5–E15.5) enter and accumulate in the MAZ. Neurons labeled at E14.5, for example, migrate in the IZ superficially and reach the CP early in the dorsomedial cortex. In the dorsolateral cortex, they sojourn transiently below the SP before entering the CP. After reaching the PCZ, labeled neurons are overtaken by newly arriving neurons. This is not clear in the dorsomedial neurons labeled at E15.5 (Figure S10A), probably because few neurons labeled later distribute in this region (Figure 7B, *).

(C) A hypothetical mechanism of regional differences in neuronal migration at these stages. The SP neurons (or some other structures in the SP) transiently decelerate the migration of neurons in the dorsolateral cortex.

(D) Migratory profiles in *reeler* brains labeled at E14.5; the SP neurons are mispositioned above the CP as superplate neurons.

Figure 9. *Continued*

(E) Migratory profiles in *Gbx2* −/− brains labeled at E14.5. The thalamocortical axons are almost absent in the cortex of *Gbx2* −/− brains.

(F) Cells labeled at very late stages (E17.0) migrate slowly through the MAZ and a dense cellular structure in the dorsal IZ or WM. Most of the labeled cells settle in the most superficial part of the dorsal GM.

behavior in a subpopulation of the labeled cells, for example, in mitotically active Pax6-positive cells that leave the VZ as early as 0.5 days after labeling in the E14.5 cohort (Figures 6A, 6I, 6K, and S8A). These comprehensive descriptions provide basic information about cortical development.

How are the regional differences formed? Time-lapse imaging suggested that cells labeled at E14.5 in the dorsolateral cortex stop transiently below the SP, whereas those in the dorsomedial cortex do not (Figure 2D). It is known that SP neurons interact with later-born neurons (Ohtaka-Maruyama et al., 2018). In *reeler* mice, we observed that more migrating neurons had already entered a zone where SP cells would normally be located in wild-type mice when most of the migrating neurons in wild-type control brains were still migrating below the SP (Figures 8B, 8D, and 8E). These observations are compatible with the idea that SP cells transiently decelerate the migration of later-born neurons as part of normal migration. In addition to the SP neurons and thalamocortical axons, there are many other structures potentially relevant to the migratory difference: corticofugal axons (Denaxa et al., 2001), catecholaminergic axons (Lidov and Molliver, 1982), and radial-fiber bending (Mission et al., 1991; Saito et al., 2019) and branching (Takahashi et al., 1990) around the SP. In addition, we cannot exclude the possibility that cell-intrinsic mechanisms in migratory neurons are also involved. Further research, including *in vivo* transplantation and specific ablation of anatomical structures, would be needed to obtain mechanistic insights.

What is the physiological role of regional differences in migratory profiles? This regional difference in migratory profiles of the E14.5 cohort was clearly visualized with FT but less clearly with thymidine analogs, a standard approach to the study of neurogenic gradients. We thus think that our findings have a biological significance different from the neurogenic gradient. Migrating neurons receive synaptic contacts from the SP neurons when they pass the SP (Ohtaka-Maruyama et al., 2018). At the same stage, thalamocortical fibers wait in the SP (Lopez-Bendito and Molnar, 2003). Thus, if migrating neurons slow down beneath the dorsolateral SP, they have a greater chance of interacting with the SP and/or thalamic afferents. Along the developmental time axis, the regional difference in neuronal migration, including sojourning beneath the SP, was clear in cohorts that contained future layer IV neurons. Histologically, the dorsomedial cortex, where labeled cells did not clearly sojourn beneath the SP, is agranular and lacks a layer IV. The dorsolateral cortex, where cells sojourn just beneath the SP, corresponds to primary somatosensory areas, where layer IV neurons are predominant. These observations suggest that sojourning beneath the SP might be implicated in thalamocortical circuit formation and/or layer IV formation. In line with this, the role of the extracellular environment is estimated to be increasingly important in refining neuronal identity as they migrate and differentiate, especially in the E14-labeled future layer IV neurons (Telley et al., 2019). In addition, abnormal migration and positioning of neurons labeled at E14.0 using *in utero* electroporation (mainly future layer IV neurons) results in abnormal differentiation (Oishi et al., 2016a, 2016b).

PP splitting involves the establishment of the CP within the PP (Goffinet and Lyon, 1979; Marin-Padilla, 1971). It has been assumed that the cells in the earliest CP are future layer VI cells and that their active reorganization drives PP splitting (Nichols and Olson, 2010; Olson, 2014). However, it is also possible that some future SP neurons actively migrate away. In the present study, in the earliest cohorts, labeled cells were first observed in the PP and then in the CP and MZ upon the formation of the CP; finally, they moved down below the CP, supporting the downward movement of some SP neurons through the CP. This observation is compatible with previous descriptions using time-lapse imaging or *in vivo* observations in which future SP neurons are labeled with *in utero* electroporation (Saito et al., 2019), genetically (*Lrp12/Mig13a-EGFP* mice) (Schneider et al., 2011) and immunohistochemically (Hpca+/Reelin- and Eaac1+/Reelin-) (Osheroff and Hatten, 2009). Historical studies using ^{3}H-TdR in cats (Luskin and Shatz, 1985) described future SP neurons transiently locating in the deep part of the histologically defined CP (Boulder-Committee, 1970) although Luskin and Shatz assumed that this is part of the SP. Bayer and Altman (1991) analyzed rats using ^{3}H-TdR and suggested that the SP neurons temporarily reside in the CP. These observations suggest that at least some neurons in the earliest CP and MZ are future SP neurons. As FT might label only a subpopulation of cells in our study, we do not exclude the possibility that some earliest-born neurons form a distinct cell layer below the CP before or immediately after the CP forms.

Neurons labeled at E17.0 are mainly distributed dorsally and relatively rarely medially or laterally (Figure 7B). However, a small number of cells labeled at E17.0 were observed at E18–19 in the dorsomedial cortex as well (Figure S12J). Some might migrate to the subiculum and hippocampus; others might fan out sparsely in the cingulate and secondary motor cortices. Another possibility is that they divide abventricularly to lose fluorescence. Around this stage, gliogenesis accelerates, but it has been shown that there are many Hopx-positive neurogenic moRG in the medial cortex at this stage (Vaid et al., 2018). Another possibility is that they undergo programmed cell death. The fate of the majority of the dorsomedial E17.0 cohort remains to be determined.

Interneurons are born in the ganglionic eminences and the preoptic area. Ventral progenitors were also labeled with FT, but FT-labeled neurons rarely entered the cortex. This can be explained by frequent abventricular division in the ventral forebrain (Katayama et al., 2013; Tan et al., 2016; Tan and Shi, 2013) (Figures S1D and S1E). However, a small number of cortical GABAergic interneurons were labeled on E17 (Figures 7D and 7E) and presumably on E15.5 (Figure S11B), which distributed into the cortex within a day. One interpretation for this retaining of the label in interneurons in the E15.5 and E17 cohorts is that FT potentially labels a certain subpopulation that undergoes final mitosis relatively late for interneurons at the ventricular surface. Another interpretation is the labeling of migrating interneurons that undergo final mitosis earlier than dye injection. Ventricle-directed migration of interneurons, some of which touch the ventricular surface, was described from E13 in mice and E15 in rats (Nadarajah et al., 2002). If some of the migrating interneurons had touched the ventricular surface and been labeled with FT, FT-labeled interneurons should have been observed in our earlier cohort as well. In our E14.5 cohort, we observed some cells with long ascending processes that left the VZ earlier than the main population (Figures 6I and 6K). However, they were mostly positive for Pax6, a dorsal progenitor marker, suggesting that they are a different population. The origin of these interneurons labeled with FT on E15.5 and E17 remains to be determined.

In the E14.5–15.5 cohorts, we observed cells that had left the VZ within 0.5 days, mainly in the dorsolateral cortex. These cells have the distribution, migratory behavior, cycling features, and morphology of the REP earlier visualized by *in utero* electroporation and subsequent BrdU incorporation (Tabata et al., 2009). Many of these cells were positive for the radial glial markers Pax6 and Sox2 (Figure 6K), supporting the view that moRG cells comprise a subpopulation of the REP (Tabata et al., 2012). In the earlier cohort (labeled at E12.5, Figures 5G, S5G, and S5H), we also observed a similar Pax6-positive population that left the VZ early. This population, however, did not share the lateral-more to the medial-less gradient of distribution of the REP that we previously reported. In the early stages of corticogenesis, when the CP is not yet formed, migrating neurons show multipolar morphology (Hatanaka et al., 2004; Tabata and Nakajima, 2003) but they do not accumulate just above the VZ to form a clear MAZ. Because the accumulated multipolar cells were shown to serve as a fence to limit the apical border of the range of interkinetic nuclear migration (Watanabe et al., 2018), these Pax6-positive cells in our E12.5 cohort that leave the VZ soon and distribute sparsely may result from the presence of an inefficient fence limiting the apical border of the VZ. Conversely, we suppose that the REP and the moRG in later cohorts (E14.5 and 15.5) may have an active mechanism for passing the MAZ/SVZ.

The application of FT to visualize neuronal migration has several strengths over conventional methods. First, FT has the potential to detect differences in neuronal migration that cannot be detected by thymidine analogs. Second, this method enables the visualization of neuronal migration in the whole brain. This feature especially compliments the whole-brain 3D approach, including FAST (Seiriki et al., 2017, 2019). Third, the methodology is simple, and FT can be a versatile approach to study neuronal migration in the whole brain in healthy and disease model mice. On the other hand, FT has several technical limitations. First, tangential migration of projection neurons (e.g., lateral dispersion of the rostromedial telencephalic wall-derived future SP neurons [Pedraza et al., 2014], ventral streaming of pallial-derived, early embryonic PP neurons [Saito et al., 2019], and abnormal tangential migration of projection neurons [Pinheiro et al., 2011]) could not be efficiently visualized because FT labels mitotic cells on the ventricular surface throughout the brain. Second, the migration profile might be biased toward the slowly exiting population (Tabata et al., 2009) or the direct progeny of apical progenitors, because the fluorescence of the secondary proliferative population would decrease upon mitosis.

In summary, we applied FT to describe neuronal migration and described the migratory profiles of early- and late-born projection neurons in normal mouse cortical development. The labeling features of FT shed

light on hitherto overlooked regional differences in neuronal migration profiles. This versatile approach would be useful in studying neuronal migration in disease models and transgenic animals.

Limitations of the study

The results of the FT experiments must be interpreted considering the following limitations. First, the mediolateral migratory difference is arguably not a true regional difference, but a simple reflection of the cortex being thinner medially. However, this is unlikely because the regional difference was preserved in the posterior cortex, where the thickness of the cortical wall is equivalent in the dorsomedial and dorsolateral cortices (Figure 2E, Video S1). Second, we measured developmental stages using embryonic days, but developmental stages are confounded with neurogenic gradients, which differ about 1 day mediolaterally (Takahashi et al., 1999). This point is especially important in discussing the regional differences in neuronal migration we observed in the E13.5 cohort. Cells labeled at E13.5 reached points just beneath the meningeal surface at approximately E14.5–15.0 in the dorsomedial cortex, upon formation of the CP (Figures S6B, S6C, and S7A). At this stage, somal translocation was previously observed (Nadarajah et al., 2001). It has also been reported that multipolar cells do not transform into bipolar locomotion cells before the CP forms (Hatanaka et al., 2004). In the dorsolateral cortex at this stage, in contrast, the CP structure is already formed, and labeled neurons need to transform from a multipolar migration mode to a bipolar locomotion mode (Figures S6B–S6D, and S7B). One may reason that this difference in migratory modes determines the mediolateral differences in neuronal migration profiles. However, this is unlikely because the mediolateral regional difference was also observed in the E14.5 and 15.5 cohorts when the dorsomedial CP is well developed.

Resource availability

Lead contact

Further information and requests for resources and reagents should be directed to and will be fulfilled by the Lead Contact, Kazunori Nakajima (kazunori@keio.jp).

Materials availability

This study did not generate new unique reagents. We did not deposit the *Gbx2* knockout mice generated in the present study, because they were designed based on a mouse line *Gbx2*^{tm1Mrt} (MGI:3665450) used in a previous study (Wassarman et al., 1997). Requests for the mice should be directed to the lead contact.

Data and code availability

This study did not generate/analyze datasets or code.

METHODS

All methods can be found in the accompanying Transparent Methods supplemental file.

SUPPLEMENTAL INFORMATION

Supplemental information can be found online at https://doi.org/10.1016/j.isci.2021.102277.

ACKNOWLEDGMENTS

This work was supported by Grants-in-Aid for Scientific Research of the Ministry of Education, Culture, Sports, Science, and Technology (MEXT), Japan/Japan Society for the Promotion of Science, Japan, Grants-in-Aid for Scientific Research (KAKENHI) (JP17J05365, JP18K19379, JP19H05227, JP18K07855, JP19H01152, JP19K08306, JP20H03649, JP20H05688, JP16H06482, JP20K21467, JP20H00492, JP19H05217, JP18H05416), the Keio Gijuku Academic Development Funds, Keio Gijuku Fukuzawa Memorial Fund for the Advancement of Education and Research, Takeda Science Foundation, and, AMED, Japan (JP20dm0207061), and PRIME, AMED, Japan (JP19gm6310004, JP20gm6310004). S.Y. was a Research Fellow of Japan Society for the Promotion of Science from fiscal year (FY) 2017 to FY 2019.

We thank Drs. Ludovic Telley and Denis Jabaudon (University of Geneva) for technical advice and valuable discussions. We also thank Core Instrumentation Facility, Collaborative Research Resources, Keio University School of Medicine, Dr. Yoshifumi Takatsume, and distinguished technicians including Emiko Shimeno, Miki Sakota, Noriko Suzuki, Chisa Konno, and Maiko Saito for technical assistance. Greatest gratitude is

expressed to all the members of Nakajima laboratory for the valuable advice, expertise, and encouragement.

AUTHOR CONTRIBUTION

Conceptualization, S.Y., K.K., and K.N.; Methodology, S.Y. M.T., A. Kasai., and H.H.; Investigation, S.Y., M.K., A. Kitazawa, K.I., and M.T.; Writing – Original Draft, S.Y.; Writing – Review & Editing, K.K. and K.N.; Visualization, S.Y., M.T., and A. Kasai; Supervision, K.-i.K. and K.N.; Funding Acquisition, S.Y., A. Kasai, H.H., K.-i.K., and K.N.

DECLARATION OF INTERESTS

The authors declare no competing interests.

Received: August 24, 2020
Revised: December 30, 2020
Accepted: March 1, 2021
Published: April 23, 2021

REFERENCES

Anderson, S.A., Eisenstat, D.D., Shi, L., and Rubenstein, J.L. (1997). Interneuron migration from basal forebrain to neocortex: dependence on Dlx genes. Science *278*, 474–476.

Angevine, J.B., Jr., and Sidman, R.L. (1961). Autoradiographic study of cell migration during histogenesis of cerebral cortex in the mouse. Nature *192*, 766–768.

Arlotta, P., Molyneaux, B.J., Chen, J., Inoue, J., Kominami, R., and Macklis, J.D. (2005). Neuronal subtype-specific genes that control corticospinal motor neuron development in vivo. Neuron *45*, 207–221.

Bayer, S.A., and Altman, J. (1991). Neocortical Development (Raven Press).

Bicknese, A.R., Sheppard, A.M., Leary, D.D., and Pearlman, A.L. (1994). Thalamocortical axons extend along a chondroitin sulfate proteoglycan-enriched pathway coincident with the neocortical subplate and distinct from the efferent path. J. Neurosci. *14*, 3500–3510.

Boulder-Committee (1970). Embryonic vertebrate central nervous system: revised terminology. The Boulder Committee. Anat. Rec. *166*, 257–261.

Brodmann, K. (1909). Vergleichende Lokalisationslehre der Großhirnrinde : in ihren Prinzipien dargestellt auf Grund des Zellenbaues (J.A. Barth).

Bystron, I., Rakic, P., Molnar, Z., and Blakemore, C. (2006). The first neurons of the human cerebral cortex. Nat. Neurosci. *9*, 880–886.

Caviness, V.S., Jr., Takahashi, T., and Nowakowski, R.S. (1995). Numbers, time and neocortical neuronogenesis: a general developmental and evolutionary model. Trends Neurosci. *18*, 379–383.

Denaxa, M., Chan, C.-H., Schachner, M., Parnavelas, J.G., and Karagogeos, D. (2001). The adhesion molecule TAG-1 mediates the migration of cortical interneurons from the ganglionic eminence along the corticofugal fiber system. Development *128*, 4635–4644.

Englund, C., Fink, A., Lau, C., Pham, D., Daza, R.A., Bulfone, A., Kowalczyk, T., and Hevner, R.F. (2005). Pax6, Tbr2, and Tbr1 are expressed sequentially by radial glia, intermediate progenitor cells, and postmitotic neurons in developing neocortex. J. Neurosci. *25*, 247–251.

Fietz, S.A., Kelava, I., Vogt, J., Wilsch-Brauninger, M., Stenzel, D., Fish, J.L., Corbeil, D., Riehn, A., Distler, W., Nitsch, R., et al. (2010). OSVZ progenitors of human and ferret neocortex are epithelial-like and expand by integrin signaling. Nat. Neurosci. *13*, 690–699.

Fujita, S. (1963). The matrix cell and cytogenesis in the developing central nervous system. J. Comp. Neurol. *120*, 37–42.

Fukuda, T., Kawano, H., Ohyama, K., Li, H.-P., Takeda, Y., Oohira, A., and Kawamura, K. (1997). Immunohistochemical localization of neurocan and L1 in the formation of thalamocortical pathway of developing rats. J. Comp. Neurol. *382*, 141–152.

Goffinet, A.M., and Lyon, G. (1979). Early histogenesis in the mouse cerebral cortex: a Golgi study. Neurosci. Lett. *14*, 61–66.

Govindan, S., Oberst, P., and Jabaudon, D. (2018). In vivo pulse labeling of isochronic cohorts of cells in the central nervous system using FlashTag. Nat. Protoc. *13*, 2297–2311.

Gurumurthy, C.B., Sato, M., Nakamura, A., Inui, M., Kawano, N., Islam, M.A., Ogiwara, S., Takabayashi, S., Matsuyama, M., Nakagawa, S., et al. (2019). Creation of CRISPR-based germline-genome-engineered mice without ex vivo handling of zygotes by i-GONAD. Nat. Protoc. *14*, 2452–2482.

Hansen, D.V., Lui, J.H., Parker, P.R., and Kriegstein, A.R. (2010). Neurogenic radial glia in the outer subventricular zone of human neocortex. Nature *464*, 554–561.

Hatanaka, Y., Hisanaga, S., Heizmann, C.W., and Murakami, F. (2004). Distinct migratory behavior of early- and late-born neurons derived from the cortical ventricular zone. J. Comp. Neurol. *479*, 1–14.

Haubensak, W., Attardo, A., Denk, W., and Huttner, W.B. (2004). Neurons arise in the basal neuroepithelium of the early mammalian telencephalon: a major site of neurogenesis. Proc. Natl. Acad. Sci. U S A *101*, 3196–3201.

Hendzel, M.J., Wei, Y., Mancini, M.A., Van Hooser, A., Ranalli, T., Brinkley, B.R., Bazett-Jones, D.P., and Allis, C.D. (1997). Mitosis-specific phosphorylation of histone H3 initiates primarily within pericentromeric heterochromatin during G2 and spreads in an ordered fashion coincident with mitotic chromosome condensation. Chromosoma *106*, 348–360.

Hevner, R.F., Miyashita-Lin, E., and Rubenstein, J.L. (2002). Cortical and thalamic axon pathfinding defects in Tbr1, Gbx2, and Pax6 mutant mice: evidence that cortical and thalamic axons interact and guide each other. J. Comp. Neurol. *447*, 8–17.

Hevner, R.F., Shi, L., Justice, N., Hsueh, Y., Sheng, M., Smiga, S., Bulfone, A., Goffinet, A.M., Campagnoni, A.T., and Rubenstein, J.L. (2001). Tbr1 regulates differentiation of the preplate and layer 6. Neuron *29*, 353–366.

Hicks, S.P., and D'Amato, C.J. (1968). Cell migrations to the isocortex in the rat. Anat. Rec. *160*, 619–634.

His, W. (1889). Die Neuroblasten und deren Entstehung im embryonalen Mark, Vol 15 (S. Hirzel).

Hoerder-Suabedissen, A., and Molnár, Z. (2015). Development, evolution and pathology of neocortical subplate neurons. Nat. Rev. Neurosci. *16*, 133–146.

Hoerder-Suabedissen, A., Wang, W.Z., Lee, S., Davies, K.E., Goffinet, A.M., Rakic, S., Parnavelas, J., Reim, K., Nicolic, M., Paulsen, O., et al. (2009). Novel markers reveal subpopulations of subplate neurons in the murine cerebral cortex. Cereb. Cortex *19*, 1738–1750.

Iacopetti, P., Michelini, M., Stuckmann, I., Oback, B., Aaku-Saraste, E., and Huttner, W.B. (1999). Expression of the antiproliferative gene TIS21 at the onset of neurogenesis identifies single

neuroepithelial cells that switch from proliferative to neuron-generating division. Proc. Natl. Acad. Sci. U S A *96*, 4639–4644.

Kanatani, S., Honda, T., Aramaki, M., Hayashi, K., Kubo, K., Ishida, M., Tanaka, D.H., Kawauchi, T., Sekine, K., Kusuzawa, S., et al. (2015). The COUP-TFII/Neuropilin-2 is a molecular switch steering diencephalon-derived GABAergic neurons in the developing mouse brain. Proc. Natl. Acad. Sci. U S A *112*, E4985–E4994.

Kanatani, S., Yozu, M., Tabata, H., and Nakajima, K. (2008). COUP-TFII is preferentially expressed in the caudal ganglionic eminence and is involved in the caudal migratory stream. J. Neurosci. *28*, 13582–13591.

Katayama, K., Imai, F., Campbell, K., Lang, R.A., Zheng, Y., and Yoshida, Y. (2013). RhoA and Cdc42 are required in pre-migratory progenitors of the medial ganglionic eminence ventricular zone for proper cortical interneuron migration. Development *140*, 3139–3145.

Kim, J.-Y., Jeong, H.S., Chung, T., Kim, M., Lee, J.H., Jung, W.H., and Koo, J.S. (2017). The value of phosphohistone H3 as a proliferation marker for evaluating invasive breast cancers: a comparative study with Ki67. Oncotarget *8*, 65064–65076.

Kostovic, I., and Rakic, P. (1990). Developmental history of the transient subplate zone in the visual and somatosensory cortex of the macaque monkey and human brain. J. Comp. Neurol. *297*, 441–470.

Kowalczyk, T., Pontious, A., Englund, C., Daza, R.A., Bedogni, F., Hodge, R., Attardo, A., Bell, C., Huttner, W.B., and Hevner, R.F. (2009). Intermediate neuronal progenitors (basal progenitors) produce pyramidal-projection neurons for all layers of cerebral cortex. Cereb. Cortex *19*, 2439–2450.

Kudo, C., Ajioka, I., Hirata, Y., and Nakajima, K. (2005). Expression profiles of EphA3 at both the RNA and protein level in the developing mammalian forebrain. J. Comp. Neurol. *487*, 255–269.

Lidov, H.G.W., and Molliver, M.E. (1982). An immunohistochemical study of serotonin neuron development in the rat: ascending pathways and terminal fields. Brain Res. Bull. *8*, 389–430.

Lopez-Bendito, G., and Molnar, Z. (2003). Thalamocortical development: how are we going to get there? Nat. Rev. Neurosci. *4*, 276–289.

Luskin, M.B., and Shatz, C.J. (1985). Studies of the earliest generated cells of the cat's visual cortex: cogeneration of subplate and marginal zones. J. Neurosci. *5*, 1062–1075.

Marin, O., and Rubenstein, J.L. (2001). A long, remarkable journey: tangential migration in the telencephalon. Nat. Rev. Neurosci. *2*, 780–790.

Marin-Padilla, M. (1971). Early prenatal ontogenesis of the cerebral cortex (neocortex) of the cat (Felis domestica). A Golgi study. Z. Anat. Entwicklungsgesch. *134*, 117–145.

Mayer, C., Hafemeister, C., Bandler, R.C., Machold, R., Batista Brito, R., Jaglin, X., Allaway, K., Butler, A., Fishell, G., and Satija, R. (2018). Developmental diversification of cortical inhibitory interneurons. Nature *555*, 457–462.

Mission, J.-P., Austin, C.P., Takahashi, T., Cepko, C.L., and Caviness, V.S., Jr. (1991). The alignment of migrating neural cells in relation to the murine neopallial radial glial fiber system. Cereb. Cortex *1*, 221–229.

Miyashita-Lin, E.M., Hevner, R., Wassarman, K.M., Martinez, S., and Rubenstein, J.L. (1999). Early neocortical regionalization in the absence of thalamic innervation. Science *285*, 906–909.

Miyata, T., Kawaguchi, A., Saito, K., Kawano, M., Muto, T., and Ogawa, M. (2004). Asymmetric production of surface-dividing and non-surface-dividing cortical progenitor cells. Development *131*, 3133–3145.

Molnár, Z., Adams, R., Goffinet, A., and Blakemore, C. (1998). The role of the first postmitotic cortical cells in the development of thalamocortical innervation in the reeler mouse. J. Neurosci. *18*, 5746–5765.

Moreno-Juan, V., Filipchuk, A., Antón-Bolaños, N., Mezzera, C., Gezelius, H., Andrés, B., Rodríguez-Malmierca, L., Susín, R., Schaad, O., Iwasato, T., et al. (2017). Prenatal thalamic waves regulate cortical area size prior to sensory processing. Nat. Commun. *8*, 14172.

Murthy, S., Niquille, M., Hurni, N., Limoni, G., Frazer, S., Chameau, P., van Hooft, J.A., Vitalis, T., and Dayer, A. (2014). Serotonin receptor 3A controls interneuron migration into the neocortex. Nat. Commun. *5*, 5524.

Nadarajah, B., Alifragis, P., Wong, R.O., and Parnavelas, J.G. (2002). Ventricle-directed migration in the developing cerebral cortex. Nat. Neurosci. *5*, 218–224.

Nadarajah, B., Brunstrom, J.E., Grutzendler, J., Wong, R.O., and Pearlman, A.L. (2001). Two modes of radial migration in early development of the cerebral cortex. Nat. Neurosci. *4*, 143–150.

Nakashiba, T., Nishimura, S., Ikeda, T., and Itohara, S. (2002). Complementary expression and neurite outgrowth activity of netrin-G subfamily members. Mech. Dev. *111*, 47–60.

Nichols, A.J., and Olson, E.C. (2010). Reelin promotes neuronal orientation and dendritogenesis during preplate splitting. Cereb. Cortex *20*, 2213–2223.

Noctor, S.C., Martinez-Cerdeno, V., Ivic, L., and Kriegstein, A.R. (2004). Cortical neurons arise in symmetric and asymmetric division zones and migrate through specific phases. Nat. Neurosci. *7*, 136–144.

Oberst, P., Fievre, S., Baumann, N., Concetti, C., Bartolini, G., and Jabaudon, D. (2019). Temporal plasticity of apical progenitors in the developing mouse neocortex. Nature *573*, 370–374.

Ogawa, M., Miyata, T., Nakajimat, K., Yagyu, K., Seike, M., Ikenaka, K., Yamamoto, H., and Mikoshibat, K. (1995). The reeler gene-associated antigen on cajal-retzius neurons is a crucial molecule for laminar organization of cortical neurons. Neuron *14*, 899–912.

Ohtaka-Maruyama, C., Okamoto, M., Endo, K., Oshima, M., Kaneko, N., Yura, K., Okado, H., Miyata, T., and Maeda, N. (2018). Synaptic transmission from subplate neurons controls radial migration of neocortical neurons. Science *360*, 313–317.

Ohtsuka, M., Sato, M., Miura, H., Takabayashi, S., Matsuyama, M., Koyano, T., Arifin, N., Nakamura, S., Wada, K., and Gurumurthy, C.B. (2018). i-GONAD: a robust method for in situ germline genome engineering using CRISPR nucleases. Genome Biol. *19*, 25.

Oishi, K., Aramaki, M., and Nakajima, K. (2016a). Mutually repressive interaction between Brn1/2 and Rorb contributes to the establishment of neocortical layer 2/3 and layer 4. Proc. Natl. Acad. Sci. U S A *113*, 3371–3376.

Oishi, K., Nakagawa, N., Tachikawa, K., Sasaki, S., Aramaki, M., Hirano, S., Yamamoto, N., Yoshimura, Y., and Nakajima, K. (2016b). Identity of neocortical layer 4 neurons is specified through correct positioning into the cortex. Elife *5*, e10907.

Olson, E.C. (2014). Analysis of preplate splitting and early cortical development illuminates the biology of neurological disease. Front. Pediatr. *2*, 121.

Osheroff, H., and Hatten, M.E. (2009). Gene expression profiling of preplate neurons destined for the subplate: genes involved in transcription, axon extension, neurotransmitter regulation, steroid hormone signaling, and neuronal survival. Cereb. Cortex *19* (*Suppl 1*), 126–134.

Ozair, M.Z., Kirst, C., van den Berg, B.L., Ruzo, A., Rito, T., and Brivanlou, A.H. (2018). hPSC modeling reveals that fate selection of cortical deep projection neurons occurs in the subplate. Cell Stem Cell *23*, 60–73.

Pedraza, M., Hoerder-Suabedissen, A., Albert-Maestro, M.A., Molnar, Z., and De Carlos, J.A. (2014). Extracortical origin of some murine subplate cell populations. Proc. Natl. Acad. Sci. U S A *111*, 8613–8618.

Pilaz, L.J., Patti, D., Marcy, G., Ollier, E., Pfister, S., Douglas, R.J., Betizeau, M., Gautier, E., Cortay, V., Doerflinger, N., et al. (2009). Forced G1-phase reduction alters mode of division, neuron number, and laminar phenotype in the cerebral cortex. Proc. Natl. Acad. Sci. U S A *106*, 21924–21929.

Pinheiro, E.M., Xie, Z., Norovich, A.L., Vidaki, M., Tsai, L.H., and Gertler, F.B. (2011). Lpd depletion reveals that SRF specifies radial versus tangential migration of pyramidal neurons. Nat. Cell Biol. *13*, 989–995.

Polleux, F., Dehay, C., Moraillon, B., and Kennedy, H. (1997). Regulation of neuroblast cell-cycle kinetics plays a crucial role in the generation of unique features of neocortical areas. J. Neurosci. *17*, 7763–7783.

Price, D.J., Aslam, S., Tasker, L., and Gillies, K. (1997). Fates of the earliest generated cells in the developing murine neocortex. J. Comp. Neurol. *377*, 414–422.

Rakic, P. (1988). Specification of cerebral cortical areas. Science *241*, 170–176.

Rakic, P. (1995). A small step for the cell, a giant leap for mankind: a hypothesis of neocortical

expansion during evolution. Trends Neurosci. *18*, 383–388.

Remedios, R., Huilgol, D., Saha, B., Hari, P., Bhatnagar, L., Kowalczyk, T., Hevner, R.F., Suda, Y., Aizawa, S., Ohshima, T., et al. (2007). A stream of cells migrating from the caudal telencephalon reveals a link between the amygdala and neocortex. Nat. Neurosci. *10*, 1141–1150.

Saito, K., Okamoto, M., Watanabe, Y., Noguchi, N., Nagasaka, A., Nishina, Y., Shinoda, T., Sakakibara, A., and Miyata, T. (2019). Dorsal-to-Ventral cortical expansion is physically primed by ventral streaming of early embryonic preplate neurons. Cell Rep. *29*, 1555–1567.

Sauer, F.C. (1935). Mitosis in the neural tube. J. Comp. Neurol. *62*, 377–405.

Schneider, S., Gulacsi, A., and Hatten, M.E. (2011). Lrp12/Mig13a reveals changing patterns of preplate neuronal polarity during corticogenesis that are absent in reeler mutant mice. Cereb. Cortex *21*, 134–144.

Seiriki, K., Kasai, A., Hashimoto, T., Schulze, W., Niu, M., Yamaguchi, S., Nakazawa, T., Inoue, K.I., Uezono, S., Takada, M., et al. (2017). High-speed and scalable whole-brain imaging in rodents and primates. Neuron *94*, 1085–1100.

Seiriki, K., Kasai, A., Nakazawa, T., Niu, M., Naka, Y., Tanuma, M., Igarashi, H., Yamaura, K., Hayata-Takano, A., Ago, Y., et al. (2019). Whole-brain block-face serial microscopy tomography at subcellular resolution using FAST. Nat. Protoc. *14*, 1509–1529.

Sekine, K., Honda, T., Kawauchi, T., Kubo, K., and Nakajima, K. (2011). The outermost region of the developing cortical plate is crucial for both the switch of the radial migration mode and the Dab1-dependent "inside-out" lamination in the neocortex. J. Neurosci. *31*, 9426–9439.

Sekine, K., Kawauchi, T., Kubo, K., Honda, T., Herz, J., Hattori, M., Kinashi, T., and Nakajima, K. (2012). Reelin controls neuronal positioning by promoting cell-matrix adhesion via inside-out activation of integrin alpha5beta1. Neuron *76*, 353–369.

Shin, M., Kitazawa, A., Yoshinaga, S., Hayashi, K., Hirata, Y., Dehay, C., Kubo, K.I., and Nakajima, K. (2019). Both excitatory and inhibitory neurons transiently form clusters at the outermost region of the developing mammalian cerebral neocortex. J. Comp. Neurol. *527*, 1577–1597.

Shitamukai, A., Konno, D., and Matsuzaki, F. (2011). Oblique radial glial divisions in the developing mouse neocortex induce self-renewing progenitors outside the germinal zone that resemble primate outer subventricular zone progenitors. J. Neurosci. *31*, 3683–3695.

Smart, I.H. (1976). A pilot study of cell production by the ganglionic eminences of the developing mouse brain. J. Anat. *121*, 71–84.

Smart, I.H., and McSherry, G.M. (1982). Growth patterns in the lateral wall of the mouse telencephalon. II. Histological changes during and subsequent to the period of isocortical neuron production. J. Anat. *134*, 415–442.

Smart, I.H., and Smart, M. (1982). Growth patterns in the lateral wall of the mouse telencephalon: I. Autoradiographic studies of the histogenesis of the isocortex and adjacent areas. J. Anat. *134*, 273–298.

Stolt, C.C., Rehberg, S., Ader, M., Lommes, P., Riethmacher, D., Schachner, M., Bartsch, U., and Wegner, M. (2002). Terminal differentiation of myelin-forming oligodendrocytes depends on the transcription factor Sox10. Genes Dev. *16*, 165–170.

Subramanian, L., Bershteyn, M., Paredes, M.F., and Kriegstein, A.R. (2017). Dynamic behaviour of human neuroepithelial cells in the developing forebrain. Nat. Commun. *8*, 14167.

Tabata, H., Kanatani, S., and Nakajima, K. (2009). Differences of migratory behavior between direct progeny of apical progenitors and basal progenitors in the developing cerebral cortex. Cereb. Cortex *19*, 2092–2105.

Tabata, H., and Nakajima, K. (2001). Efficient in utero gene transfer system to the developing mouse brain using electroporation: visualization of neuronal migration in the developing cortex. Neuroscience *103*, 865–872.

Tabata, H., and Nakajima, K. (2002). Neurons tend to stop migration and differentiate along the cortical internal plexiform zones in the Reelin signal-deficient mice. J. Neurosci. Res. *69*, 723–730.

Tabata, H., and Nakajima, K. (2003). Multipolar migration: the third mode of radial neuronal migration in the developing cerebral cortex. J. Neurosci. *23*, 9996–10001.

Tabata, H., and Nakajima, K. (2008). Labeling embryonic mouse central nervous system cells by in utero electroporation. Dev. Growth Differ. *50*, 507–511.

Tabata, H., Yoshinaga, S., and Nakajima, K. (2012). Cytoarchitecture of mouse and human subventricular zone in developing cerebral neocortex. Exp. Brain Res. *216*, 161–168.

Takabayashi, S., Aoshima, T., Kabashima, K., Aoto, K., Ohtsuka, M., and Sato, M. (2018). i-GONAD (improved genome-editing via oviductal nucleic acids delivery), a convenient in vivo tool to produce genome-edited rats. Sci. Rep. *8*, 12059.

Takahashi, T., Goto, T., Miyama, S., Nowakowski, R.S., and Caviness, V.S. (1999). Sequence of neuron origin and neocortical laminar fate: relation to cell cycle of origin in the developing murine cerebral wall. J. Neurosci. *19*, 10357–10371.

Takahashi, T., Misson, J.-P., and Caviness, V.S., Jr. (1990). Glial process elongation and branching in the developing murine neocortex: a qualitative and quantitative immunohistochemical analysis. J. Comp. Neurol. *302*, 15–28.

Takahashi, T., Nowakowski, R.S., and Caviness, V.S., Jr. (1996). The leaving or Q fraction of the murine cerebral proliferative epithelium: a general model of neocortical neuronogenesis. J. Neurosci. *16*, 6183–6196.

Tamamaki, N., Fujimori, K.E., and Takauji, R. (1997). Origin and route of tangentially migrating neurons in the developing neocortical intermediate zone. J. Neurosci. *17*, 8313–8323.

Tamamaki, N., Yanagawa, Y., Tomioka, R., Miyazaki, J., Obata, K., and Kaneko, T. (2003). Green fluorescent protein expression and colocalization with calretinin, parvalbumin, and somatostatin in the GAD67-GFP knock-in mouse. J. Comp. Neurol. *467*, 60–79.

Tan, X., Liu, W.A., Zhang, X.J., Shi, W., Ren, S.Q., Li, Z., Brown, K.N., and Shi, S.H. (2016). Vascular influence on ventral telencephalic progenitors and neocortical interneuron production. Dev. Cell *36*, 624–638.

Tan, X., and Shi, S.-H. (2013). Neocortical neurogenesis and neuronal migration. Wiley Interdiscip. Dev. Biol. *2*, 443–459.

Tatsumi, K., Isonishi, A., Yamasaki, M., Kawabe, Y., Morita-Takemura, S., Nakahara, K., Terada, Y., Shinjo, T., Okuda, H., Tanaka, T., et al. (2018). Olig2-Lineage astrocytes: a distinct subtype of astrocytes that differs from GFAP astrocytes. Front. Neuroanat. *12*, 8.

Telley, L., Agirman, G., Prados, J., Amberg, N., Fievre, S., Oberst, P., Bartolini, G., Vitali, I., Cadilhac, C., Hippenmeyer, S., et al. (2019). Temporal patterning of apical progenitors and their daughter neurons in the developing neocortex. Science *364*, eaav2522.

Telley, L., Govindan, S., Prados, J., Stevant, I., Nef, S., Dermitzakis, E., Dayer, A., and Jabaudon, D. (2016). Sequential transcriptional waves direct the differentiation of newborn neurons in the mouse neocortex. Science *351*, 1443–1446.

Vaid, S., Camp, J.G., Hersemann, L., Eugster Oegema, C., Heninger, A.-K., Winkler, S., Brandl, H., Sarov, M., Treutlein, B., Huttner, W.B., et al. (2018). A novel population of Hopx-dependent basal radial glial cells in the developing mouse neocortex. Development *145*, dev169276.

Vue, T.Y., Lee, M., Tan, Y.E., Werkhoven, Z., Wang, L., and Nakagawa, Y. (2013). Thalamic control of neocortical area formation in mice. J. Neurosci. *33*, 8442–8453.

Wang, X., Tsai, J.W., LaMonica, B., and Kriegstein, A.R. (2011). A new subtype of progenitor cell in the mouse embryonic neocortex. Nat. Neurosci. *14*, 555–561.

Wassarman, K., Lewandoski, M., Campbell, K., Joyner, A.L., Rubenstein, J.L., Martínez, S., and Martin, G.R. (1997). Specification of the anterior hindbrain and establishment of a normal mid/hindbrain organizer is dependent on Gbx2 gene function. Development *124*, 2923–2934.

Watanabe, Y., Kawaue, T., and Miyata, T. (2018). Differentiating cells mechanically limit the interkinetic nuclear migration of progenitor cells to secure apical cytogenesis. Development *145*, dev162883.

Yoshinaga, S., Ohkubo, T., Sasaki, S., Nuriya, M., Ogawa, Y., Yasui, M., Tabata, H., and Nakajima, K. (2012). A phosphatidylinositol lipids system, lamellipodin, and Ena/VASP regulate dynamic morphology of multipolar migrating cells in the developing cerebral cortex. J. Neurosci. *32*, 11643–11656.

Zhou, Q., Wang, S., and Anderson, D.J. (2000). Identification of a novel family of oligodendrocyte lineage-specific basic helix-loop-helix transcription factors. Neuron *25*, 331–343.

iScience, Volume *24*

Supplemental information

Comprehensive characterization of migration profiles of murine cerebral cortical neurons during development using FlashTag labeling

Satoshi Yoshinaga, Minkyung Shin, Ayako Kitazawa, Kazuhiro Ishii, Masato Tanuma, Atsushi Kasai, Hitoshi Hashimoto, Ken-ichiro Kubo, and Kazunori Nakajima

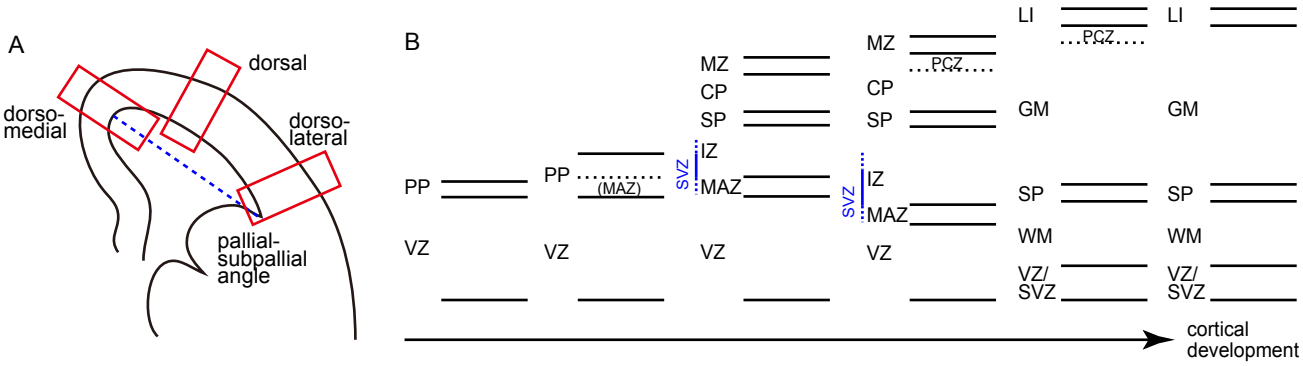
A
dorsal
dorso-
medial
dorso-
lateral
pallial-
subpallial
angle
B
PP
VZ
PP
(MAZ)
VZ
SVZ
MZ
CP
SP
IZ
MAZ
VZ
SVZ
MZ
CP
SP
IZ
MAZ
VZ
PCZ
LI
GM
SP
WM
VZ/
SVZ
LI
PCZ
GM
SP
WM
VZ/
SVZ
cortical
development

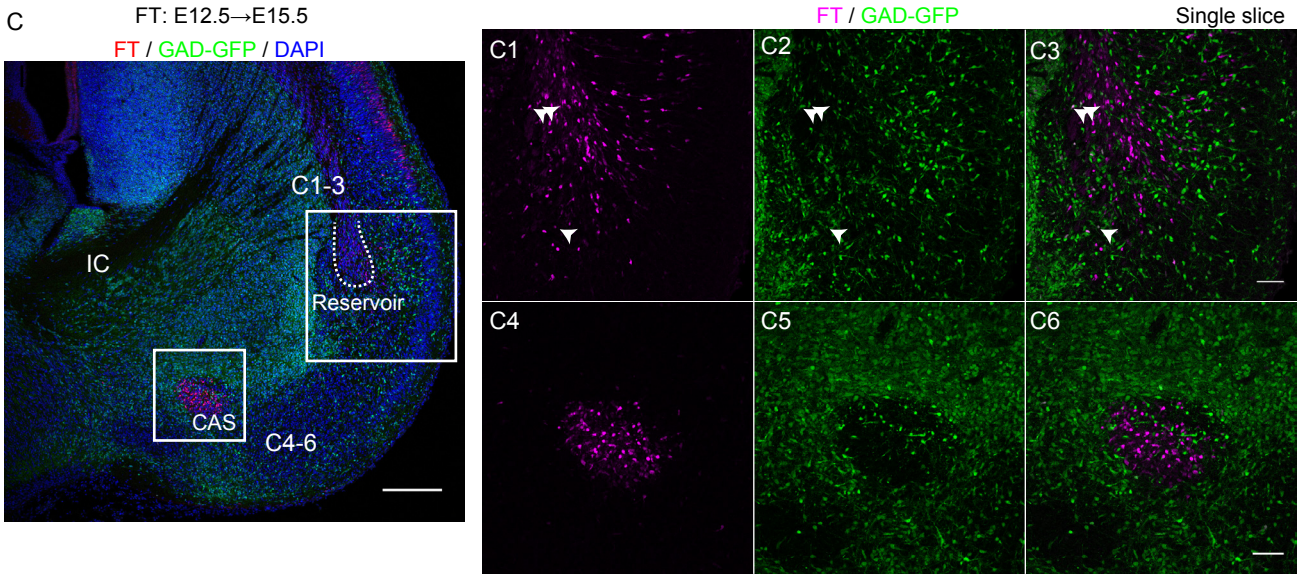
C
FT: E12.5→E15.5
FT / GAD-GFP / DAPI
C1-3
IC
Reservoir
CAS
C4-6
FT / GAD-GFP
Single slice
C1
C2
C3
C4
C5
C6

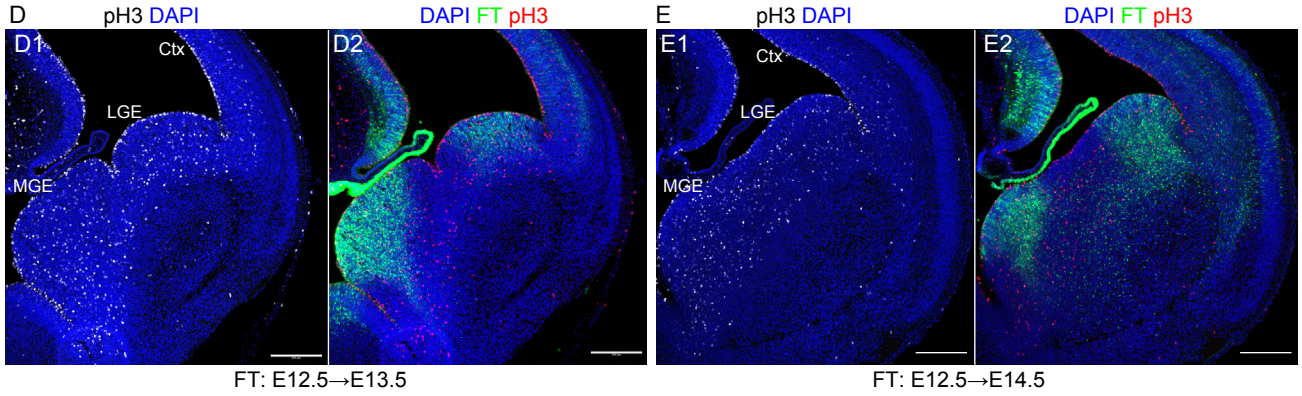
D
pH3 DAPI
DAPI FT pH3
D1
Ctx
LGE
MGE
D2
FT: E12.5→E13.5
E
pH3 DAPI
DAPI FT pH3
E1
Ctx
LGE
MGE
E2
FT: E12.5→E14.5

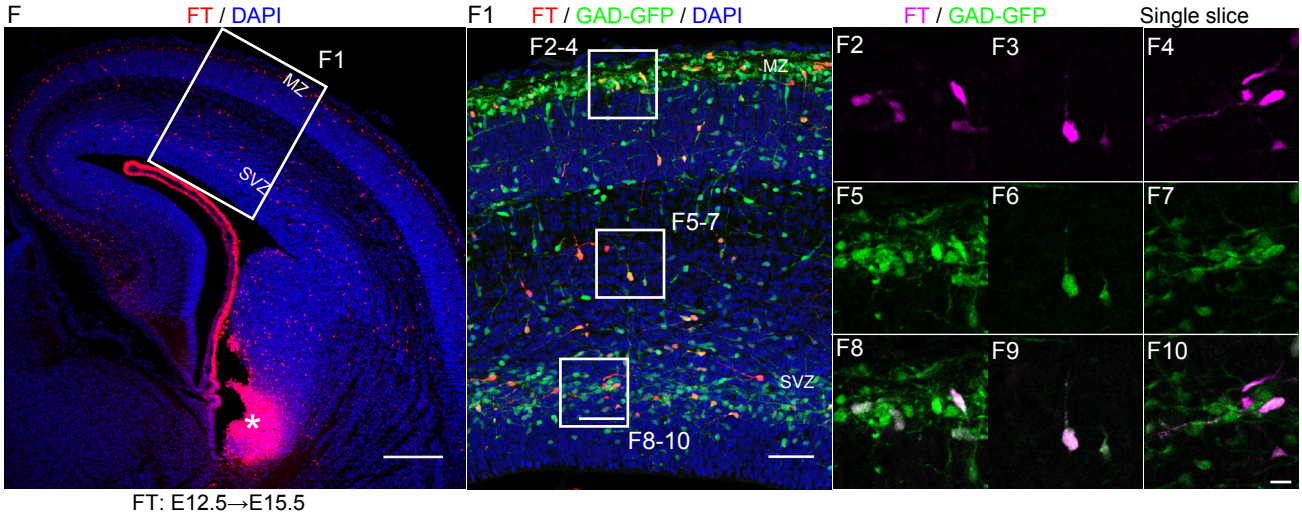
F
FT / DAPI
F1
MZ
SVZ
*
FT: E12.5→E15.5
F1
FT / GAD-GFP / DAPI
F2-4
MZ
F5-7
SVZ
F8-10
FT / GAD-GFP
Single slice
F2
F3
F4
F5
F6
F7
F8
F9
F10

Figure S1, related to Figure 1

Characterization of the FT-labeled cell population.

A: The definitions of “dorsomedial,” “dorsal,” and “dorsolateral” cortices used in the current study.

B: Schematic representation of the histological zones in this study. See the *histological terminology* section of the Transparent Methods for discussion.

C: CytoTell Blue was injected into the LV of the E12.5 *GAD67-GFP* brains. A coronal section of E15.5 brains slightly caudal to the section shown in Figure 1M is shown. In the “reservoir” (Altman & Bayer, 1991), there are many migrating cells that are mostly negative for GFP (C1–C3). More ventrally, labeled cells are identified in the caudal amygdaloid stream (CAS) and are negative for GFP (C4–C6). Arrowheads show rare examples of cells positive for both FT and GFP.

D–E: Immunohistochemistry against pH3 was performed in E13.5 (D) and E14.5 (E) wild-type brains in which CFSE was injected at E12.5. Abventricular mitosis labeled with pH3 is abundant in the ganglionic eminences (GE) (D, E). In the medial ganglionic eminence (MGE) at E13.5, many FT-labeled cells are observed in the VZ and apical half of the SVZ (D). At E14.5, FT-labeled interneurons enter the cortex when fluorescent dyes were injected into the parenchyma of the GE (data not shown); FT-labeled cells are again observed in the VZ and apical half of the SVZ (E). Note that a relatively small number of cells migrate in the deep part of the SVZ of the MGE and in the presumptive pallidum and that few labeled cells with interneuron-like morphology are observed in the cortex.

F: CytoTell Blue was injected into the parenchyma of the GE of the heterozygous *GAD67-GFP* mice at E12.5. The asterisk in (F) indicates the retrospectively identified injection site. Strongly labeled cells are distributed throughout the hemispheres, especially in the SVZ and marginal zone (MZ) (F, F1). They often show tangential morphology and are positive for GFP (F1–F10).

Scale bars, 200 μm (C, D, E, F), 50 μm (F1), 20 μm (C1–6), 10 μm (F10).

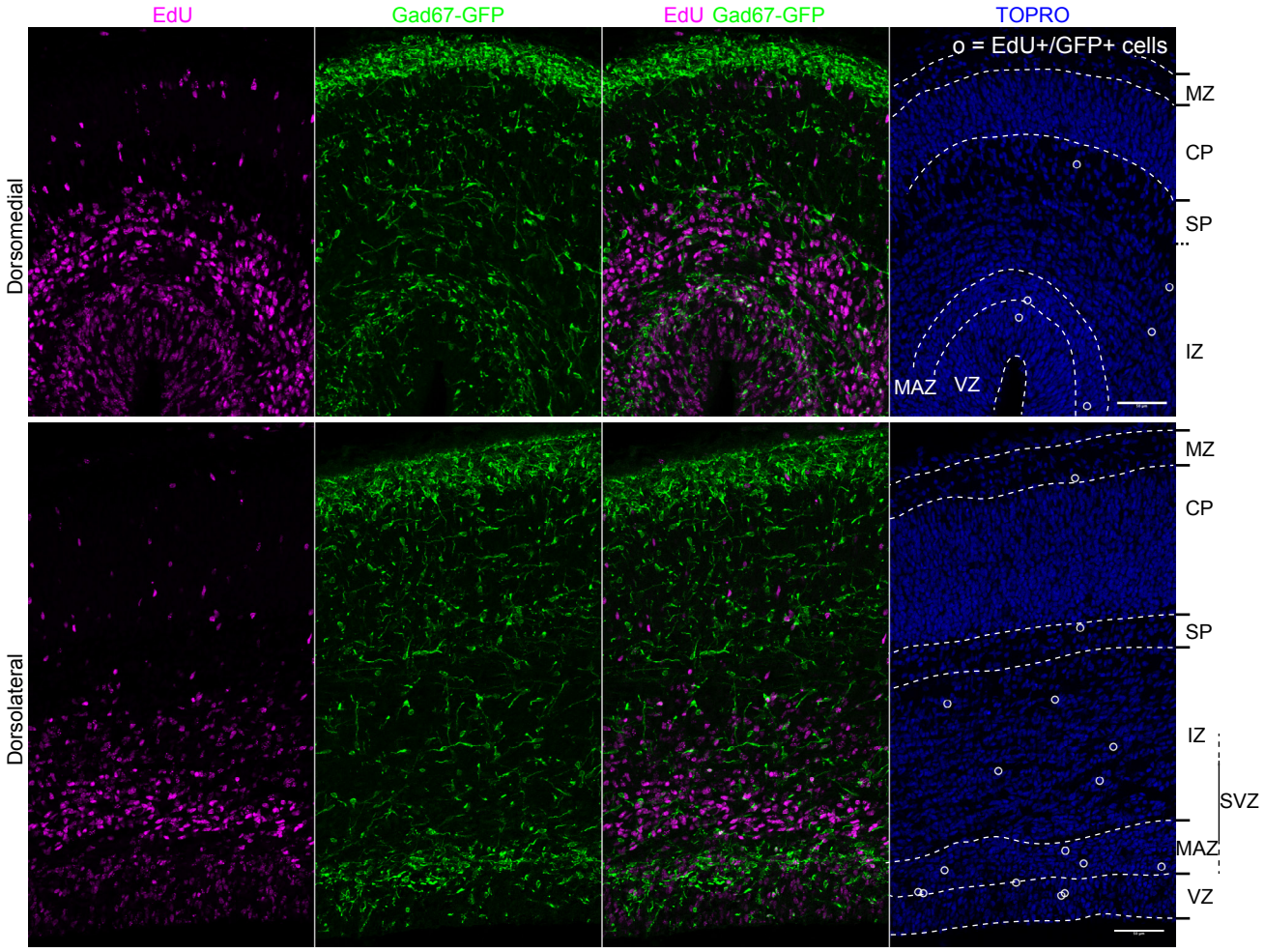
EdU
Gad67-GFP
EdU Gad67-GFP
TOPRO
o = EdU+/GFP+ cells
Dorsomedial
Dorsolateral
MZ
CP
SP
IZ
SVZ
MAZ
VZ

Figure S2, related to Figure 2

GABAergic interneurons in EdU-labeled brains.

The same experiment as in Figures 2A–C was performed using *GAD67-GFP* mice to visualize GABAergic interneurons. EdU-labeled interneurons (EdU+/GFP+) are sparsely distributed in the cerebral cortex. The distribution is mainly in the multipolar cell accumulation zone and intermediate zone, or in the subventricular zone. Scale bars, 50 μm.

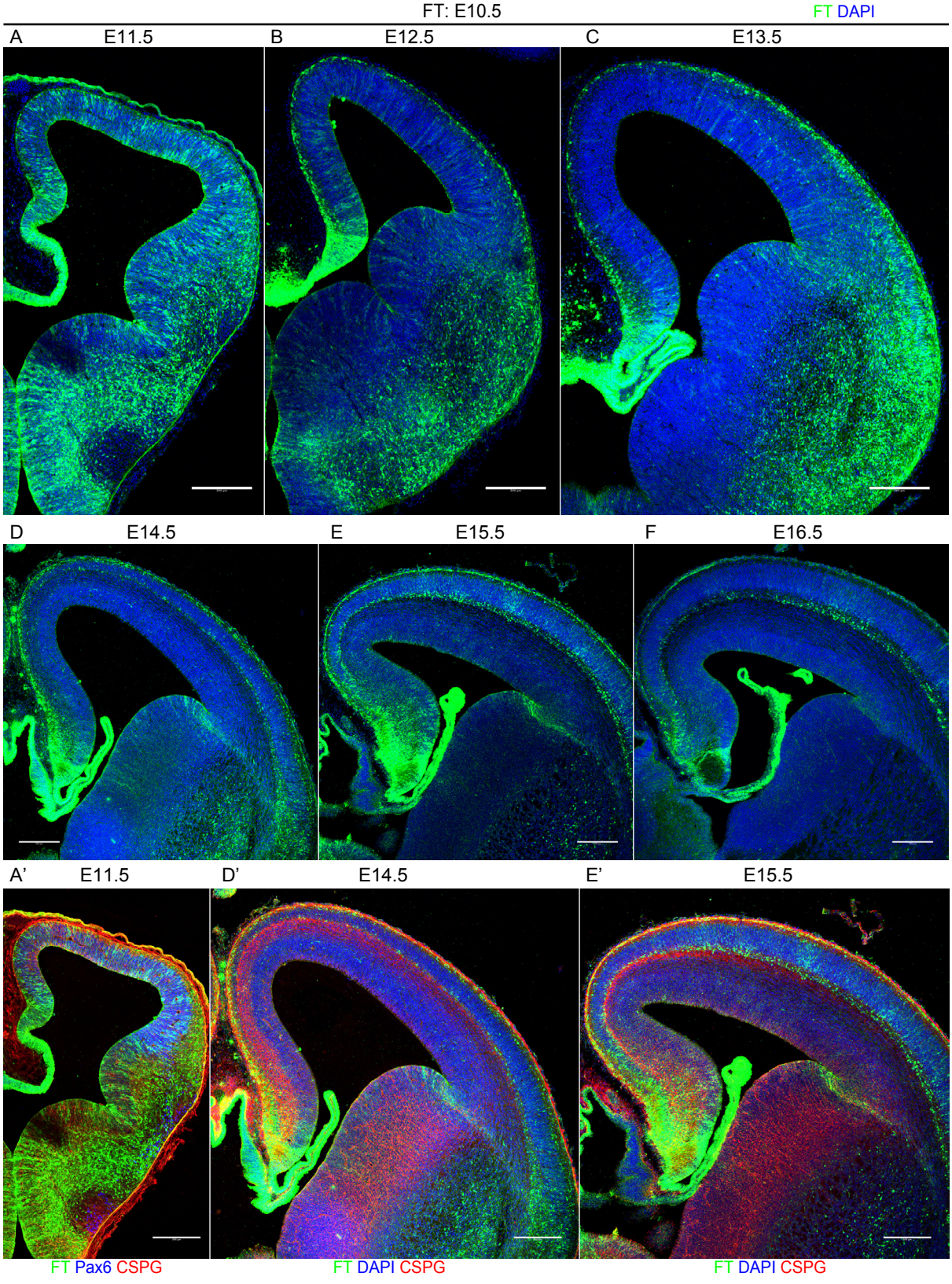
FT: E10.5
FT DAPI
A
E11.5
B
E12.5
C
E13.5
D
E14.5
E
E15.5
F
E16.5
A'
E11.5
D'
E14.5
E'
E15.5
FT Pax6 CSPG
FT DAPI CSPG
FT DAPI CSPG
G
FT E10.5: E16.5 Dorsolateral
MZ
CP
SP
FT / DAPI
FT / Tbr1
FT / Reelin

Figure S3*,* related to Figure 3

Cohort of cells born at E10.5.

A–F: Coronal sections of E11.5 (A, A'), 12.5 (B), 13.5 (C), 14.5 (D, D'), 15.5 (E, E') and 16.5 (F) brains labeled at E10.5. See also Figure 3 for higher magnifications. As early as E11.5, some cells are found in the preplate (PP), which is very thin in the dorsomedial cortex, and in the VZ (A, A'). At E12.5, many cells are observed in the PP (B). In the dorsomedial cortex at E13.5, the labeled cells are in the PP (C). In the dorsolateral cortex, on the other hand, many labeled cells are in the CP and MZ (C). At E14.5, a thin CP is also identified in the dorsomedial cortex (D, D'). Some labeled cells are observed in the deep part of the CP in the dorsomedial cortex, but many labeled cells are found in the MZ (D, D'). In the dorsolateral cortex, many labeled cells are found near the boundary between the CP and SP (D, D'). At E15.5, labeled cells are found at the boundary between the SP and CP as well as in the MZ in the dorsomedial cortex (E), which is like the dorsolateral cortex at E14.5 (D). In the E15.5 dorsolateral cortex, many labeled cells are found in the CSPG-positive SP (E, E'). At E16.5, labeled cells are mainly found in the SP in both the dorsomedial and dorsolateral cortex and some cells are also found in the MZ (F).

G: At E16.5, in both the dorsomedial and dorsolateral cortex, labeled cells are mainly found in the SP and are Tbr1-positive. Some cells are also found in the MZ and are positive for Reelin, suggesting that they are Cajal–Retzius neurons.

Scale bars, 200 μm (A–F) and 50 μm (G).

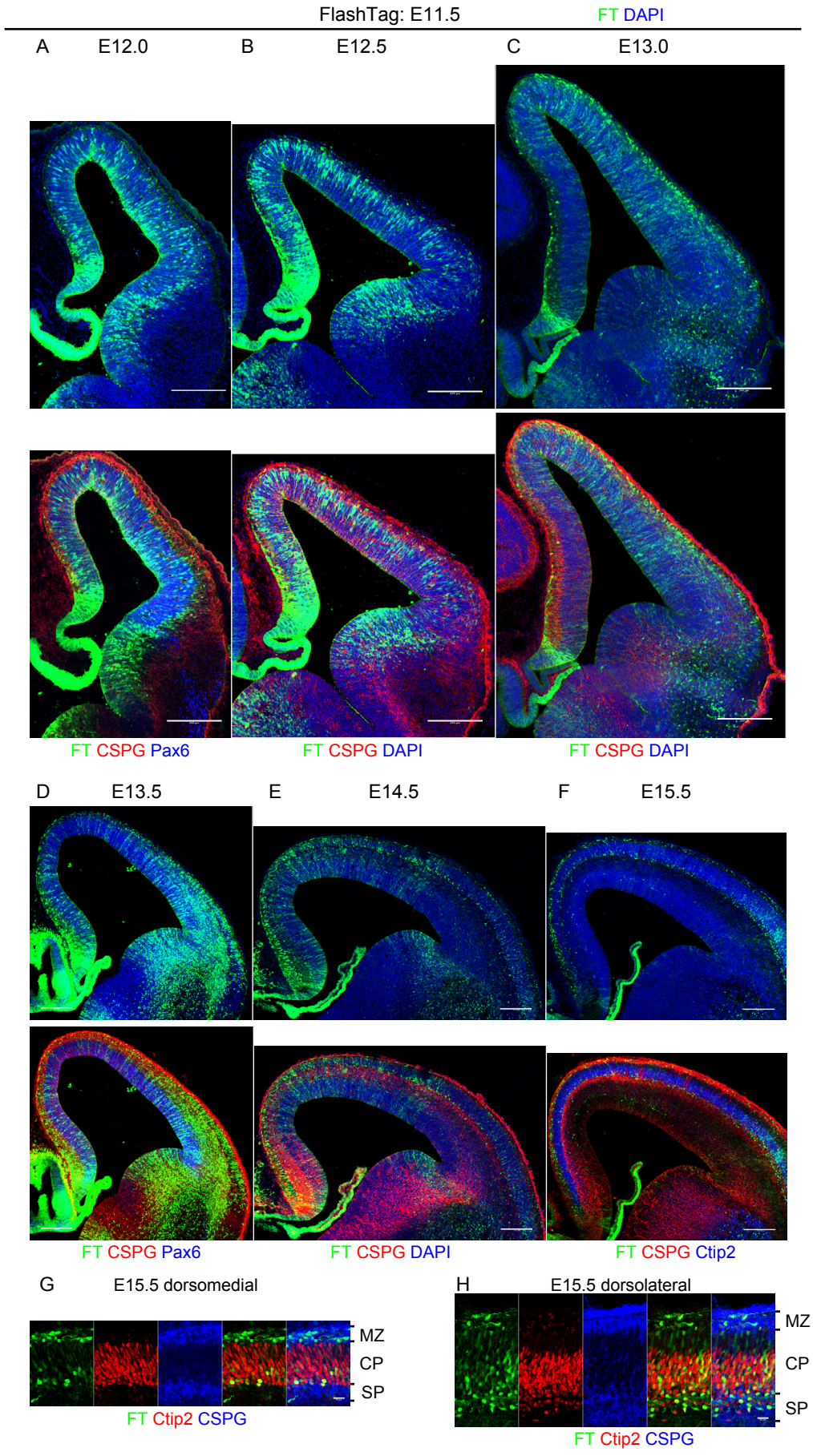
FlashTag: E11.5
FT DAPI
A
E12.0
B
E12.5
C
E13.0
FT CSPG Pax6
FT CSPG DAPI
FT CSPG DAPI
D
E13.5
E
E14.5
F
E15.5
FT CSPG Pax6
FT CSPG DAPI
FT CSPG Ctip2
G
E15.5 dorsomedial
MZ
CP
SP
FT Ctip2 CSPG
H
E15.5 dorsolateral
MZ
CP
SP
FT Ctip2 CSPG

Figure S4*,* related to Figure 4

Cohort of cells born at E11.5.

A–F: Coronal sections of E12.0 (A), E12.5 (B), E13.0 (C), E13.5 (D), E14.5 (E), and E15.5 (F) brains, all labeled at E11.5. See the legend of Figure 4 for explanations.

G–H: Immunohistochemistry against Ctip2 and CSPG in E15.5 brains in which FT injection was performed at E11.5. Images (G), dorsomedial, and (H), dorsolateral, are taken from insets in Figures 4D and E, respectively. At E15.5, many cells are in the lower part of the CP and, to a lesser extent, the MZ. Some cells are also found in the SP in the dorsolateral cortex. Most of the labeled cells in the CP at E15.5 are positive for Ctip2, a deep-layer marker.

Scale bars, 200 μm (A–F), 20 μm (G, H).

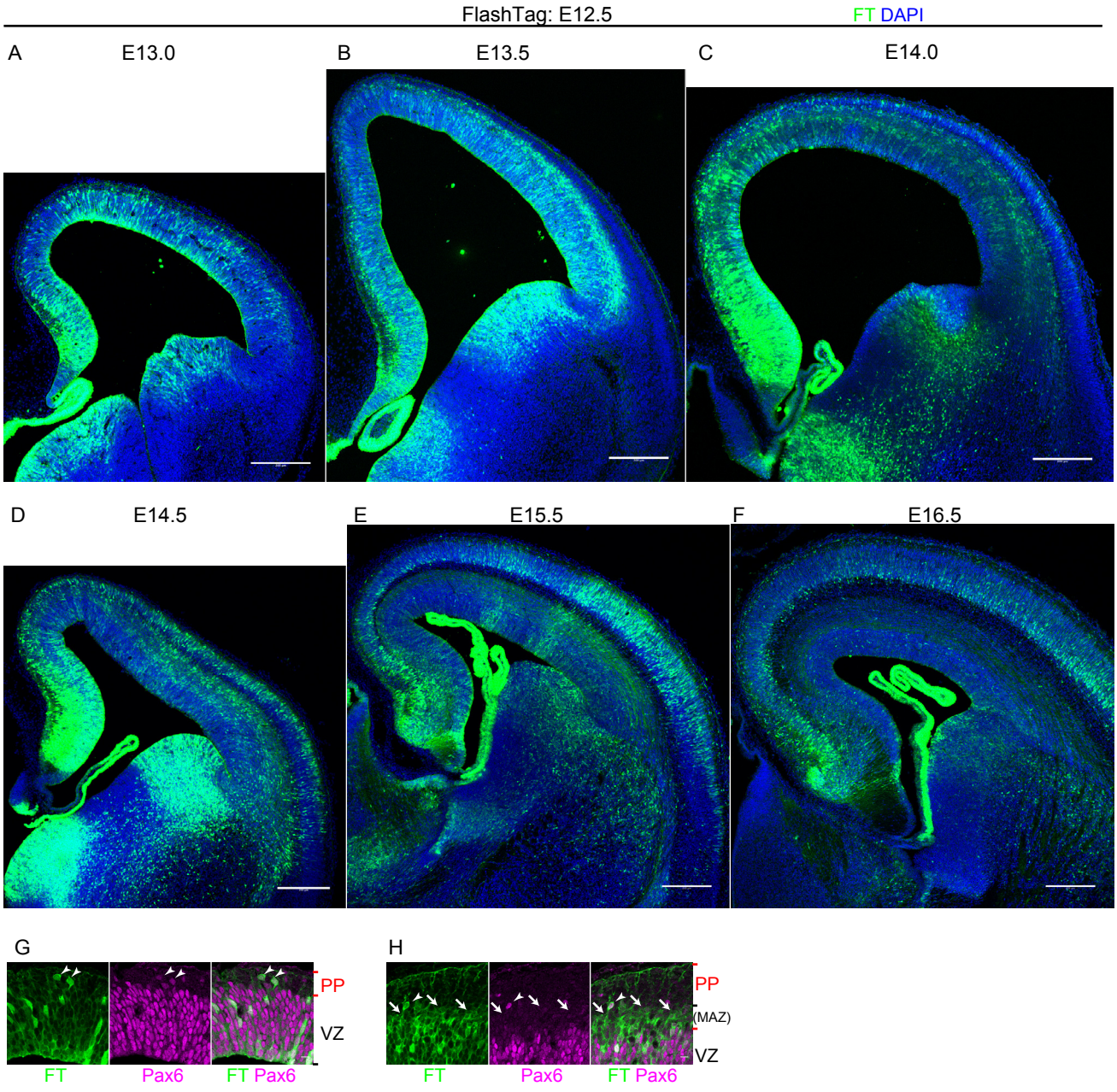
FlashTag: E12.5
FT DAPI
A
E13.0
B
E13.5
C
E14.0
D
E14.5
E
E15.5
F
E16.5
G
PP
VZ
FT
Pax6
FT Pax6
H
PP
(MAZ)
VZ
FT
Pax6
FT Pax6

Figure S5*,* related to Figure 5

Cohort of cells born at E12.5.

A–F: Coronal sections of E13.0 (A), 13.5 (B), 14.0 (C), 14.5 (D), 15.5 (E), and 16.5 (F) brains, all labeled at E12.5, are shown with nuclear staining. See the legend of Figure 5 for explanations.

G–H: Single optical slices of E13.0 brains taken from the dorsomedial and dorsolateral cortices are shown in (G) and (H), respectively. In the dorsomedial cortex at E13.0, many labeled cells are observed in the VZ, but a small number of labeled cells are also found in the PP (Figure 5A, G). The latter cells are often weakly positive for Pax6 (G, arrowheads). In the dorsolateral cortex, many labeled cells are located in regions just above the VZ in addition to the VZ itself, and they are often negative for Pax6 (H; arrows). FT+ / Pax6+ cells outside the VZ are relatively rare (H, an arrowhead).

Scale bars, 200 μm (A–F) and 10 μm (G, H).

FlashTag: E13.5

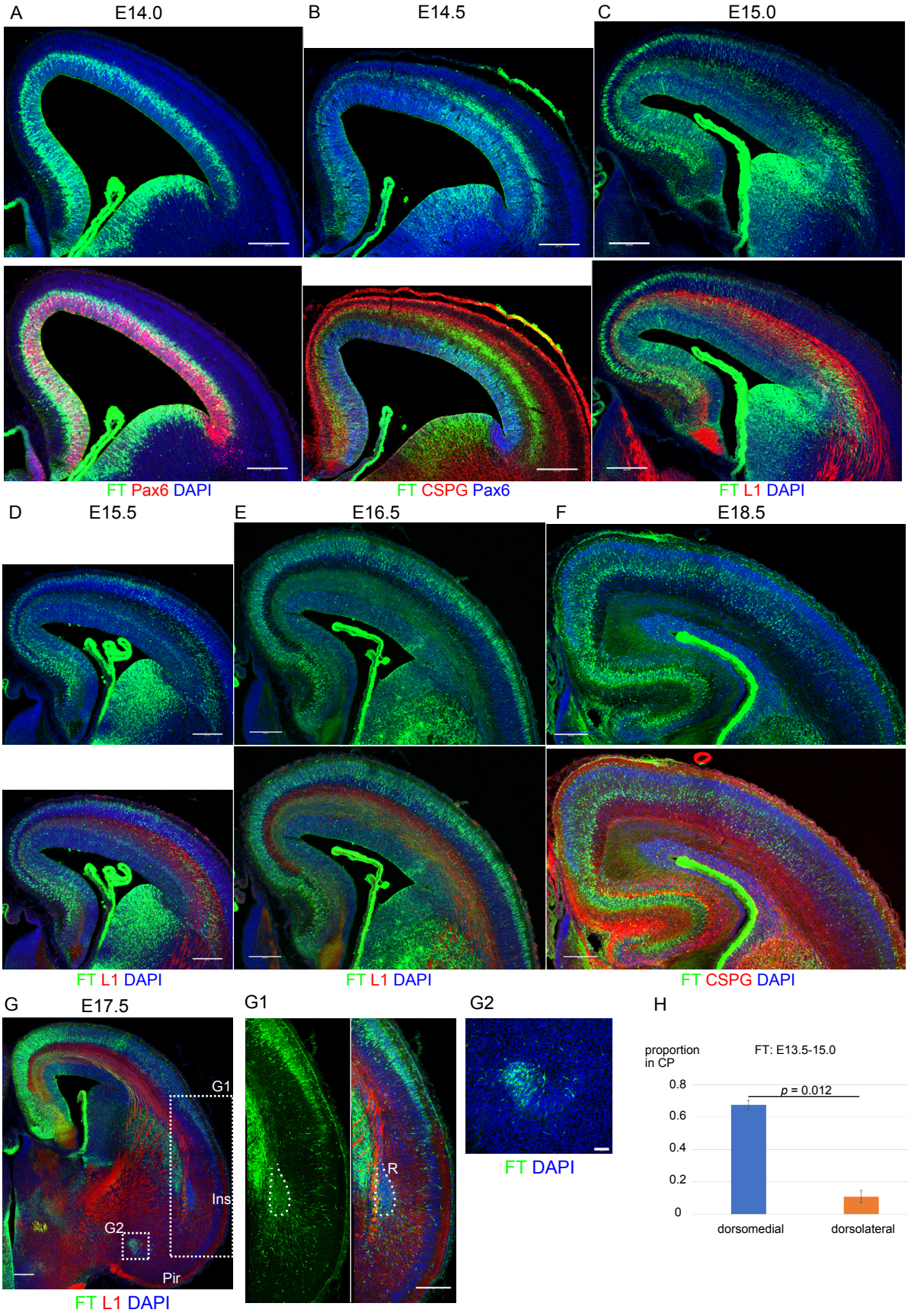

Figure S6, related to Figures 6 and S7

Cohort of cells born at E13.5.

A–H: Coronal sections of E14.0 (A), 14.5 (B), 15.0 (C), 15.5 (D), 16.5 (E), 18.5 (F), and 17.5 (G) brains labeled at E13.5. Higher magnification micrographs from the dorsomedial and dorsolateral cortices from E14.0–17.5 are shown in Figure S7. A quantitative analysis of migrating neurons reaching the CP of E15.0 (C) is shown in (H). At E14.0, most of the labeled cells are in the VZ and zones just above the VZ in both the dorsomedial and dorsolateral cortices (A, see also Figures S7A, and S7B). At E14.5, many labeled neurons migrate in the IZ below the SP as revealed by immunohistochemistry for CSPG (B, Figures S7A, S7B). At E15.0, most of the labeled cells reach points just beneath the pial surface in the dorsomedial cortex (C, Figure S7A), but most of the labeled cells in the dorsolateral cortex are in the IZ below the SP (C, Figure S7B). The proportion of labeled cells in the CP was calculated (H; dorsomedial: 67.6 ± 2.7%, 114 cells from 3 brains, dorsolateral: 10.9 ± 3.8%, 183 cells from 3 brains; paired *t*-test, $p = 0.012$, $n = 3$ brains). At E15.5, some of the labeled cells enter the CP, while many neurons are still migrating in the IZ and SP in the dorsolateral cortex (D, Figure S7B). At E16.5, most of the labeled cells in the dorsomedial cortex are in the CP (E, Figure S7A). Most of the labeled cells in the dorsolateral cortex reach the superficial part of the CP (E, Figure S7A). Note the FT-labeled axon bundles in the IZ. At E17.5 and 18.5, many strongly labeled neurons are in the deeper part of the CP, suggesting that later-born neurons pass through the neuronal layers that are born at E13.5 (F, G, Figures S7A, and S7B). As late as E17.5, in the most lateral part of the cortex (G), many labeled cells are still migrating radially or are about to leave the reservoir (R) (Bayer and Altman, 1991) (G1). Labeled cells are also found in the caudal amygdaloid stream (CAS) (G2).

Scale bars, 200 μm (A–G, G1), and 50 μm (G2). Data are presented as mean ± SEM.

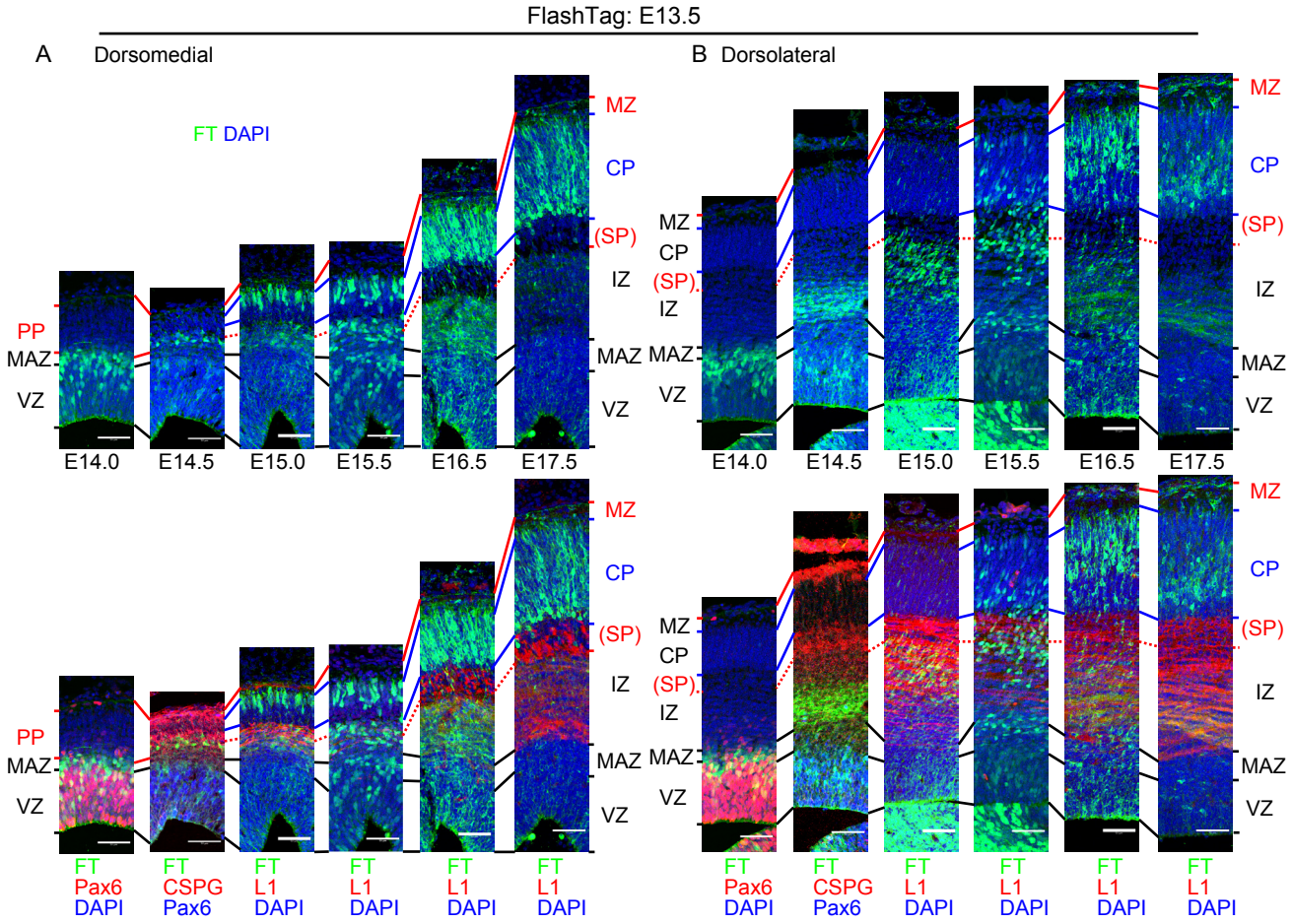
FlashTag: E13.5
A Dorsomedial
B Dorsolateral
FT DAPI
MZ
CP
(SP)
IZ
MAZ
VZ
PP
E14.0
E14.5
E15.0
E15.5
E16.5
E17.5
FT Pax6 DAPI
FT CSPG Pax6
FT L1 DAPI

Figure S7, related to Figures 6 and S6

Higher magnification micrographs of the cohort of cells born at E13.5.

A-B: Higher magnification micrographs from the dorsomedial and dorsolateral cortices from E14.0–17.5 are shown in A and B, respectively. Refer to the legend of Figure S6 for a detailed explanation. Scale bars, 50 μm.

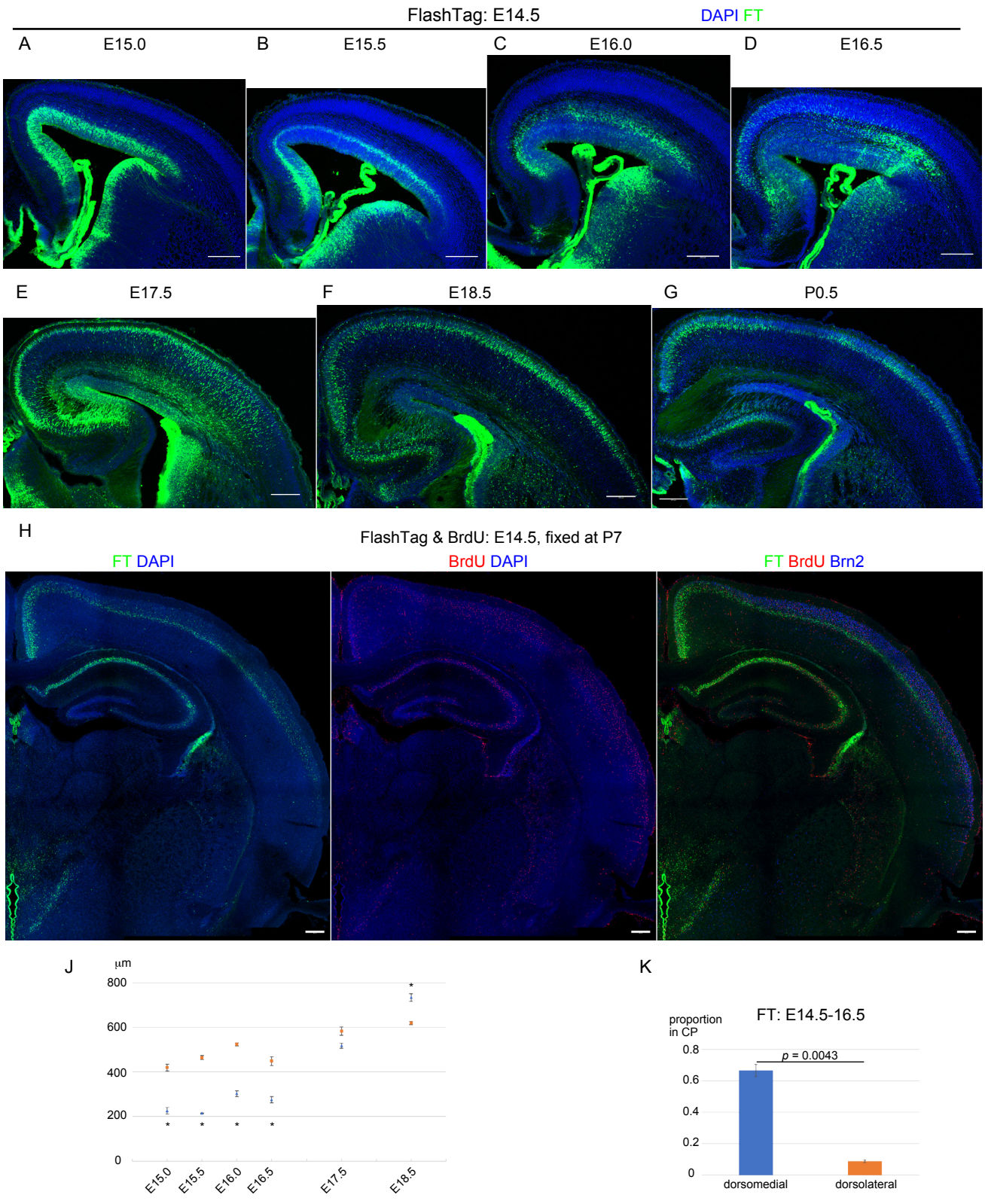
FlashTag: E14.5
DAPI FT
A
E15.0
B
E15.5
C
E16.0
D
E16.5
E
E17.5
F
E18.5
G
P0.5
H
FlashTag & BrdU: E14.5, fixed at P7
FT DAPI
BrdU DAPI
FT BrdU Brn2
J
µm
800
600
400
200
0
E15.0
E15.5
E16.0
E16.5
E17.5
E18.5
K
FT: E14.5-16.5
proportion in CP
0.8
0.6
0.4
0.2
0
p = 0.0043
dorsomedial
dorsolateral

Figure S8, related to Figure 6

Cohort of cells born at E14.5.

A–G: Coronal sections of E15.0 (A), 15.5 (B), 16.0 (C), 16.5 (D), 17.5 (E), 18.5 (F), and P0.5 (G) brains labeled at E14.5. Channels for FT and nuclear staining are shown. See the legend of Figure 6 for explanations.

H: A coronal section of a P7 brain in which FT labeling and intraperitoneal BrdU injection were performed at E14.5. Brn2 was used as a marker for layers II/III and V. In the dorsolateral cortex, FT-labeled cells are mainly distributed in layer IV. In the dorsomedial and lateral cortex, FT-labeled cells are mainly distributed in layer II/III. BrdU-positive cells are mainly detected in the superficial layers.

J: Longitudinal changes in the thickness of the dorsomedial and dorsolateral cortices, where quantitative analyses of migratory profiles were conducted (Figure 6J). The thickness of the dorsomedial cortex (blue) is smaller at earlier stages, but it gradually catches up with that of the dorsolateral cortex (orange). *$p < 0.05$ (*t*-test; E15.0, $n = 4$ brains; E15.5, $n = 3$; E15.5, $n = 3$; E16.5, $n = 4$; E17.5, $n = 3$; E18.5, $n = 3$).

K: The proportion of FT-labeled cells in the CP. Significantly more neurons are found in the CP in the dorsomedial cortex than in the dorsolateral cortex (dorsomedial, 66.7 ± 3.9%, 218 cells from 3 brains; dorsolateral, 8.7 ± 0.8%, 220 cells from 3 brains; paired *t*-test, $p = 0.0043$, $n = 3$ brains). Scale bars, 200 μm. Data are presented as mean ± SEM.

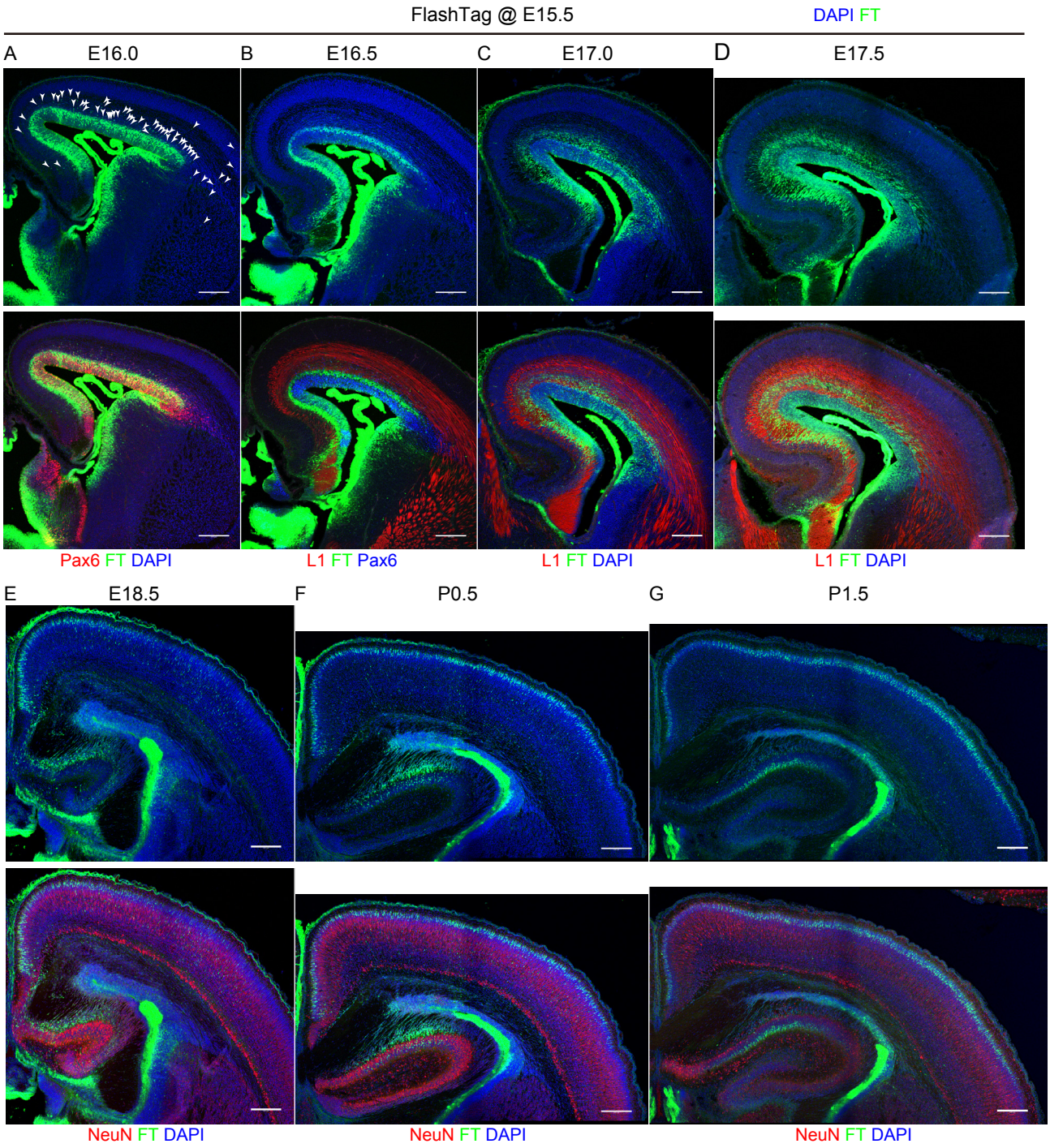
FlashTag @ E15.5
DAPI FT
A
E16.0
B
E16.5
C
E17.0
D
E17.5
Pax6 FT DAPI
L1 FT Pax6
L1 FT DAPI
L1 FT DAPI
E
E18.5
F
P0.5
G
P1.5
NeuN FT DAPI
NeuN FT DAPI
NeuN FT DAPI

Figure S9, related to Figures 6, S10, and S11

Cohort of cells labeled at E15.5.

A–G: Coronal sections of E16.0 (A), 16.5 (B), 17.0 (C), 17.5 (D), 18.5 (E), P0.5 (F), and P1.5 (G) brains labeled at E15.5. Higher-magnification micrographs from the dorsomedial and dorsolateral cortices are shown in Figures S10 and S11, respectively. At E16.0, most of the labeled cells are in the VZ (A, Figure S10A, S11A). Some labeled cells, often positive for Pax6, are outside the VZ (A, Figure S11A; arrowheads). One day (E16.5; B, Figure S10A, S11A) and 1.5–2 days (E17.0–17.5; C, D, Figures S10A, S11A) after injection, most of the labeled cells are in the MAZ and IZ, respectively. At E17.5, most of the labeled cells migrate in the superficial and deep part of the IZ in the dorsomedial cortex (D, Figure S10A). In the dorsolateral cortex, migrating cells are found mainly in the deep part of the IZ (D, Figure S11A). At E18.5, in the dorsomedial cortex, most of the labeled cells are found in the PCZ (E, Figure S10A). In the dorsolateral cortex, on the other hand, only a small population of labeled cells have reached the PCZ, and others are still migrating in the CP and SP with a locomotion morphology (E, Figure S11A). At P0.5, the vast majority of labeled cells have settled in the PCZ in the dorsomedial cortex (F, Figure S10A). In the dorsolateral cortex, many labeled cells have reached the PCZ (F, Figure S11A). At P1.5, cells labeled at E15.5 settle in the GM in the dorsolateral cortex (G, Figures S10A, S11A). In the dorsolateral cortex, some of these labeled cells change their position slightly deeper to leave the PCZ (G, Figure S11A).

Scale bars, 200 μm.

A Dorsomedial FlashTag: E15.5 FT DAPI

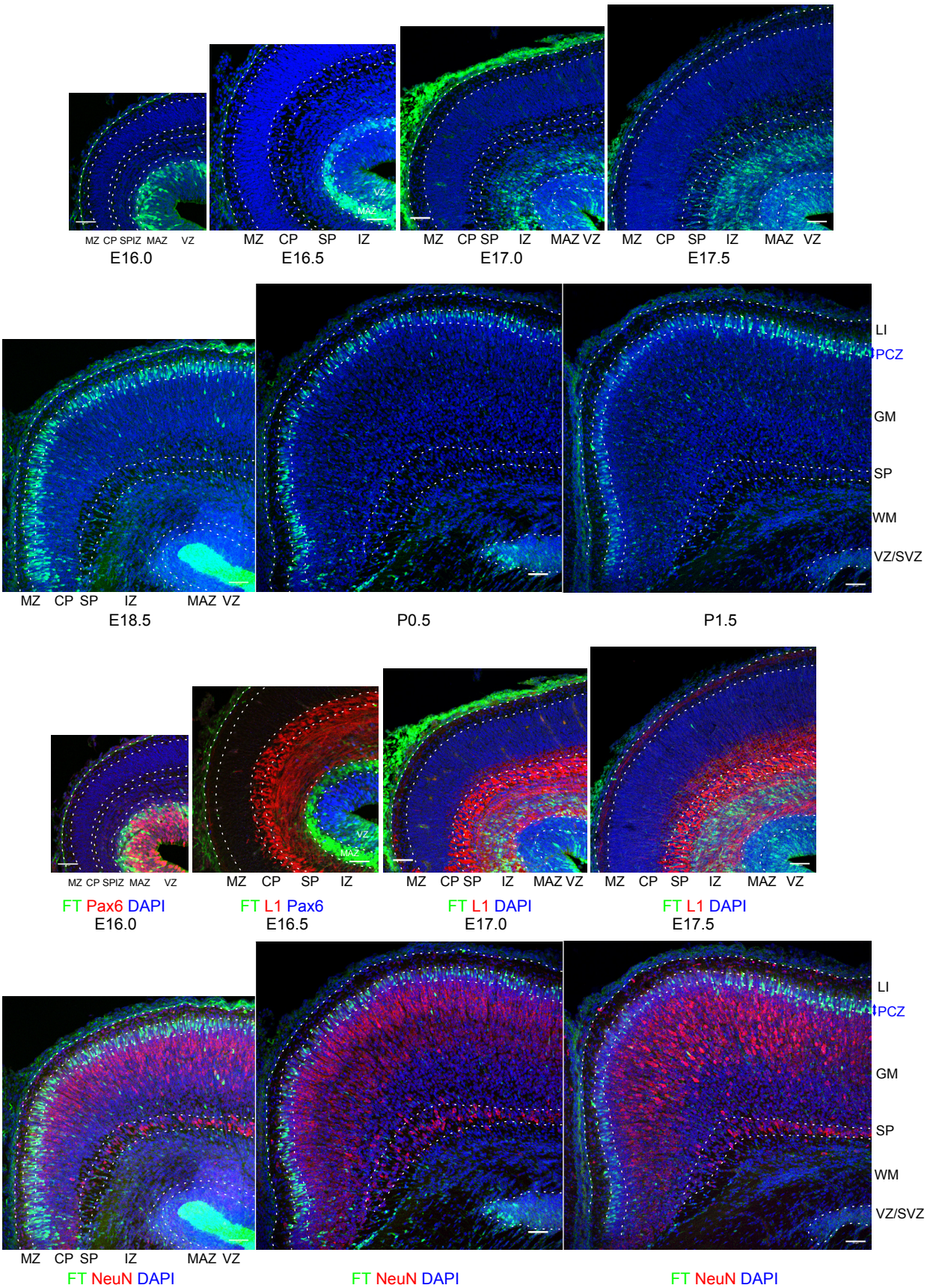

Figure S10, related to Figures 6, S9, and S11

Dorsomedial higher-magnification micrographs of the cohort of cells born at E15.5.

A: Higher magnification micrographs from the dorsomedial cortices from E16.0–P1.5 are shown. Refer to the legend of Figure S9 for a detailed explanation.

Scale bars, 50 μm.

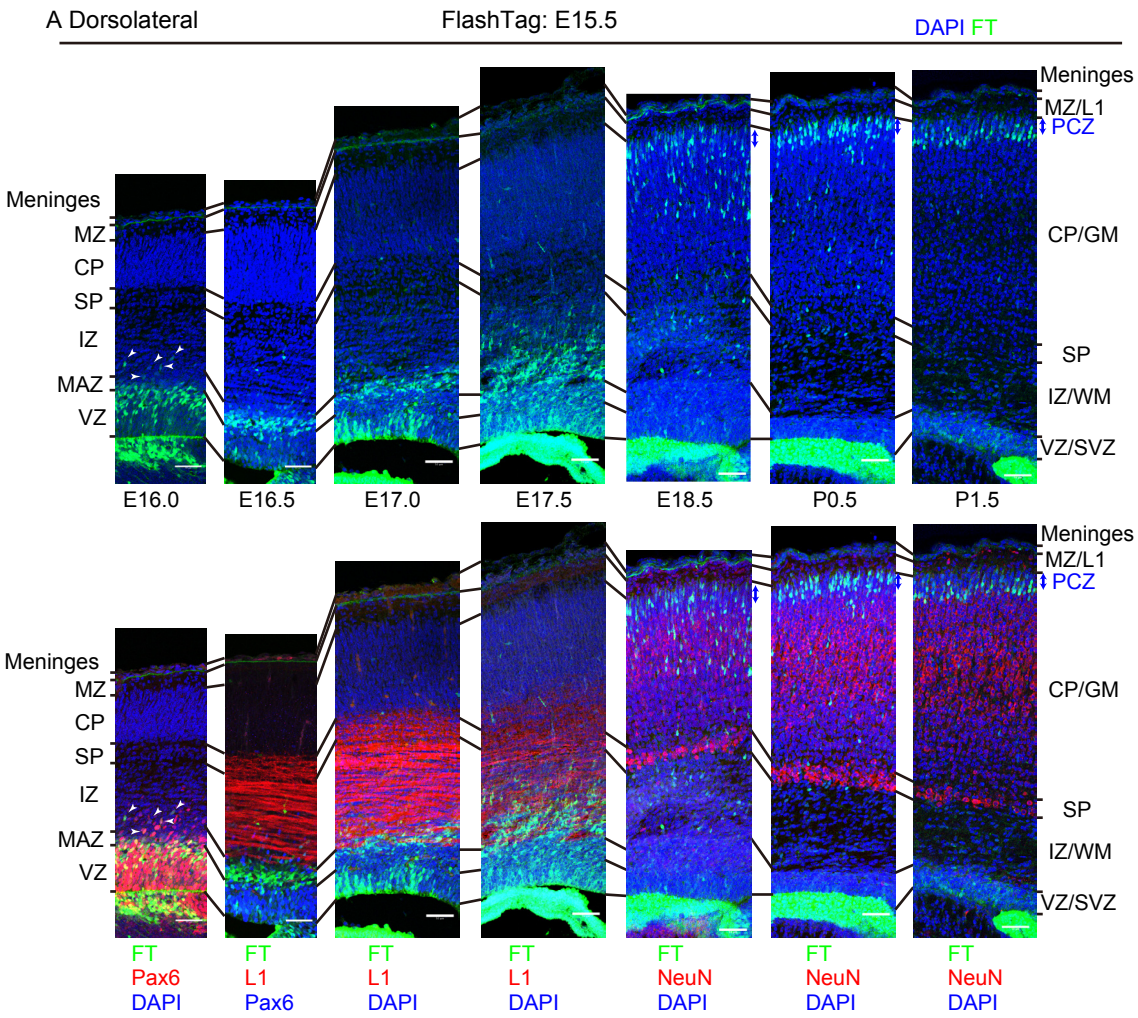
A Dorsolateral
FlashTag: E15.5
DAPI FT
Meninges
MZ
CP
SP
IZ
MAZ
VZ
MZ/L1
PCZ
CP/GM
SP
IZ/WM
VZ/SVZ
E16.0
E16.5
E17.0
E17.5
E18.5
P0.5
P1.5
FT Pax6 DAPI
FT L1 Pax6
FT L1 DAPI
FT L1 DAPI
FT NeuN DAPI
FT NeuN DAPI
FT NeuN DAPI

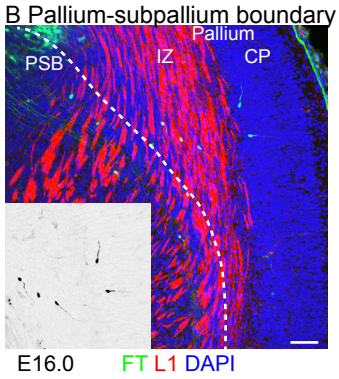
B Pallium-subpallium boundary
Pallium
PSB
IZ
CP
E16.0
FT L1 DAPI

Figure S11, related to Figure 6, S9, and S10

Dorsolateral higher-magnification micrographs of the cohort of cells born at E15.5.

A: Higher magnification micrographs from the dorsomedial cortices from E16.0–P1.5 are shown. Please refer to the legend of Figure S9 for a detailed explanation.

B: Higher-magnification of the pallial-subpallial boundaries (PSB) of E16.0 (0.5 day after injection) brains is shown. Around the PSB, a small number of labeled cells are seen in the IZ and CP with long leading processes.

Scale bars, 50 μm.

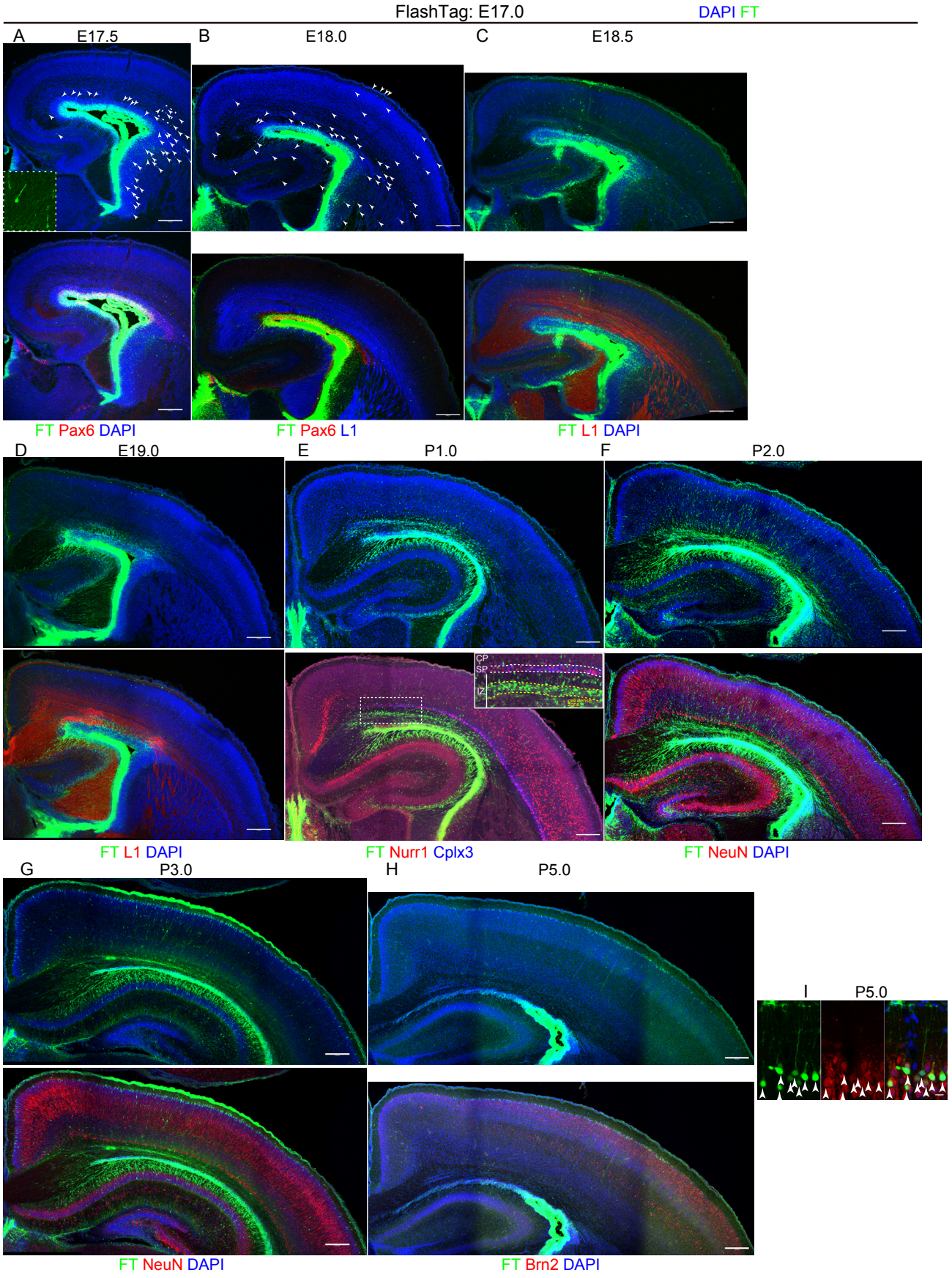
FlashTag: E17.0
DAPI FT
A E17.5
B E18.0
C E18.5
FT Pax6 DAPI
FT Pax6 L1
FT L1 DAPI
D E19.0
E P1.0
F P2.0
CP
SP
IZ
FT L1 DAPI
FT Nurr1 Cplx3
FT NeuN DAPI
G P3.0
H P5.0
I P5.0
FT NeuN DAPI
FT Brn2 DAPI
J FT at E17.0; fix at P1.0
J1
J2
J3
FT DAPI
J2
J3
J4
J5
J6
FT Hu DAPI
J4
J5
J6
FT Hu

Figure S12, related to Figure 7

Cohort of cells labeled at E17.0.

A–I: Coronal section of E17.5 (A), 18.0 (B), 18.5 (C), 19.0 (D), P1.0 (E), P2.0 (F), P3.0 (G), and P5.0 (H) brains labeled at E17.0. Higher-magnification images of these brains are shown in Figure 7C. At E17.5, most of the labeled cells are in the VZ (A). Some of the labeled cells are scattered in the brain parenchyma (arrowheads in A). At E18.0, most of the labeled cells are in the VZ and MAZ (B). Again, a small number of labeled cells are distributed throughout the cortex (arrowheads in B). At E18.5, many labeled cells are found in the MAZ (C). Some labeled cells are sparsely distributed throughout the cortex. At E19.0, many cells enter the L1-positive IZ dorsally (D). At P1.0, many labeled cells migrate in the IZ (E). Migrating cells migrate in a denser cellular zone sandwiched between L1-positive axon bundles (Figure 7A). This zone is deeper than the SP, as visualized by Nurr1 and Cplx3, SP neuron markers. At P2.0, many neurons migrate in the CP/cortical gray matter with a bipolar morphology (F). At P3.0, many labeled cells reach the dorsal PCZ (G). At P5.0, most of the labeled cells are in the most superficial part of the cortical gray matter (H) and are positive for NeuN (I).

J: At P1.0, labeled cells are migrating dorsally, ventrally (to the hippocampus), and, to a lesser extent, medially. Some labeled cells are also found in the VZ/SVZ. Most of these are positive for the neuronal marker Hu (J2–J6).

Scale bars, 200 μm (A–H, J1), 50 μm (J2–3), 20 μm (J4–6), 10 μm (I).

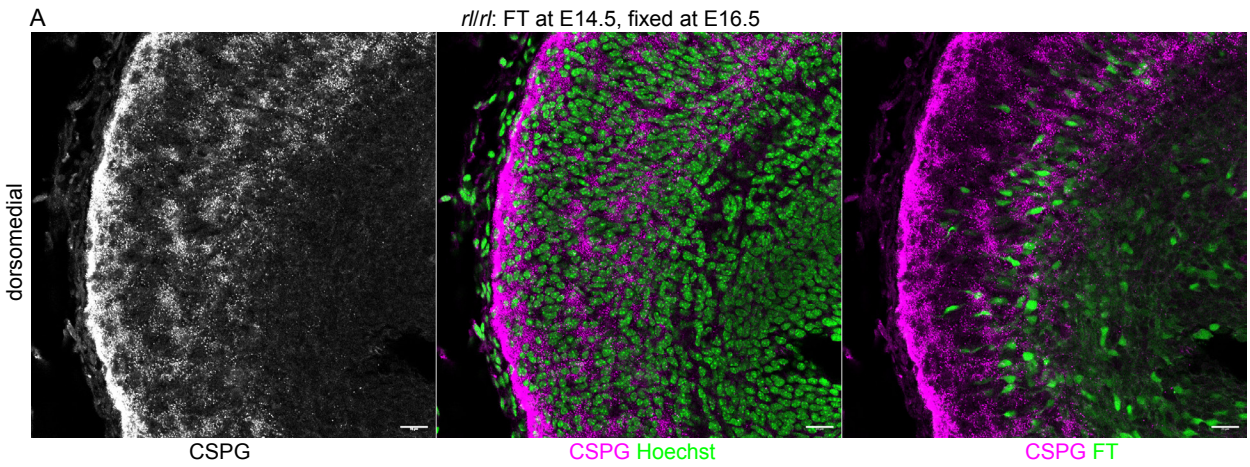
A
rl/rl: FT at E14.5, fixed at E16.5
dorsomedial
CSPG
CSPG Hoechst
CSPG FT

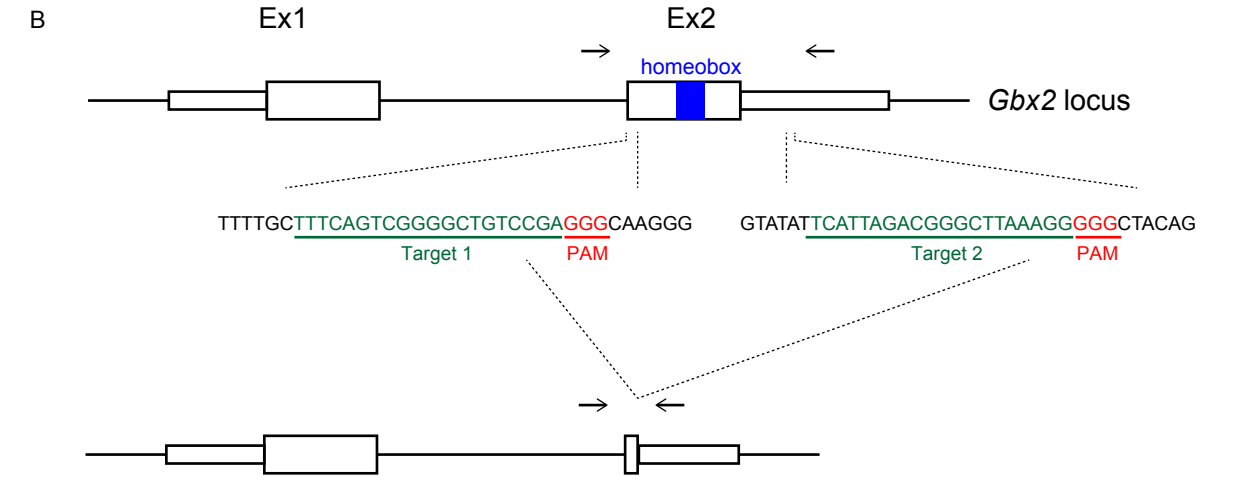
B
Ex1
Ex2
homeobox
Gbx2 locus
TTTTGCTTTCAGTCGGGGCTGTCCGAGGGCAAGGG
Target 1
PAM
GTATATTCATTAGACGGGCTTAAAGGGGGCTACAG
Target 2
PAM

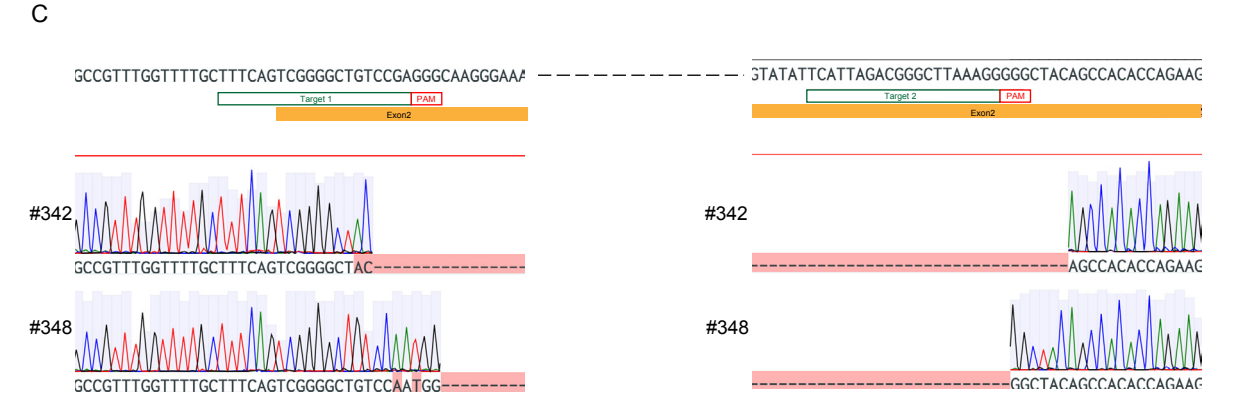
C
GCCGTTTGGTTTTGCTTTCAGTCGGGGCTGTCCGAGGGCAAGGGAAA
GTATATTCATTAGACGGGCTTAAAGGGGGCTACAGCCACACCAGAAG
Target 1
PAM
Exon2
Target 2
PAM
Exon2
#342
GCCGTTTGGTTTTGCTTTCAGTCGGGGCTAC----------
#342
----------AGCCACACCAGAAG
#348
GCCGTTTGGTTTTGCTTTCAGTCGGGGCTGTCCAATGG--------
#348
----------GGCTACAGCCACACCAGAAG

Figure S13, related to Figure 8

The internal plexiform zone in *reeler* mice and generation of *Gbx2* knockout mice using Crispr/Cas9.

A: A representative image of E16.5 dorsomedial *reeler* brains in which FT was performed at E14.5. FT-labeled cells tend to position along the internal plexiform zone labeled by CSPG. Scale bars, 20 μm.

B: A schematic diagram of our strategy to make a deletion in a region containing a homeobox domain. Key concepts of this strategy were based on mice generated in a previous study (Wassarman et al., 1997). Animals with an allele in which a region between Target 1 and Target 2 was deleted were screened by an electrophoretic band shift of the PCR products and were further confirmed by sequencing.

C: Direct sequencing of the PCR products amplified from the G0 mice.

Transparent Methods

KEY RESOURCES TABLE

REAGENT or RESOURCE	SOURCE	IDENTIFIER
Antibodies		
mouse monoclonal anti-BrdU	BD Biosciences	Cat# 347580; RRID:AB_2313824
goat polyclonal anti-Brn2	Santa Cruz	Cat# sc-6029; RRID:AB_2167385
mouse monoclonal anti-COUPTF2 (H7147)	R&D	Cat# PP-H7147-00; RRID:AB_2155627
rabbit polyclonal anti-Cplx3	Synaptic Systems	Cat# 122 302; RRID:AB_2281240
mouse monoclonal anti-CSPG (IgM; CS-56)	Abcam	Cat# ab11570; RRID:AB_298176
rat monoclonal anti-CTIP2 (25B6)	Abcam	Cat# ab18465; RRID:AB_2064130
goat polyclonal anti-fluorescein	Abcam	Cat# ab6655; RRID:AB_305628
chick polyclonal anti-GFAP	Abcam	Cat# ab4674; RRID:AB_304558
mouse monoclonal anti-Hu (16A11)	Molecular Probes	Cat# A-21271; RRID:AB_221448
rabbit polyclonal anti-KI67	Lab Vision	Cat# RB-1510-P1; RRID:AB_60160
rat monoclonal anti-L1 (clone 324)	Chemicon	Cat# MAB5272; RRID:AB_2133200
mouse monoclonal anti-Map2 (AP20)	Santa Cruz	Cat# sc-32791; RRID:AB_627948
Goat polyclonal anti-Netrin G1	R&D	Cat# AF1166; RRID:AB_2154822
rabbit polyclonal anti-NeuN	Millipore	Cat# ABN78; RRID:AB_10807945

goat polyclonal anti-Nurr1	R&D	Cat# AF2156; RRID:AB_2153894
goat polyclonal anti-OLIG2 (biotin-conjugated)	R&D	Cat# BAF2418; RRID:AB_2251803
rabbit polyclonal anti-Pax6	Covance	Cat# PRB-278P; RRID:AB_291612
rabbit polyclonal anti-phosphohistone H3 (Ser10)	Upstate	Cat# 06-570; cf. RRID:AB_310177
mouse monoclonal anti-Reelin (G10)	Abcam	Cat# ab78540; RRID:AB_1603148
goat polyclonal anti-SOX10	R&D	Cat# AF2864, RRID:AB_442208
goat polyclonal anti-SOX2	Santa Cruz	Cat# sc-17320, RRID:AB_2286684
rabbit polyclonal anti-Tbr1	Abcam	Abcam Cat# ab31940, RRID:AB_2200219
Chemicals and Proteins		
5- or 6-(N-Succinimidyloxycarbonyl) fluorescein 3',6'-diacetate (Cellstain CFSE)	Dojindo Molecular Technologies	Cat# C309
CytoTell Blue	AAT Bioquest	Cat# 22251
Dimethyl sulfoxide	Sigma-Aldrich	Cat# D2650
Hepes-buffered saline	Sigma-Aldrich	Cat# 51558
Ritodrine hydrochloride	WAKO	Cat# R3477
5-ethynyl-2'-deoxyuridine (EdU)	Invitrogen	Cat# A10044
5-bromo-2′-deoxyuridine (BrdU)	Sigma-Aldrich	Cat# B5002
Alt-R® S.p. Cas9 Nuclease V3, 100 µg	Integrated DNA Technologies	Cat# 1081058
Critical Commercial Assays		
Click-iT™ Plus EdU Cell Proliferation Kit for Imaging, Alexa Fluor™ 555 dye	Invitrogen	Cat# C10638
Experimental Models: Organisms/Strains		
wildtype ICR mice	Japan SLC	RRID:MGI:5462094

Wildtype C57BL/6NJcl mice	CLEA Japan	RRID:MGI:5659218
GAD67-GFP (∆*Neo*) mice (Tamamaki et al., 2003)	A gift from Dr. Yanagawa	RRID:IMSR_RBRC03674
B6CFe a/a-Relnrl/J mice	Jackson Laboratory	RRID:IMSR_JAX:000235
Gbx2 knockout mice	This manuscript	
Oligonucleotides		
A probe set for mouse *Htr3a* (NM_013561.2, probe number = 30)	Molecular Instruments	N/A, https://www.molecularinstruments.com/
fluorescence-labeled hairpins (B5-AlexaFluor647)	Molecular Instruments	N/A, https://www.molecularinstruments.com/
crRNA for *Gbx2* mutant, protospacer sequence for Target 1: UUUCAGUCGGGGCUGUCCGA	Integrated DNA Technologies	N/A, https://sg.idtdna.com/pages
crRNA for *Gbx2* mutant, protospacer sequence for Target 2: UCAUUAGACGGGCUUAAAGG	Integrated DNA Technologies	N/A, https://sg.idtdna.com/pages
Alt-R® CRISPR-Cas9 tracrRNA, 100 nmol	Integrated DNA Technologies	Cat# 1072534
Gbx2 primer, forward: CAGGAAATCGCAATGTGTTAATGTGG	Integrated DNA Technologies	N/A, https://sg.idtdna.com/pages
Gbx2 primer, reverse: TCAAAACACTGCAGCTGAGATCC	Integrated DNA Technologies	N/A, https://sg.idtdna.com/pages
Software and Algorithms		
CHOPCHOP	(Labun et al., 2019)	RRID:SCR_015723, http://chopchop.cbu.uib.no/
Fiji	(Schindelin et al., 2012)	RRID:SCR_002285, https://imagej.net/Fiji

LAS-X software	Leica	RRID:SCR_013673
Microsoft Excel for Mac	Microsoft	RRID:SCR_016137
Python 3.6	Python Software Foundation	RRID:SCR_008394, https://www.python.org/
Imaris 8.4.1	Oxford Instruments	RRID:SCR_007370, https://imaris.oxinst.com/packages

Experimental Model

Animals

Pregnant wild-type ICR (RRID:MGI:5462094) and C57BL/6NJcl mice (RRID:MGI:5659218) were purchased from Japan SLC (Shizuoka, Japan) and CLEA Japan (Tokyo, Japan). *GAD67-GFP* (ΔNeo) mice (Tamamaki et al., 2003) were provided by Dr. Yanagawa (Gunma University, Gunma, Japan), and heterozygous progenies were backcrossed to wild-type ICR mice. Heterozygous males were mated with wild-type ICR mice and used in the experiments. *Reeler* mice (B6CFe a/a-*Reln*^{rl}/J; RRID:IMSR_JAX:000235) were obtained from the Jackson Laboratory and maintained by mating heterozygous females with homozygous males. The day on which a vaginal plug was detected was considered embryonic day (E) 0. Dams, pups, and weaned animals were kept under a 12/12-hour light/dark cycle in a temperature-controlled room. The animals had free access to food and water. Embryos and pups of both sexes were indiscriminately analyzed because sexes cannot be macroscopically determined. All animal experiments were performed according to the Institutional Guidelines on Animal Experimentation at Keio University. The experimental protocols for the animal experiments were approved by the Keio University Institutional Animal Care and Use Committee.

Methodological Details

FT Surgical procedures

Pregnant mice were deeply anesthetized, the uterine horns were exposed, and the lateral and third ventricles of the embryos were identified. The trans-illumination method (Shimogori and Ogawa, 2008), in which the tip of a flexible fiber light, moistened with warm phosphate-buffered saline (PBS), was gently pushed against the uterine horn, was utilized to visualize small embryos of

E10.5 and 11.5. At these early stages, 200 μL of 0.1 mg/mL ritodrine hydrochloride (WAKO, now FUJIFILM Wako Pure Chemical Corporation, Osaka, Japan) was injected intraperitoneally to relax the myometrium (Nishiyama et al., 2012; Takeo, 2016; Takeo et al., 2015). FT (Telley et al., 2016) was performed in their intrauterine embryos with some modifications. A 10 mM 5- or 6-(N-succinimidyloxycarbonyl) fluorescein 3',6'-diacetate (Cellstain CFSE, C309, Dojindo Molecular Technologies, Inc., Kumamoto, Japan) working stock was prepared by dissolving CFSE in dimethyl sulfoxide (DMSO) (Hybri-Max™, Sigma-Aldrich, St. Louis, MO). The working solution was further diluted with 1X Hepes-buffered saline (HBS) to make a 1-mM solution just before surgery. The solution was colored with Fast Green (final concentration 0.01–0.05%) to monitor successful injection. In experiments using GAD67-GFP mice, CytoTell Blue (22251, AAT Bioquest, Sunnyvale, CA) was used instead of CFSE. Approximately 0.5 μL of the prepared FT solution was injected into the lateral ventricle. After applying plenty of PBS into the abdominal cavity and onto the surface of manipulated uterine horns, injected embryos were placed back into the abdominal cavity.

Administration of thymidine analogs

EdU and BrdU (Sigma) were dissolved in PBS at 5 mg/mL and 10 mg/mL, respectively. Bolus intraperitoneal injection of EdU or BrdU solution was performed at 25 μg/g body weight (BW) and 50 μg/gBW, respectively.

Histological terminology

The VZ and SVZ were determined according to the definition provided by Boulder's Committee (Boulder-Committee, 1970). Because the VZ is a pseudostratified columnar epithelium, the nuclei, by definition, are mostly radially oriented. The basal border of the VZ nuclei could also be determined by staining with a radial glial marker, Pax6 (Englund et al., 2005) or acute administration of a thymidine analog (Tabata et al., 2012) because the nuclei of radial glia in the S-phase occupy a basal zone of the VZ (interkinetic nuclear migration). Just above the VZ is a zone that we previously named the MAZ (Tabata et al., 2009), where multipolar cells that have just exited the VZ transiently accumulate. The cell density of this zone is high, and nuclei are randomly oriented (Bayer and Altman, 1991; Yoshinaga et al., 2012). Although many cells in the MAZ are postmitotic (Tabata et al., 2009), there are some cycling cells in the MAZ. The MAZ and the lower part of the SVZ, which was originally characterized as abventricular cells with proliferative activity by Boulder's Committee, overlaps. Just above the MAZ is a zone rich in L1-positive axonal fibers (Yoshinaga et al., 2012) and the somata of immature migrating neurons. We called this zone the IZ

according to Boulder's Committee's suggestion. The SP layer, which was described after Boulder's Committee, defined histological terminology, was excluded from the IZ in the current study because the main component is relatively mature SP neurons. The original description by the Boulder Committee defined the IZ and SVZ as distinct regions, but because we observed many proliferative cells in the axon-rich area (Tabata et al., 2009; Vaid et al., 2018) (Figures 1A–D), the IZ in our definition and the SVZ inevitably overlap. Collectively, the SVZ starts from the MAZ extending into the IZ in our definition. Therefore, we preferred the use of MAZ and IZ to describe neuronal migration more precisely, except for contexts stressing abventricular mitosis. We defined the SP according to cytoarchitectonic criteria and the presence of abundant CSPG (Bicknese et al., 1994) and/or other SP markers. The CP was determined by cytoarchitectonic criteria (high cellularity, radial orientation of the nuclei (Olson, 2014)) and/or weak immunoreactivity for CSPG (Bicknese et al., 1994). The primitive cortical zone, or PCZ (Sekine et al., 2011; Shin et al., 2019), was determined by weak or absent NeuN staining in the CP. The marginal zone was determined by cytoarchitectonic criteria–the most superficial hypocellular zones just above the CP. Before the formation of the CP, the zone between the proliferative zone (i.e., the VZ at this stage) and the meningeal surface was named the PP (Bystron et al., 2008), although this area might include intermediate progenitors (Vasistha et al., 2015). The cytoarchitecture changes as development proceeds, as summarized in Figure S1B.

The definition of the dorsomedial, dorsal, and dorsolateral cortex in coronal sections is provided in Figure S1A. We obtained images at the rostrocaudal axis of the foramina of Monro unless otherwise specified. We obtained dorsolateral high-magnification images from the lateral borders of regions that cross the pallial-subpallial angles. We obtained dorsomedial high-magnification images from regions adjacent to the medial protrusion of the lateral ventricles. In most cases, the images were corrected so that the apicobasal axes were parallel to a line that passed the medial protrusion of the lateral ventricles and the ipsilateral pallial-subpallial angles. In the late stages of cortical development, dorsomedial high-magnification images were shown dorsal-up because lines that pass the medial protrusion of the lateral ventricles and the ipsilateral pallial-subpallial angels are no longer parallel to the apicobasal axes nor perpendicular to the meningeal surfaces.

Histological sample preparation.

The harvested embryonic brains were fixed by immersion in 4% paraformaldehyde (PFA) at 4°C with gentle agitation for 1 h to overnight. The postnatal embryos were perfused with ice-cold

4% PFA, and their brains were further fixed by immersing in 4% PFA at 4°C with gentle agitation for several hours overnight. The brains were cryoprotected by immersion in 20% and 30% sucrose in PBS at 4°C for several hours to overnight sequentially, embedded in 75% O.C.T. compound (Sakura, Tokyo, Japan) (O.C.T: 30% sucrose = 3:1) and frozen with liquid nitrogen. Brains were cryosectioned coronally at 20 μm thickness on MAS-coated slides (MAS-02; Matsunami Glass Ind., Ltd., Osaka, Japan).

For immunohistochemistry, sections were immersed in PBS with 0.01% Triton X-100 (Sigma-Aldrich, St. Louis, MO) (PBS-Tx) for more than 30 min at room temperature (RT). Antigen retrieval was performed in most of the experiments by incubating in 1x HistoVT ONE (NACALAI TESQUE, INC., Kyoto, Japan) at 70°C for 20 min. To detect BrdU, sections were treated with sodium citrate buffer (pH 6) at 105°C for 5 min and with 2 M hydrogen chloride at 37°C for 30 min. To detect EdU, sections were treated with 2 M hydrogen chloride at 37°C for 30 min in some experiments. The sections were blocked with 10% normal goat serum in PBS-Tx at RT and incubated with the primary antibody overnight at 4°C. After washing with PBS-Tx three times, the sections were incubated with secondary antibodies for 1 h at RT. The details of the primary antibodies are shown in the Key Resources Table and the antibody characterization section.

Histological detection of EdU was performed using the Click-iT™ EdU Cell Proliferation Kit for Imaging and Alexa Fluor™ 555 dye (C10338, Thermo Fisher Scientific) according to the manufacturer's protocol.

When nuclear staining was performed without immunohistochemistry, sections were immersed in PBS for more than 30 min at RT and incubated with 2.5 ng/μL of 4',6-diamidino-2-phenylindole (DAPI; D3571; Thermo Fisher Scientific, Waltham, MA), 0.5 μM of TO-PRO3 Iodide (T3605, Thermo Fisher Scientific), or 10 ng/μL of Hoechst 33342 (H-3570; Molecular Probes, Eugene, OR) at RT for 1 h. When nuclear staining was performed with immunohistochemistry, DAPI was added to the secondary antibody solution. Sections were mounted using PermaFluor ® (TA-030-FM; Thermo Fisher Scientific).

Antibody Characterization

The antibodies used in this study were listed in Key Resource Table. The mouse anti-BrdU antibody (clone B44) (Tabata et al., 2009) was used to detect nuclei of cells that were in the S phase when BrdU was administered. This antibody is derived from hybridization of mouse Sp2/0-Ag14 myeloma cells with spleen cells from BALB/c mice immunized with iodouridine-conjugated ovalbumin (manufacturer's datasheet and a previous report (Gratzner, 1982)). This antibody detects

BrdU (but not thymidine) in single-stranded DNA, free BrdU, or BrdU coupled to a protein carrier. The antibody also reacts with iodouridine, which was not used in this study.

An anti-Brn2 antibody was used as a layer II/III/V marker (Oishi et al., 2016). This antibody was raised against a peptide mapping at the C-terminus of *BRN2* of human origin (manufacturer's datasheet). Although previous study suggested that this antibody detects both Brn1 and Brn2 in western blotting (Yamanaka et al., 2010), we believe that this antibody predominantly detects Brn2 in immunohistochemistry of perinatal cortical slices, because electroporation of a shRNA against *Brn2* significantly diminished immunoreactivity of this antibody but not of anti-Brn1 antibody while electroporation of a shRNA against *Brn1* did not significantly diminish immunoreactivity of this antibody in immunohistochemistry (Oishi et al., 2016). Even if this antibody detects Brn1 as well, its expression pattern is similar to that of Brn2 in the developing cerebral cortex and the use of this antibody as a layer marker would be justified.

An anti-COUP-TF II antibody was used to label CGE- and PoA-derived interneurons (Kanatani et al., 2015; Kanatani et al., 2008). This mouse monoclonal antibody was raised against recombinant human COUP-TF II (amino acids 43-64) (manufacturer's datasheet). The specificity of this antibody was previously confirmed by absence of immunohistochemical staining in a Couptf2 conditional knockout tissue (Suh et al., 2006).

An anti-Cplx3 antibody was used to label the SP in the postnatal stage (Hoerder-Suabedissen et al., 2009). This antibody was raised against recombinant mouse Complexin3 (amino acids 1-158) (manufacturer's datasheet). The specificity of this antibody was previously confirmed by absence of signals in a *Cplx3* knockout tissue in immunohistochemistry and western blotting (Reim et al., 2009).

An anti-CSPG antibody was used to label the PP, MZ and SP (Bicknese et al., 1994). This antibody was well characterized elsewhere (Yi et al., 2012).

Ctip2/Bcl11b was used as a deep layer marker (Arlotta et al., 2005). Anti-CTIP2 rat monoclonal antibody was raised against a fusion protein corresponding to human CTIP2 (amino acids 1-150). This antibody detects two bands representing Ctip2 at about 120kD (manufacturer's datasheet). This antibody detected nuclear staining in wildtype mice while no signals in *Ctip2*-null mice on immunohistochemistry (Zhang et al., 2012).

A goat anti-fluorescein antibody was used to boost FT signals when brains were analyzed days after FT injection and fluorescent labeling was weak. This antibody was raised against fluorescein conjugated to goat IgG. Western blotting detected BSA conjugated fluorescein

(manufacturer's datasheet). This antibody enhanced fluorescence from FT-labeled cells, but no signal was detected in untreated (CFSE was not injected) brains (data not shown).

A mouse anti-Hu monoclonal antibody was used as a neuronal marker (Marusich et al., 1994; Tabata and Nakajima, 2003). This antibody was raised against a human HuD peptide (QAQRFRLDNLLN-C)-Keyhole Limpet Hemocyanin conjugate, and recognizes HuC, HuD and HuDpro in western blotting (Marusich et al., 1994). This antibody showed immunoreactivity similar to human anti-Hu autoantibody in western blotting of human neuron extract, which was blocked by synthetic HuD peptide (Marusich et al., 1994).

A rabbit anti-Ki-67polyclonal antibody was used to label proliferating cells. This antibody was raised against a synthetic peptide from the human Ki-67 protein. Immunohistochemistry of human lymph nodes resulted in nuclear staining of germinal center (manufacturer's datasheet). Proliferating reactive astrocytes (Chen et al., 2017) and colorectal carcinoma foci (Zhao et al., 2017) were reported to be specifically labeled. Immunohistochemistry of developing mouse cortex resulted in nuclear staining of the proliferative zones including VZ and SVZ, as previously published (Watanabe et al., 2018).

L1 immunohistochemistry was performed to label the IZ rich in axons including thalamocortical and corticofugal axons (Fukuda et al., 1997; Kudo et al., 2005; Yoshinaga et al., 2012). The antibody used was raised against glycoprotein fraction from cerebellum of 8-10 day old C57BL/6J mice. The same clone from the previous vendor did not stain fiber bundles in the *L1*-null mice (Fransen et al., 1998).

An anti-Map2 monoclonal antibody [AP20] was used as a SP marker (Ohtaka-Maruyama et al., 2013; Ohtaka-Maruyama et al., 2018). This antibody was raised against cow MAP-2 (amino acids 997-1332), and detects bands corresponding to MAP2A/B on western blotting (manufacturer's datasheet). Immunohistochemistry of developing mouse cortex resulted in an identical staining pattern previously reported with another antibody against MAP2 (AB5622; Merck Millipore) (Ohtaka-Maruyama et al., 2013; Ohtaka-Maruyama et al., 2018).

Netrin G1 immunohistochemistry was used to mark thalamocortical axons (Nakashiba et al., 2002). The anti-Netrin G1a antibody was raised against purified insect cell line *Sf* 21-derived recombinant mouse Netrin-G1a (rmNetrin-G1a) (manufacturer's datasheet). Mouse Netrin-G1a specific IgG was purified by mouse Netrin-G1a affinity chromatography. Manufacturer's datasheet states that this antibody shows less than 2% cross-reactivity with rmNetrin-1, rchNetrin-2 and rhNetrin-4. Cortical immunoreactivity was lost in *Gbx2* conditional knockout mice, in which thalamocortical axons failed to innervate (Vue et al., 2013).

NeuN immunohistochemistry was used to label neuronal cells. The anti-NeuN antibody used is an affinity purified rabbit polyclonal antibody raised against GST-tagged recombinant mouse NeuN N-terminal fragment (ABN78, Millipore) (manufacturer's datasheet). This antibody is a rabbit polyclonal version of anti NeuN antibody (mouse monoclonal, MAB377, Millipore, clone A60), and has been widely used as a neuronal marker by authors of many different literatures [e.g. (Ataka et al., 2013; Huang et al., 2015; Lundgaard et al., 2015).] Immunohistochemistry of *Rbfox3/NeuN*-null tissue using this antibody and the mouse monoclonal antibody (clone A60), which also has been widely used as a neuronal marker and was extensively characterized by western blotting and 2D electrophoresis (Lind et al., 2005), detected no signals (Lin et al., 2018). Double immunohistochemistry using ABN78 and A60 resulted in an identical staining pattern (data not shown).

A goat anti-Nurr1 antibody was used to label the SP neurons. This antibody was raised against *E. coli*-derived recombinant mouse Nurr1 (Val332-Lys558) (manufacturer's datasheet), and reported to detect the nuclei of the SP neurons (Hoerder-Suabedissen et al., 2009; Ozair et al., 2018; Pedraza et al., 2014). No signal was detected in *Nurr1*-deficient mice (data not shown).

A rabbit polyclonal anti-phospho-histone H3 antibody (Ser10) (06-570, Upstate, Spartanburg, SC) was used to label mitotic cells (Hendzel et al., 1997; Kim et al., 2017). This antibody was raised against a short peptide from the amino-terminus of H3 from amino acids 7-20 (A7RKSTGGKAPRKQL20C) synthesized containing a single phosphorylated serine at position 10 (Hendzel et al., 1997). This antibody detected a single band in whole cell protein and acid-soluble nuclear protein from Colcemid-treated mitotic Hela cells but did not detect in whole cell protein and acid-soluble nuclear protein from interphase enriched preparation (Hendzel et al., 1997).

A rabbit anti-Pax6 antibody was used to label radial glial cells. This antibody was raised against a peptide (QVPGSEPDMSQYWPRLQ) derived from the C-terminus of the mouse Pax-6. Western blotting of mouse Raw264.7 cells detects a single band (manufacturer's datasheet). In the cerebellum of chimera mice made from wildtype and Pax6-null cells, nuclear immunoreactivity was detected in wildtype granular cells while no signal was detected in Pax6 null cells (Swanson and Goldowitz, 2011). In our study, nuclear immunoreactivity was detected in the majority of the VZ cells (Englund et al., 2005) and small number of extra-VZ cells, as expected (Shitamukai et al., 2011; Vaid et al., 2018).

Reelin was used as a marker for Cajal-Retzius cells (Ogawa et al., 1995). Anti-Reelin monoclonal antibody [G10] was raised against a recombinant fusion protein, corresponding to amino acids 164-496 of Mouse Reelin. This antibody detects an expected 388kDa band on western

blotting (manufacturer's technical information). On immunohistochemistry, this antibody detected Cajal-Retzius cells in the marginal zone in the developing wildtype cortex but no signal was detected in the *reeler* cortex except for blood vessels (Ishii et al., 2019), confirming its specificity.

A goat anti-Sox2 polyclonal antibody was used to label nuclei of radial glia. This antibody is an affinity purified antibody raised against a peptide mapping near the C-terminus of human SOX2. Western blotting of human and mouse embryonic stem cells detected a single band at 34 kDa (manufacturer's datasheet). Immunohistochemistry of developing mouse (Vaid et al., 2018; Watanabe et al., 2018) and human cortex (Nowakowski et al., 2016) resulted in labeling of radial glial cells in the VZ and SVZ.

Tbr1 has been widely used as a marker for postmitotic neurons of the PP, SP and deep layer (Hevner et al., 2001). The detailed information about the antibody used in the current study was described elsewhere (Betancourt et al., 2014).

A chicken anti-GFAP antibody was used to label astrocytes. This chicken polyclonal IgY antibody was raised against a recombinant full-length protein corresponding to Human GFAP, isotype 1. Western blotting of mouse and rat cortical lysates detected a single band (manufacturer's datasheet). A number of studies have used this antibody to label astrocytes (Saliu et al., 2014). In GFAP-Cre driven GFP transgenic mice, immunoreactivity from this antibody showed excellent colocalization with GFP signals (Suarez-Mier and Buckwalter, 2015), confirming its specificity.

A goat anti-SOX10 antibody and goat anti-OLIG2 antibody was used to label oligodendrocyte (Stolt et al., 2002; Zhou et al., 2000) progenitors and oligodendrocyte + astrocyte progenitors(Tatsumi et al., 2018), respectively. The anti-SOX10 antibody was raised against *E. coli*-derived recombinant human SOX10 (Met1-Ala118) (manufacturer's datasheet) and has been widely used to label cells of the oligodendrocyte lineage in many literatures including mouse spinal cord (Kelenis et al., 2018) and dorsal cortex (Winkler et al., 2018) in immunohistochemistry. The anti-OLIG2 antibody used in this study was raised against *E. coli*-derived recombinant human SOX10 (Met1-Ala118). In Western blots, less than 5% cross-reactivity with recombinant human (rh) OLIG1 and rhOLIG3 is observed, according to the manufacturer's technical information. This antibody has been used to label cells of the glial progenitors on immunohistochemistry (Tabata et al., 2009).

In situ HCR

Fluorescent *in situ* hybridization was performed using in situ HCR v3.0 (Choi et al., 2018). E18.0 brains, in which FT was performed at E17.0, were perfused with ice-cold 4% PFA and post-fixed overnight at 4°C. Brains were embedded in 3% low-melting agarose gel and vibratomed at

100 μm. Brain slices were preserved at -20°C in a cryoprotectant solution (30% w/v sucrose, 1% w/v polyvinyl-pyrrolidone (PVP)-40, 30% v/v ethylene glycol in PBS) until use. Brain slices were washed in PBS for 5 min at RT, and incubated in a hybridization solution (Molecular Instruments, Los Angeles, CA) at 37°C in a 96-well plate with agitation (a round shaker, 200 rpm). The probe set for mouse *Htr3a* (NM_013561.2, probe number = 30) was designed and purchased from Molecular Instruments. Brain slices were incubated with 4-nM probes overnight at 37°C with agitation. After washing with a prewarmed wash solution (Molecular Instruments) for 15 min three times at 37°C with agitation, and with 5x SSC with 0.1% Tween20 (5x SSCT) for 5 min three times at RT with agitation, sections were incubated with fluorescence-labeled hairpins (B5-AlexaFluor647) reconstituted with an amplification solution (Molecular Instruments) overnight at RT with agitation. After washing with 5x SSCT for more than 5 min three times at RT with agitation, and counterstaining with DAPI, brain slices were mounted using PermaFluor on MAS-coated glass slides. This resulted in essentially the same staining pattern as previously described (Murthy et al., 2014).

Image Acquisition from glass-slide samples

Fluorescence images were acquired using confocal laser scanning microscopy (FV1000; Olympus, Tokyo, Japan & TCS SP8; Leica, Wetzlar, Germany). Stitching was performed with LAS-X software (Leica) (RRID:SCR_013673) equipped with a Leica confocal microscope, when necessary. Images were analyzed with Fiji (RRID:SCR_002285) (Schindelin et al., 2012). Linear changes in tone and background subtraction were performed. Maximum projection images of optical slices were obtained to show the morphology of the entire cortical wall. Single optical slices were shown to evaluate the colocalization of signals from different channels.

Whole-brain imaging and generation of 3D movies

Three-dimensional imaging of the whole brain was performed using block-face serial microscopy tomography (FAST) (Seiriki et al., 2017; Seiriki et al., 2019) with some modifications. Briefly, brains were perfused with ice-cold PBS and ice-cold 4% PFA. The harvested brains were post-fixed for one week at 4°C. The fixed brains were stained with Hoechst33258 (Seiriki et al., 2019) and embedded in the previously reported 4% oxidized agarose (Ragan et al., 2012). Subsequently, whole-brain images were obtained at a spatial resolution of 1.0 × 1.0 × 5.0 μm^3. The resulting section images were stitched by FASTitcher, written in Python 3.6 (Seiriki et al., 2019). We

generated 3D-rendered movies from 2D stacks of serial stitched images using Imaris 8.4.1 (Bitplane, Belfast, UK).

Time-Lapse Analyses

Coronal brain slices (200 μm thick) were prepared by a vibratome and cultured in Neurobasal medium (NB) containing 2% B27 (Invitrogen) on MilliCell-CM culture plate inserts (PICM03050; Merck KGaA, Darmstadt, Germany). The dishes were then mounted in a CO_2 incubator (40% O_2, 65% N_2, 5% CO_2 at 37°C) fitted onto a confocal microscope, TCS SP8. Approximately 10–20 optical Z-sections were obtained automatically every 30 min. Using Fiji, photobleaching was linearly corrected afterward to maintain the signal strength of the labeled cells, to enable visual evaluation of the migration profiles.

i-GONAD

CRISPR guide RNAs were designed using CHOPCHOP (Labun et al., 2019). The synthetic crRNAs, tracrRNA, and Cas9 protein were commercially obtained as Alt-R™ CRISPR guide RNAs from Integrated DNA Technologies (Coralville, IA) and Alt-R™S.p. Cas9 Nuclease V3. Adult ICR mice were purchased from Japan SLC. Females in estrus were mated with stud males. The females used were not superovulated. Surgical procedures for i-GONAD (Gurumurthy et al., 2019; Ohtsuka et al., 2018) were performed at around E0.7 (around 4 pm of the day in which a vaginal plug was detected) under deep anesthesia. A mixture of 15 μM gRNA for Target 1, 15 μM gRNA for Target 2, and 1 μg/L Cas9 protein was prepared in Opti-MEM. A 0.02% Fast Green solution was used to monitor successful injection. Approximately 1.5 μL of electroporation solution was injected into the oviduct from upstream of the ampulla using a glass micropipette. Electroporation was performed using NEPA21 (NEPA GENE, Tokyo, Japan) (poring pulse: 50 V, 5 ms pulse, 50 ms pulse interval, 4 pulses, 10% decay, single pulse orientation, and transfer pulse: 10 V, 50 ms pulse, 50 ms pulse interval, 3 pulses, 40% decay, ± pulse orientation). Animals carrying the expected deletion were mated with wild-type ICR mice.

Quantification and Statistical Analysis

Histological samples were evaluated by visual inspection. Careful anatomical and qualitative analyses were performed in most of the experiments. All quantitative data presented are expressed as arithmetic mean ± SEM, and the exact values of n (number of brains) are provided in

the Results section and in the Figure Legends. Descriptive statistical values, including mean, SEM, proportion, and *t*-test were calculated using Microsoft Excel for Mac (RRID:SCR_016137).

Supplemental References

Arlotta, P., Molyneaux, B.J., Chen, J., Inoue, J., Kominami, R., and Macklis, J.D. (2005). Neuronal subtype-specific genes that control corticospinal motor neuron development in vivo. Neuron 45, 207-221.

Ataka, K., Asakawa, A., Nagaishi, K., Kaimoto, K., Sawada, A., Hayakawa, Y., Tatezawa, R., Inui, A., and Fujimiya, M. (2013). Bone marrow-derived microglia infiltrate into the paraventricular nucleus of chronic psychological stress-loaded mice. PLoS One 8, e81744.

Bayer, S.A., and Altman, J. (1991). Neocortical development (Raven Press New York).

Betancourt, J., Katzman, S., and Chen, B. (2014). Nuclear factor one B regulates neural stem cell differentiation and axonal projection of corticofugal neurons. J. Comp. Neurol. 522, 6-35.

Bicknese, A.R., Sheppard, A.M., Leary, D.D., and Pearlman, A.L. (1994). Thalamocortical axons extend along a chondroitin sulfate proteoglycan- enriched pathway coincident with the neocortical subplate and distinct from the efferent path. J. Neurosci. 14, 3500-3510.

Boulder-Committee (1970). Embryonic vertebrate central nervous system: revised terminology. The Boulder Committee. Anat. Rec. 166, 257-261.

Bystron, I., Blakemore, C., and Rakic, P. (2008). Development of the human cerebral cortex: Boulder Committee revisited. Nat. Rev. Neurosci. 9, 110-122.

Chen, J., He, W., Hu, X., Shen, Y., Cao, J., Wei, Z., Luan, Y., He, L., Jiang, F., and Tao, Y. (2017). A role for ErbB signaling in the induction of reactive astrogliosis. Cell Discov 3, 17044.

Choi, H.M.T., Schwarzkopf, M., Fornace, M.E., Acharya, A., Artavanis, G., Stegmaier, J., Cunha, A., and Pierce, N.A. (2018). Third-generation in situ hybridization chain reaction: multiplexed, quantitative, sensitive, versatile, robust. Development 145, dev165753.

Englund, C., Fink, A., Lau, C., Pham, D., Daza, R.A., Bulfone, A., Kowalczyk, T., and Hevner, R.F. (2005). Pax6, Tbr2, and Tbr1 are expressed sequentially by radial glia, intermediate progenitor cells, and postmitotic neurons in developing neocortex. J. Neurosci. 25, 247-251.

Fransen, E., D'Hooge, R., Van Camp, G., Verhoye, M., Sijbers, J., Reyniers, E., Soriano, P., Kamiguchi, H., Willemsen, R., Koekkoek, S.K.*, et al.* (1998). L1 knockout mice show dilated ventricles, vermis hypoplasia and impaired exploration patterns. Hum. Mol. Genet. 7, 999-1009.

Fukuda, T., Kawano, H., Ohyama, K., Li, H.-P., Takeda, Y., Oohira, A., and Kawamura, K. (1997). Immunohistochemical localization of neurocan and L1 in the formation of thalamocortical pathway of developing rats. J. Comp. Neurol. 382, 141-152.

Gratzner, H.G. (1982). Monoclonal antibody to 5-bromo- and 5-iododeoxyuridine: A new reagent for detection of DNA replication. Science 218, 474.

Gurumurthy, C.B., Sato, M., Nakamura, A., Inui, M., Kawano, N., Islam, M.A., Ogiwara, S., Takabayashi, S., Matsuyama, M., Nakagawa, S.*, et al.* (2019). Creation of CRISPR-based germline-genome-engineered mice without ex vivo handling of zygotes by i-GONAD. Nat. Protoc. 14, 2452-2482.

Hendzel, M.J., Wei, Y., Mancini, M.A., Van Hooser, A., Ranalli, T., Brinkley, B.R., Bazett-Jones, D.P., and Allis, C.D. (1997). Mitosis-specific phosphorylation of histone H3 initiates primarily within pericentromeric heterochromatin during G2 and spreads in an ordered fashion coincident with mitotic chromosome condensation. Chromosoma : Zeitschrift für Zellkern-und Chromosomenforschung. 106, 348-360.

Hevner, R.F., Shi, L., Justice, N., Hsueh, Y., Sheng, M., Smiga, S., Bulfone, A., Goffinet, A.M., Campagnoni, A.T., and Rubenstein, J.L. (2001). Tbr1 regulates differentiation of the preplate and layer 6. Neuron 29, 353-366.

Hoerder-Suabedissen, A., Wang, W.Z., Lee, S., Davies, K.E., Goffinet, A.M., Rakic, S., Parnavelas, J., Reim, K., Nicolic, M., Paulsen, O.*, et al.* (2009). Novel markers reveal subpopulations of subplate neurons in the murine cerebral cortex. Cereb. Cortex 19, 1738-1750.

Huang, B., Wei, W., Wang, G., Gaertig, M.A., Feng, Y., Wang, W., Li, X.J., and Li, S. (2015). Mutant huntingtin downregulates myelin regulatory factor-mediated myelin gene expression and affects mature oligodendrocytes. Neuron 85, 1212-1226.

Ishii, K., Kohno, T., and Hattori, M. (2019). Differential binding of anti-Reelin monoclonal antibodies reveals the characteristics of Reelin protein under various conditions. Biochem. Biophys. Res. Commun. 514, 815-820.

Kanatani, S., Honda, T., Aramaki, M., Hayashi, K., Kubo, K., Ishida, M., Tanaka, D.H., Kawauchi, T., Sekine, K., Kusuzawa, S.*, et al.* (2015). The COUP-TFII/Neuropilin-2 is a molecular switch steering diencephalon-derived GABAergic neurons in the developing mouse brain. Proc. Natl. Acad. Sci. U. S. A. 112, E4985-4994.

Kanatani, S., Yozu, M., Tabata, H., and Nakajima, K. (2008). COUP-TFII Is Preferentially Expressed in the Caudal Ganglionic Eminence and Is Involved in the Caudal Migratory Stream. J. Neurosci. 28, 13582–13591.

Kelenis, D.P., Hart, E., Edwards-Fligner, M., Johnson, J.E., and Vue, T.Y. (2018). ASCL1 regulates proliferation of NG2-glia in the embryonic and adult spinal cord. Glia 66, 1862-1880.
Kim, J.-Y., Jeong, H.S., Chung, T., Kim, M., Lee, J.H., Jung, W.H., and Koo, J.S. (2017). The value of phosphohistone H3 as a proliferation marker for evaluating invasive breast cancers: A comparative study with Ki67. Oncotarget 8, 65064-65076.
Kudo, C., Ajioka, I., Hirata, Y., and Nakajima, K. (2005). Expression profiles of EphA3 at both the RNA and protein level in the developing mammalian forebrain. J. Comp. Neurol. 487, 255-269.
Labun, K., Montague, T.G., Krause, M., Torres Cleuren, Y.N., Tjeldnes, H., and Valen, E. (2019). CHOPCHOP v3: expanding the CRISPR web toolbox beyond genome editing. Nucleic Acids Res. 47, W171-W174.
Lin, Y.S., Kuo, K.T., Chen, S.K., and Huang, H.S. (2018). RBFOX3/NeuN is dispensable for visual function. PLoS One 13, e0192355.
Lind, D., Franken, S., Kappler, J., Jankowski, J., and Schilling, K. (2005). Characterization of the neuronal marker NeuN as a multiply phosphorylated antigen with discrete subcellular localization. J. Neurosci. Res. 79, 295-302.
Lundgaard, I., Li, B., Xie, L., Kang, H., Sanggaard, S., Haswell, J.D., Sun, W., Goldman, S., Blekot, S., Nielsen, M.*, et al.* (2015). Direct neuronal glucose uptake heralds activity-dependent increases in cerebral metabolism. Nat. Commun. 6, 6807.
Marusich, M.F., Furneaux, H.M., Henion, P.D., and Weston, J.A. (1994). Hu neuronal proteins are expressed in proliferating neurogenic cells. J. Neurobiol. 25, 143-155.
Murthy, S., Niquille, M., Hurni, N., Limoni, G., Frazer, S., Chameau, P., van Hooft, J.A., Vitalis, T., and Dayer, A. (2014). Serotonin receptor 3A controls interneuron migration into the neocortex. Nat. Commun. 5, 5524.
Nakashiba, T., Nishimura, S., Ikeda, T., and Itohara, S. (2002). Complementary expression and neurite outgrowth activity of netrin-G subfamily members. Mech. Dev. 111, 47-60.
Nishiyama, J., Hayashi, Y., Nomura, T., Miura, E., Kakegawa, W., and Yuzaki, M. (2012). Selective and regulated gene expression in murine Purkinje cells by in utero electroporation. Eur. J. Neurosci. 36, 2867-2876.
Nowakowski, T.J., Pollen, A.A., Sandoval-Espinosa, C., and Kriegstein, A.R. (2016). Transformation of the Radial Glia Scaffold Demarcates Two Stages of Human Cerebral Cortex Development. Neuron 91, 1219-1227.

Ogawa, M., Miyata, T., Nakajimat, K., Yagyu, K., Seike, M., Ikenaka, K., Yamamoto, H., and Mikoshibat, K. (1995). The reeler gene-associated antigen on cajal-retzius neurons is a crucial molecule for laminar organization of cortical neurons. Neuron 14, 899-912.

Ohtaka-Maruyama, C., Hirai, S., Miwa, A., Heng, J.I., Shitara, H., Ishii, R., Taya, C., Kawano, H., Kasai, M., Nakajima, K.*, et al.* (2013). RP58 regulates the multipolar-bipolar transition of newborn neurons in the developing cerebral cortex. Cell Rep. 3, 458-471.

Ohtaka-Maruyama, C., Okamoto, M., Endo, K., Oshima, M., Kaneko, N., Yura, K., Okado, H., Miyata, T., and Maeda, N. (2018). Synaptic transmission from subplate neurons controls radial migration of neocortical neurons. Science 360, 313-317.

Ohtsuka, M., Sato, M., Miura, H., Takabayashi, S., Matsuyama, M., Koyano, T., Arifin, N., Nakamura, S., Wada, K., and Gurumurthy, C.B. (2018). i-GONAD: a robust method for in situ germline genome engineering using CRISPR nucleases. Genome Biol. 19, 25.

Oishi, K., Aramaki, M., and Nakajima, K. (2016). Mutually repressive interaction between Brn1/2 and Rorb contributes to the establishment of neocortical layer 2/3 and layer 4. Proc. Natl. Acad. Sci. U. S. A. 113, 3371-3376.

Olson, E.C. (2014). Analysis of preplate splitting and early cortical development illuminates the biology of neurological disease. Front Pediatr 2, 121.

Ozair, M.Z., Kirst, C., van den Berg, B.L., Ruzo, A., Rito, T., and Brivanlou, A.H. (2018). hPSC Modeling Reveals that Fate Selection of Cortical Deep Projection Neurons Occurs in the Subplate. Cell Stem Cell 23, 60-73.

Pedraza, M., Hoerder-Suabedissen, A., Albert-Maestro, M.A., Molnar, Z., and De Carlos, J.A. (2014). Extracortical origin of some murine subplate cell populations. Proc. Natl. Acad. Sci. U. S. A. 111, 8613-8618.

Ragan, T., Kadiri, L.R., Venkataraju, K.U., Bahlmann, K., Sutin, J., Taranda, J., Arganda-Carreras, I., Kim, Y., Seung, H.S., and Osten, P. (2012). Serial two-photon tomography for automated ex vivo mouse brain imaging. Nat. Methods 9, 255-258.

Reim, K., Regus-Leidig, H., Ammermüller, J., El-Kordi, A., Radyushkin, K., Ehrenreich, H., Brandstätter, J.H., and Brose, N. (2009). Aberrant function and structure of retinal ribbon synapses in the absence of complexin 3 and complexin 4. J. Cell Sci. 122, 1352-1361.

Saliu, A., Adise, S., Xian, S., Kudelska, K., and Rodríguez-Contreras, A. (2014). Natural and lesion-induced decrease in cell proliferation in the medial nucleus of the trapezoid body during hearing development. J. Comp. Neurol. 522, 971-985.

Schindelin, J., Arganda-Carreras, I., Frise, E., Kaynig, V., Longair, M., Pietzsch, T., Preibisch, S., Rueden, C., Saalfeld, S., Schmid, B.*, et al.* (2012). Fiji: an open-source platform for biological-image analysis. Nat. Methods 9, 676-682.

Seiriki, K., Kasai, A., Hashimoto, T., Schulze, W., Niu, M., Yamaguchi, S., Nakazawa, T., Inoue, K.I., Uezono, S., Takada, M.*, et al.* (2017). High-Speed and Scalable Whole-Brain Imaging in Rodents and Primates. Neuron 94, 1085-1100.

Seiriki, K., Kasai, A., Nakazawa, T., Niu, M., Naka, Y., Tanuma, M., Igarashi, H., Yamaura, K., Hayata-Takano, A., Ago, Y.*, et al.* (2019). Whole-brain block-face serial microscopy tomography at subcellular resolution using FAST. Nat. Protoc. 14, 1509-1529.

Sekine, K., Honda, T., Kawauchi, T., Kubo, K., and Nakajima, K. (2011). The outermost region of the developing cortical plate is crucial for both the switch of the radial migration mode and the Dab1-dependent "inside-out" lamination in the neocortex. J. Neurosci. 31, 9426-9439.

Shimogori, T., and Ogawa, M. (2008). Gene application with in utero electroporation in mouse embryonic brain. Dev. Growth Differ. 50, 499-506.

Shin, M., Kitazawa, A., Yoshinaga, S., Hayashi, K., Hirata, Y., Dehay, C., Kubo, K.I., and Nakajima, K. (2019). Both excitatory and inhibitory neurons transiently form clusters at the outermost region of the developing mammalian cerebral neocortex. J. Comp. Neurol. 527, 1577-1597.

Shitamukai, A., Konno, D., and Matsuzaki, F. (2011). Oblique radial glial divisions in the developing mouse neocortex induce self-renewing progenitors outside the germinal zone that resemble primate outer subventricular zone progenitors. J. Neurosci. 31, 3683-3695.

Stolt, C.C., Rehberg, S., Ader, M., Lommes, P., Riethmacher, D., Schachner, M., Bartsch, U., and Wegner, M. (2002). Terminal differentiation of myelin-forming oligodendrocytes depends on the transcription factor Sox10. Genes Dev. 16, 165-170.

Suarez-Mier, G.B., and Buckwalter, M.S. (2015). Glial Fibrillary Acidic Protein-Expressing Glia in the Mouse Lung. ASN Neuro 7, 1759091415601636.

Suh, J.M., Yu, C.-T., Tang, K., Tanaka, T., Kodama, T., Tsai, M.-J., and Tsai, S.Y. (2006). The Expression Profiles of Nuclear Receptors in the Developing and Adult Kidney. Mol. Endocrinol. 20, 3412-3420.

Swanson, D.J., and Goldowitz, D. (2011). Experimental Sey mouse chimeras reveal the developmental deficiencies of Pax6-null granule cells in the postnatal cerebellum. Dev. Biol. 351, 1-12.

Tabata, H., Kanatani, S., and Nakajima, K. (2009). Differences of migratory behavior between direct progeny of apical progenitors and basal progenitors in the developing cerebral cortex. Cereb. Cortex 19, 2092-2105.
Tabata, H., and Nakajima, K. (2003). Multipolar migration: the third mode of radial neuronal migration in the developing cerebral cortex. J. Neurosci. 23, 9996-10001.
Tabata, H., Yoshinaga, S., and Nakajima, K. (2012). Cytoarchitecture of mouse and human subventricular zone in developing cerebral neocortex. Exp. Brain Res. 216, 161-168.
Takeo, Y.H. (2016). In utero Electroporation of Mouse Cerebellar Purkinje Cells. Bio-protocol 6, e1835.
Takeo, Y.H., Kakegawa, W., Miura, E., and Yuzaki, M. (2015). RORα Regulates Multiple Aspects of Dendrite Development in Cerebellar Purkinje Cells In Vivo. J. Neurosci. 35, 12518-12534.
Tamamaki, N., Yanagawa, Y., Tomioka, R., Miyazaki, J., Obata, K., and Kaneko, T. (2003). Green fluorescent protein expression and colocalization with calretinin, parvalbumin, and somatostatin in the GAD67-GFP knock-in mouse. J. Comp. Neurol. 467, 60-79.
Tatsumi, K., Isonishi, A., Yamasaki, M., Kawabe, Y., Morita-Takemura, S., Nakahara, K., Terada, Y., Shinjo, T., Okuda, H., Tanaka, T.*, et al.* (2018). Olig2-Lineage Astrocytes: A Distinct Subtype of Astrocytes That Differs from GFAP Astrocytes. Front. Neuroanat. 12, 8-8.
Telley, L., Govindan, S., Prados, J., Stevant, I., Nef, S., Dermitzakis, E., Dayer, A., and Jabaudon, D. (2016). Sequential transcriptional waves direct the differentiation of newborn neurons in the mouse neocortex. Science 351, 1443-1446.
Vaid, S., Camp, J.G., Hersemann, L., Eugster Oegema, C., Heninger, A.-K., Winkler, S., Brandl, H., Sarov, M., Treutlein, B., Huttner, W.B.*, et al.* (2018). A novel population of Hopx-dependent basal radial glial cells in the developing mouse neocortex. Development 145, dev169276.
Vasistha, N.A., Garcia-Moreno, F., Arora, S., Cheung, A.F., Arnold, S.J., Robertson, E.J., and Molnar, Z. (2015). Cortical and Clonal Contribution of Tbr2 Expressing Progenitors in the Developing Mouse Brain. Cereb. Cortex 25, 3290-3302.
Vue, T.Y., Lee, M., Tan, Y.E., Werkhoven, Z., Wang, L., and Nakagawa, Y. (2013). Thalamic control of neocortical area formation in mice. J.Neurosci. 33, 8442-8453.
Watanabe, Y., Kawaue, T., and Miyata, T. (2018). Differentiating cells mechanically limit the interkinetic nuclear migration of progenitor cells to secure apical cytogenesis. Development 145, dev162883.

Winkler, C.C., Yabut, O.R., Fregoso, S.P., Gomez, H.G., Dwyer, B.E., Pleasure, S.J., and Franco, S.J. (2018). The Dorsal Wave of Neocortical Oligodendrogenesis Begins Embryonically and Requires Multiple Sources of Sonic Hedgehog. J. Neurosci. 38, 5237-5250.
Yamanaka, T., Tosaki, A., Miyazaki, H., Kurosawa, M., Furukawa, Y., Yamada, M., and Nukina, N. (2010). Mutant huntingtin fragment selectively suppresses Brn-2 POU domain transcription factor to mediate hypothalamic cell dysfunction. Hum. Mol. Genet. 19, 2099-2112.
Yi, J.-H., Katagiri, Y., Susarla, B., Figge, D., Symes, A.J., and Geller, H.M. (2012). Alterations in sulfated chondroitin glycosaminoglycans following controlled cortical impact injury in mice. J. Comp. Neurol. 520, 3295-3313.
Yoshinaga, S., Ohkubo, T., Sasaki, S., Nuriya, M., Ogawa, Y., Yasui, M., Tabata, H., and Nakajima, K. (2012). A Phosphatidylinositol Lipids System, Lamellipodin, and Ena/VASP Regulate Dynamic Morphology of Multipolar Migrating Cells in the Developing Cerebral Cortex. J. Neurosci. 32, 11643-11656.
Zhang, L.J., Bhattacharya, S., Leid, M., Ganguli-Indra, G., and Indra, A.K. (2012). Ctip2 is a dynamic regulator of epidermal proliferation and differentiation by integrating EGFR and Notch signaling. J. Cell Sci. 125, 5733-5744.
Zhao, T., Li, H., and Liu, Z. (2017). Tumor necrosis factor receptor 2 promotes growth of colorectal cancer via the PI3K/AKT signaling pathway. Oncol. Lett. 13, 342-346.
Zhou, Q., Wang, S., and Anderson, D.J. (2000). Identification of a Novel Family of Oligodendrocyte Lineage-Specific Basic Helix-Loop-Helix Transcription Factors. Neuron 25, 331-343.